8-2021

Terrestrial laser scanning technology for measuring streambank retreat along East Fork Poplar Creek and calculating the effect on mercury release.

José L. Martínez Collado
University of Tennessee, Knoxville, jmart199@vols.utk.edu

To the Graduate Council:

I am submitting herewith a thesis written by José L. Martínez Collado entitled "Terrestrial laser scanning technology for measuring streambank retreat along East Fork Poplar Creek and calculating the effect on mercury release.." I have examined the final electronic copy of this thesis for form and content and recommend that it be accepted in partial fulfillment of the requirements for the degree of Master of Science, with a major in Environmental Engineering.

Frank Loeffler, Major Professor

We have read this thesis and recommend its acceptance:

Melanie Mayes, John Schwartz, Frank Loeffler, Alex Johs

Accepted for the Council:
Dixie L. Thompson

Vice Provost and Dean of the Graduate School

(Original signatures are on file with official student records.)

Terrestrial laser scanning technology for measuring streambank retreat along East Fork Poplar Creek and calculating the effect on mercury release.

A Thesis Presented for the

Master of Science

Degree

University of Tennessee, Knoxville

José L. Martínez Collado

August 2021

Dedication

I humbly dedicate this thesis project to my beloved mother for always encouraging me to do my best to achieve my dreams. To my friends who supported me on the way and to my mentors for all their support. Especially to Dr. Melanie Mayes for being such a dedicated mentor and guide through this journey. I also want to thank Dr. Alex Johs, Dr. John Schwartz, and Dr. Frank Loeffler for always being there whenever I needed advice and being part of my committee. Also, I would like to thanks Mr. Kenneth Lowe and Mr. Leroy Goñez-Rodríguez for all their help during fieldwork.

Acknowledgment

This work was funded by the U.S. Department of Energy's (DOE) Oak Ridge Office of Environmental Management (ORO-EM) and URS| CH2M Oak Ridge LLC (UCOR) and is a product of ORNL's Mercury Remediation Technology Development Program.

ORNL is managed by UT-Battelle, LLC, for the U.S. DOE under contract No. DE-AC05-00OR22725.

Abstract

Mercury (Hg) is a globally distributed inorganic pollutants of human concern. The high toxicity is mainly related to the capacity of Hg species to accumulate and biomagnify along aquatic food webs. Along East Fork Poplar Creek (EFPC), erosion represents the principal mercury input into the local waters, eventually reaching humans through the food chain. This research project aimed to monitor streambank erosion along a mercury-contaminated creek using Light Detention and Ranging (Lidar) technology and erosion pins. A Terrestrial Laser Scanner (TLS) was used to generate high-resolution point clouds from August 2020 to January 2021 across nine streambank locations to detect changes in soil volumes. These volumes were simultaneously monitored using erosion pins, and with the results, estimates of soil input into the creek from streambank erosion were obtained. For all the sites, the volumes of soil introduced into the EFPC for the erosion pins ranged between 0-6.29 m^3 and 3.93-14.18m^3 for the TLS. Using erosion estimates, bulk density measurements, and known concentrations of Hg in bank soils, estimates for the mass of Hg entering EFPC were obtained. Estimates of Hg released into the EFPC ranged between 0-11.84 kg and 0-0.4 kg for the erosion pins and TLS, respectively. Erosion pin estimates of Hg and soil introduced into EFPC were both on average of 64 times greater than those given by the TLS. Measurements obtained with the TLS can be considered more reliable than those given by the erosion pins since this new technique has more spatial coverage, higher resolution and can account for irregularities and changes within the whole streambank, compared to erosion pins which interrogate only a tiny fraction of the volume of a streambank. This assessment identified locations in EFPC where soil erosion and mercury release are highest, thereby targeting specific locations for possible future remediation actions to prevent mercury mobilization.

Keywords:
Erosion, Light Detention and Ranging, Terrestrial Laser Scanner, Erosion Pins, Streambanks, Mercury, Contamination, East Fork Poplar Creek.

Table of Contents

List of Tables

List of Figures

List of Abbreviations

ALS	Airborne Laser Scanning
ARP	Autodesk Recap Pro
CC	CloudCompare
EFK	East Fork Kilometer
EFPC	East Fork Poplar Creek
Hg	Mercury
HRD	Historical Release Deposit
Lidar	Light Detention and Ranging
MeHg	Monomethyl Mercury/Methyl Mercury
ORR	Oak Ridge Reservation
SBR	Streambank Retreat
TLS	Terrestrial Laser Scanner
TRW	Trimble RealWorks
TS	Total Station

Chapter I: Introduction

1.1 Mercury Contamination Background

Mercury can be released into the environment by natural (volcanic eruptions or ore degradation) or anthropogenic sources (mercury and artisanal gold mining, industrial use, disposal of medical waste) (Oken et al., 2008; Bhan et al., 2005). Global anthropogenic activities, including ore mining and processing, coal combustion, and metal production, are responsible for more than 2,220 metric tons of mercury (Hg) emitted each year, according to the 2018 Global Mercury Assessment (United Nations Environment, 2018). This inorganic pollutant is a persistent neurotoxin that can easily spread across the environment (Di Natale et al., 2016). In nature, mercury may occur in three oxidation states (0, +1, and +2) such as elemental (Hg^0), mercurous (Hg^{+1}), mercuric (Hg^{2+}) mercury as well as other organomercury compounds (Poulain et al., 2013, Guzzi et al., 2008). In combination with environmental physical, chemical, and biological factors and other species present, the chemical speciation of Hg dictates the ecological and toxicological effects. Some prevailing conditions may facilitate the conversion of inorganic Hg into a more toxic species such as methyl mercury (MeHg), a potent neurotoxin that is readily accumulated by aquatic biota at each trophic level (Poulain et al., 2013; Ullrich et al., 2001).

Despite the fact that inorganic Hg is the main form of this element being introduced into the environment, the biggest threat to wildlife and human health comes from the bioaccumulation of MeHg (United Nations Environmental Program, 2009). International efforts from the United Nations Environment Programme (UNEP) have been around for several years, intending to locate existing Hg-contaminated zones that continuously affect public and environmental health. These efforts lead to the location of more than 3,000 high Hg contamination systems associated with industries, manufacturing sites, and mining processes (United Nations Environment, 2018). In most cases, Hg releases into aquatic environments from contaminated sites have not been extensively documented. Although there are many site-specific studies, they only use observations from short periods, and they do not always consider external factors such as meteorological conditions (Kocman et al., 2013).

Inorganic Hg emitted into the environment may enter watersheds either by direct release from contaminated sites or by atmospheric deposition, where it may be transformed to MeHg (Kraepiel et al., 2003). Anaerobic bacteria and archaea carrying the gene pair hgcAB are responsible for the methylation of Hg (Parks et al., 2013; Podar et al., 2015 and Gilmour et al., 2013). The primary methylators in freshwater systems and estuaries are sulfate-reducing bacteria (Poulain et al., 2013, Rhoades et al., 2009, Gilmour et al., 1992 and Fitzgerald et al., 1991). Methylmercury enters aquatic food webs through uptake by phytoplankton, where it bioaccumulates and biomagnifies up the trophic levels, as shown in

Figure 1 (Oken et al., 2008). Consequently, people whose diet relies on predatory fish (higher trophic levels) such as king mackerel, shark, swordfish, and bigeye tuna are at higher risk of developing Hg-related neurological diseases (Whiteacre et al., 2009).

The first report on MeHg poisoning was published as early as 1940 by Hunter et al. However, it was not until the 1960s that a relationship between seafood consumption and Hg-related diseases was established (Semionov, 2018; Harada, 1992; Hunter et al., 1940). Thousands of people were exposed to high levels of MeHg through the consumption of fish and shellfish contaminated by the wastewater dumped into a bay by a chemical factory in Minamata, Japan. Patients presented numbness, difficulty seeing, hearing, swallowing, coma, and many died. This condition was eventually known as the Minamata disease, and since then, Hg has been a critical contaminant of concern around the globe (Seminov, 2018; Timothy, 2001).

In the United States, Federal and state governments have been actively alerting communities about the risk of consuming certain kinds of fish (Roe, 2003). Simultaneously, efforts led to identifying Hg sources and also prompted research to investigate Hg transformations and the development of technologies to reduce and remediate Hg contamination. Even though Hg mobilization pathways are not clear, one of the major Hg sources in the environment is the erosion of Hg-rich historical deposits in stream banks (Rhoades, 2008).

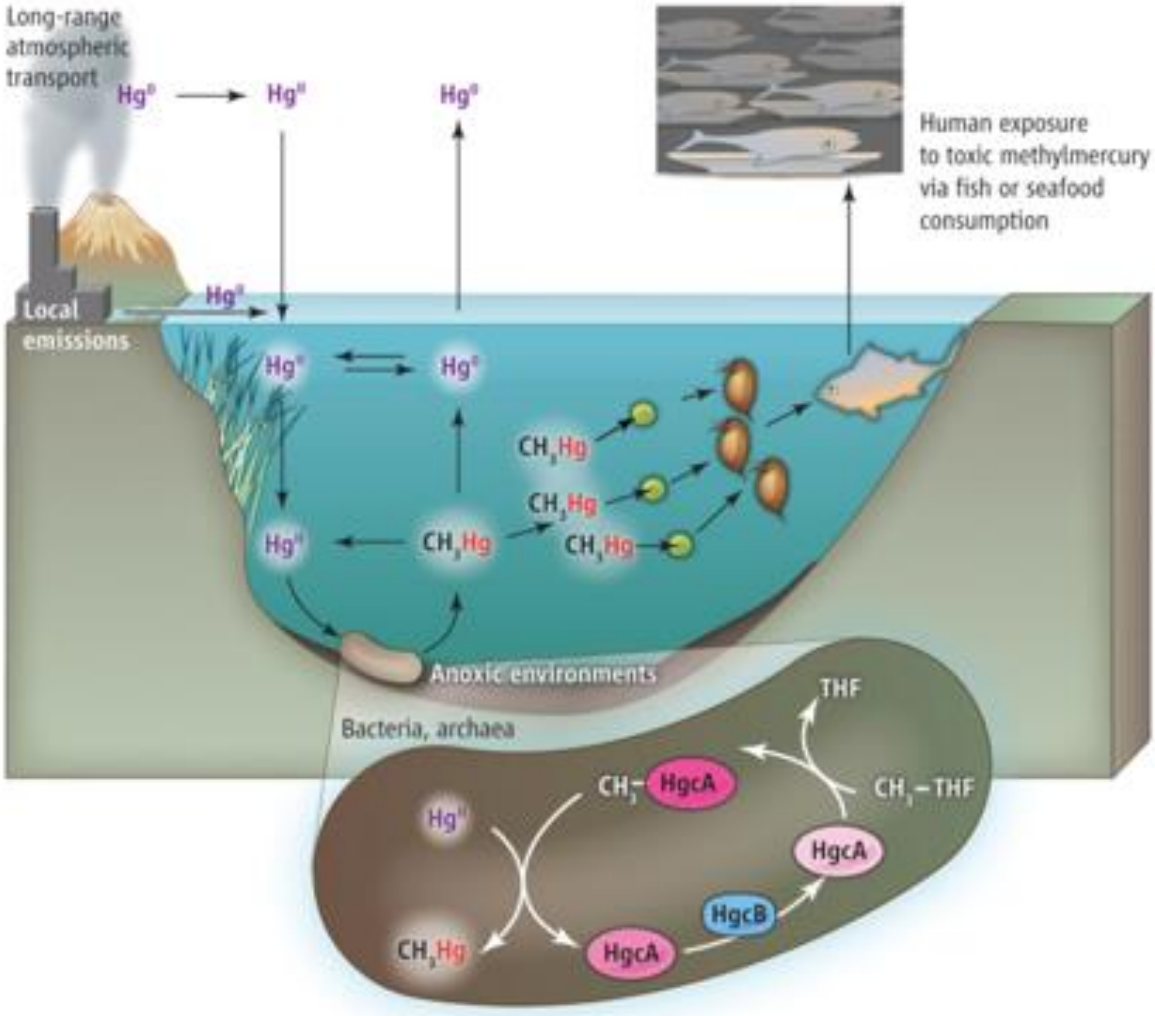

Figure 1: Mercury methylation in the environment (Poulain, A. J. et al. 2013).

1.2 Site Background

An example of widespread Hg contamination is the Oak Ridge Reservation (ORR) in eastern Tennessee, USA. The ORR was established during World War II, beginning in 1942, as part of the Manhattan Project. A facility to separate lithium isotopes for thermonuclear weapons was constructed within the Y-12 plant on the ORR. The lithium isotope separation process involved the amalgamation of lithium and required large amounts of metallic Hg. Even though the plant took precautions to avoid Hg release into the environment, by the end of the lithium isotope enrichment activities in 1963, around 128,000 ± 35,000 kg of Hg were discharged to the headwaters East Fork Poplar Creek (EFPC), which is within the boundary of Y-12 (Brooks et al., 2011) as seen in Figure 2.

The EFPC flows through the city of Oak Ridge until it reaches a confluence with Poplar Creek. Active use of Hg by Y-12 no longer occurs, but smaller amounts of Hg continue to enter the EFPC from residual contaminated infrastructure and soils at Y-12. The yearly average concentrations of total Hg exiting Y-12 and entering EFPC are around 300 ng/L, from which 60% of the Hg is in a dissolved form (Watson et al., 2017; Southworth et al., 2010).

The streambank soil along EFPC has been sampled to understand additional Hg sources along the creek downstream of the Y-12 facility. Studies showed that the stream banks throughout the EFPC can be classified as loam and silty loam soils (Dickson et al., 2017). Dickson et al. (2018) attempted to understand the role of the streambank and the streambed as Hg sources to the contaminated stream. Locations within EFPC were represented with the identifier East Fork (EFK), followed by a number that designates the creek kilometer measured upstream from the creek's mouth. The main focus of this study was the characterization of Hg contamination in streambanks and sediments in EFPC downstream of Y-12, beginning at EFK 23 throughout the following 19 km downstream to EFK 4. The survey was divided into four reaches; these were made based on the similarities of the floodplain properties and stream channel gradients, as shown in Figure 3 (Watson et al., 2016).

In the previously mentioned study, scientists were able to identify the historical release deposit (HRD) as a primary contributor of Hg into the stream. The HRD is a layer rich in coal fines deposited during historical Y-12 Hg discharge events. It was previously identified as a Hg-rich horizon in the bank soil (Southworth et al. 2010, 2013) with elevated Hg concentrations (Watson et al., 2017). The HRD contains Hg concentrations up to 4,600 ppm and is typically found between 2 to 120 cm below the ground surface with a thickness ranging between 5 and 45 cm (Dickson et al., 2018). The HRD is not continuous, but around 1,500 m of the stream may contain exposures of HRD along the banks of the EFPC (Dickson et al., 2018). That layer represents an essential visual aid in the creek banks for locating Hg hotspots. It was shown that the areas with HRD soils had an order of magnitude higher Hg than in the rest of the streambank soils (Figure 4). Identification of these high Hg zones was critical, especially since erosion plays a major role in the creek configuration and the transport of this chemical of concern.

1.3 Erosion Monitoring Approaches

For the past few years, there have been investigations to understand the streambank erosion along EFPC. The primary approach to measure erosion involved a conventional technique that uses erosion pins placed at different locations along a creek bank surface. This technique provides a simple and generalized input for erosion calculations. The first reference to this technique being used for bank erosion comes from Wolman (1959), and since then, it has been extensively used by many researchers for many applications (Thorne, 1981). It consists of using a rod (metal or fiberglass) of a determined length that is fully inserted into the bank, leaving no portion of it exposed. As bank erosion manifests, the rod will be continuously exposed (Lawler, 1993), as seen in

Figure 5 (Watson et al., 2016). After some time, especially following significant rain events, measurements are taken from the pin tip to the bank on each side of the rod (top, right, bottom, and left), then a mean of these values is obtained (Kiesel et al., 2009). As well as erosion, deposition can be easily estimated by measuring the depth to which the rod is buried. Apart from being an economical and straightforward alternative for measuring erosion, this technique possesses high sensitivity. It can detect small amounts of bank erosion (on the order of millimeters) with considerable accuracy (Lawler, 1993).

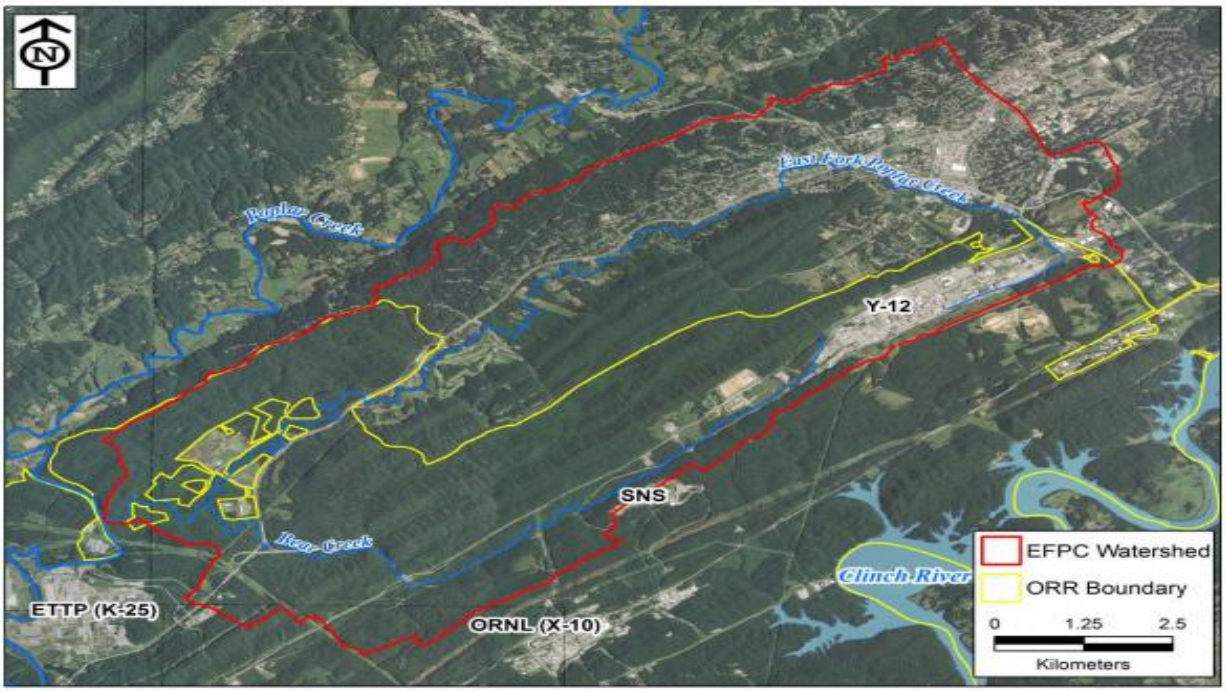

Figure 2: Map of the EFPC watershed (Watson et al., 2016).

(Notes: EFPC = East Fork Poplar Creek; ORR = Oak Ridge Reservation; ETTP = East Tennessee Technology Park; ORNL = Oak Ridge National Laboratory; SNS = Spallation Neutron Source; Y-12 = Y-12 National Security Complex.)

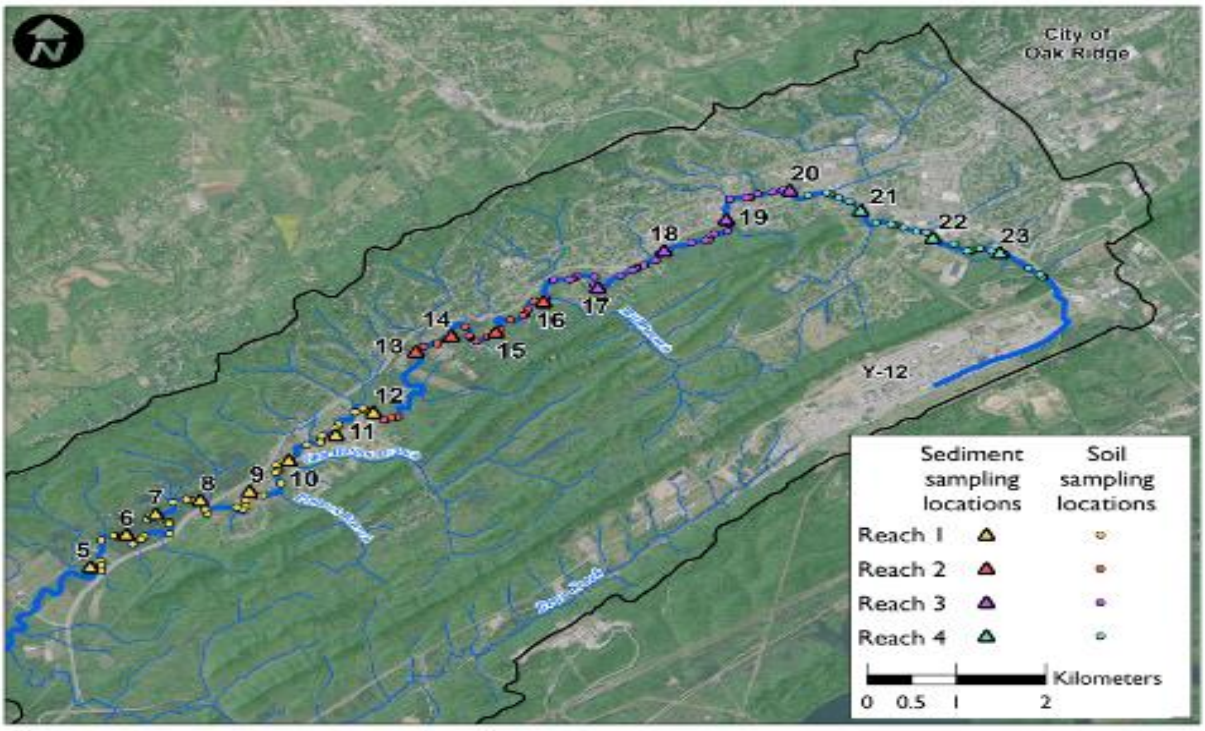

Figure 3: Map of EFPC with the four reaches and soil sampling locations (Watson et al., 2016).

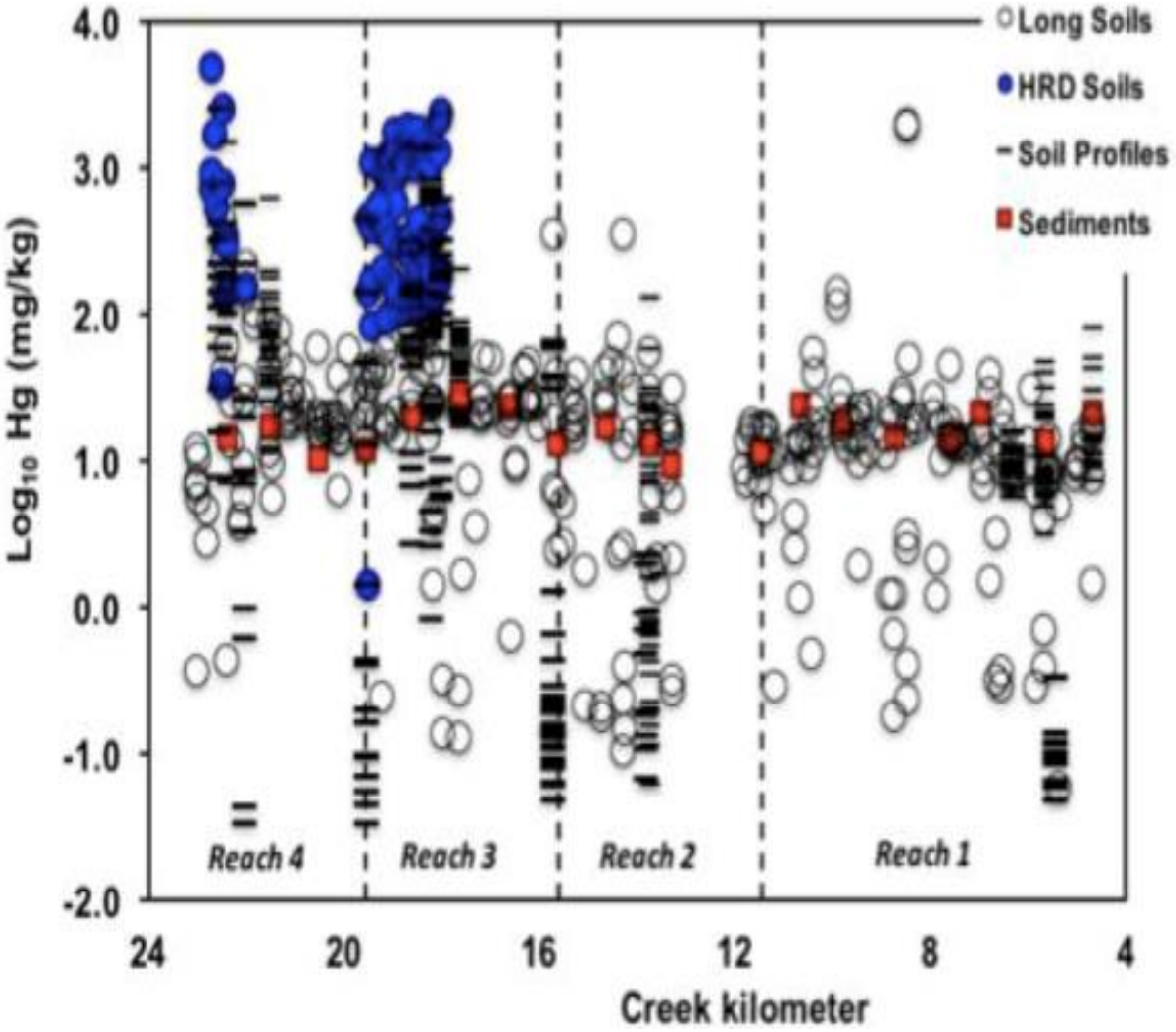

Figure 4: Mercury concentration distribution in streambank soils and sediment. (Dickson et al., 2018).

(Note: data from different studies was used, including a longitudinal soil sampling (2014 and 2015), Historical Release Deposit (HRD), vertical and horizontal soil profiles (Southworth et al., 2010), and streambed sediment sampling.)

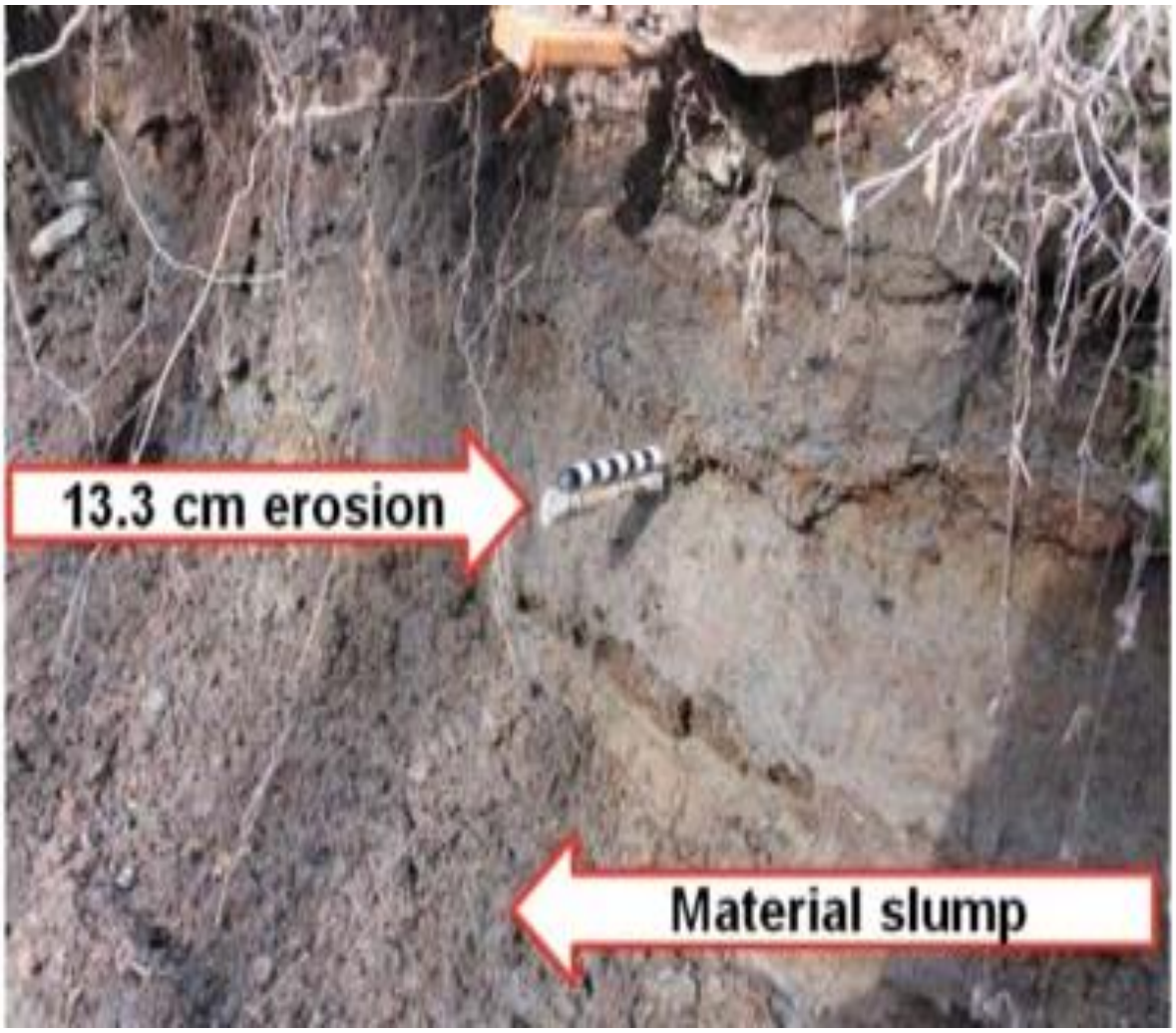

Figure 5: Streambank at EFK (January 2014), 96 days after erosion pin installation (Watson et al., 2016).

1.3.1 Erosion pin measurements in EFPC

A significant outcome from these erosion pin measurements at different locations along EFPC was estimates of net erosion and deposition over time. As illustrated in Figure 6 (Watson et al., 2016), the various lines represent the distance in centimeters (from the top of the bank) at which the erosion pins were located (Watson et al., 2016). In addition to using bulk densities to obtain a volume of soil eroded or deposited, two other essential assumptions were made. First, volume measurements were derived from a single length scale. The best way to acquire streambanks eroded soil volumes is by measuring erosion or deposition in every dimension within the bank. Since scientists only measured the length of exposure and burial of the erosion pin, they missed essential information such as the actual loss in the bank's horizontal and vertical axis. They obtained volumes by assuming equivalent erosion or deposition in every single direction on the streambank. As represented in Figure 7 (Mathews et al., 2019), they used the length of exposure or burial, then multiplied that value by the height and width of the bank, therefore extrapolating from one-dimensional distance value to three-dimensional volume. This approach may result in significant errors in the volume of eroded soil measured since the bank face is entirely non-uniform; instead of measuring erosion at multiple points along the entire bank length and height, only one measurement from the erosion pin is used. Second, it was assumed that the bulk soil densities are equivalent along the streambank, which is flawed because the creek bank locations where an HRD layer is present are not uniform. In addition, EFPC contains areas where clay is predominant and zones where very soft and loose soil predominates. When multiplying the volume and the bulk density (both based on assumptions), the resulting mass measurements have a high degree of uncertainty. Despite the many assumptions and high degree of uncertainties, by combining the information from Figure 6, an estimate for net erosion and deposition at different locations as a function of bank height was obtained (Figure 8, Mathews et al., 2019).

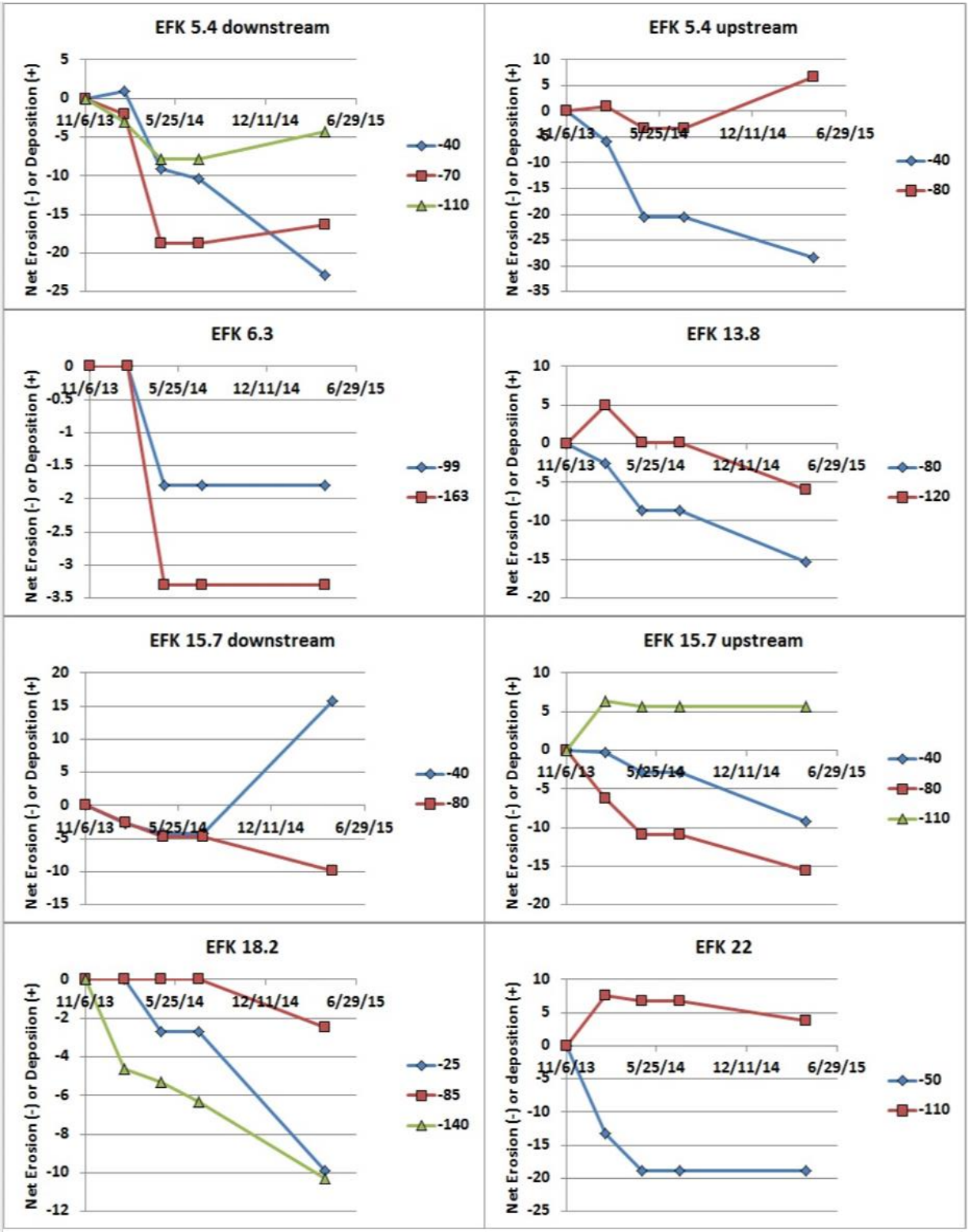

Figure 6: Estimates of net erosion and deposition (y-axis in centimeters) over time obtained from the erosion pin experiment at different locations along the EFPC (Watson et al., 2016). Colored lines indicate the distance from the top of the bank to the pin in cm.

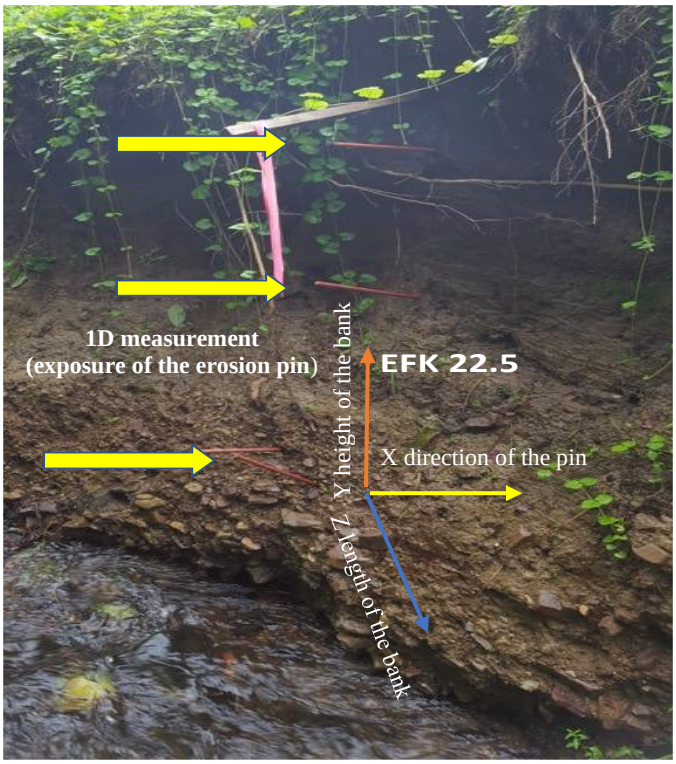

Figure 7: Erosion pin experiment used to obtain volume estimates of the streambank retreat (Mathews et al., 2019).

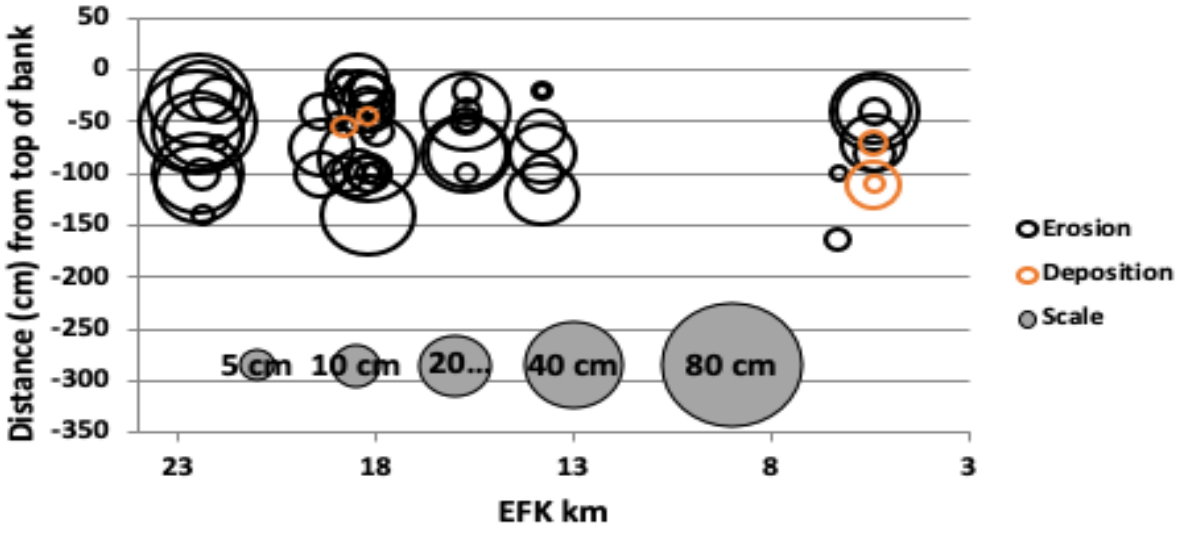

Figure 8: Cumulative erosion and deposition as a function of distance along EFPC (Mathews et al., 2019).

Despite their limitations, these preliminary measurements provide sufficient background data to compare future erosion assessments along the creek. Although this approach provides highly sensitive data, it is a point-specific technique, resulting in a high random spatial variability. This can lead to overestimates of erosion, a significant factor when cost-intensive remedial actions, such as bank restoration, are considered (Lawler, 1993). Also, volume estimates lack accuracy since this method can only measure one-dimensional length scales and not three-dimensional volumes lost due to erosion. Consequently, erosion pins may be most useful to provide qualitative rather than quantitative estimates of erosion (Mathews et al., 2019).

1.4 Proposed Technology for Erosion Monitoring: Terrestrial Laser Scanning

Terrestrial laser scanning (TLS) is a modern technology designed for surveying applications, including measuring exact distances and angles. This technology allows the acquisition of complex spatial profile data in combination with high-resolution images from buildings, machines, and other physical objects. The TLS system uses Light Detection and Ranging (Lidar) technology, which uses light emitted by a pulsed laser to measure distances between a fixed location and a surface with high spatial resolution. After the laser emits light, it is reflected from a surface and detected by a sensor. The equipment measures the time it took for the light pulse to travel from the laser source back to the sensor and calculates the distance between the equipment and the surface. That way, it can generate a spatially accurate 3D model ("point cloud") of the area of interest. This technology, in contrast to previous methods, can repeatedly create high spatial resolution 3D maps. This approach has been used to generate digital terrain models (DTM) because it can detect continuous changes in a monitored area with vast data.

One of the most commonly known applications of Lidar is Airborne Laser Scanning (ALS). The ALS is a commonly used surveying technique used to accurately mapping the earth's topography as well as man-made structures. Although both technologies are based on the Lidar application, the way they are implemented is different. The ALS is usually attached to an airplane, helicopter, or drone, and it works by emitting the light pulses downwards. On the other hand, the TLS is a stationary device, usually attached to a tripod on the ground and usually used to capture specific areas around the instrument. One of the studies where ALS is tested compared to the TLS

was performed by Goodwin et al., 217. The study aimed to assess the ability and synergies to detect geomorphic changes for a gully located in Aratula, southeast Queensland, Australia. The outcome of the experiment showed that both technologies separately provide unique assessments. The ALS analyzed bigger data sets of a greater area and used rainfall events to generate estimates of volumetric changes. The TLS was able to detect more subtle intra-annual changes but was limited in its spatial coverage. Data proved that the TLS is optimum for specific sites and that in combination with ALS, data accuracy and general values of volumes can be estimated with more reliability.

Another relevant experiment was performed in the Piedmont geological region near Raleigh, North Carolina, USA (Starek et al., 2013). The goal was to analyze a region with banks composed of different kinds of sediments and develop digital terrain models using TLS point cloud data. The authors conducted a series of nine TLS surveys within an 11.5 m wide by 3.2 m height area, forming eight sequential data epochs. For the study, data was collected periodically using a Leica Geosystem ScanStation 2 mounted on a tripod over a timeframe of 18 months. Once point cloud data and images were acquired and processed with Leica Cyclone software, a visual comparison between the DTM at different periods demonstrates significant erosion. A quantitative estimate of the erosion was obtained by staking the DTMs at different times into a voxel model (small and distinguishable element of a 3D model) to form a space-time cube. The space-time cube provided a compact representation of the spatiotemporal evolution of the bank using the TLS images. TLS provided much more accurate 3D measurements of bank erosion compared to traditional methods like erosion pins.

Other recently developed technologies have evolved with advanced capabilities; they focus on applications such as calculating distances and shapes via triangulation. For example, the total station (TS) is an electronic, optical instrument used for surveying and many other architectural applications. Although both technologies are capable of generating volume estimates, the TLS generates a complete coverage of the surface while the TS uses horizontal and vertical angles and distances interpolated to generate the image. This technology has also been proposed as an alternative for measuring stream bank erosion. An experiment was performed comparing the TS technology with TLS to measure streambank retreat (SBR, or erosion) (Resop et al. 2010). This study's final objective was to find a technology to efficiently quantify the sediment load of a

streambank along Stroubles Creek downstream of Virginia Tech's main campus. The 11 m long streambank was measured with a Leica TC 307 for the TS surveying and an Optech ILRIS-3D for the TLS measurements. One of the most significant advantages of the TLS over TS was the amount of data scientists collected to evaluate the variability of SBR. Also, TLS allowed creating maps of the entire zone over time. This aspect is advantageous as it is useful to have a faster and better visualization of erosion and deposition areas.

In conclusion, the study proves that this technology is adequate to calculate SBR and volume changes without perturbing the streambank and with improved point density measurements compared to the TS. Even though it is a useful instrument, the TS is not easy to operate. It requires a skilled surveyor, more software manipulation and is troublesome for the user since they cannot check the data from the field (Resop et al., 2010; Myers et al., 2019).

1.5 Mercury Calculations

As previously mentioned, Hg contamination across the EFPC streambanks represents a significant concern for the local community and government. For this reason, quantifying how much of this contaminant is being introduced into the EFPC waters is crucial. Although different studies aim to understand streambank processes using multiple technologies (erosion pins, Lidar, TS), almost none address streambanks with specific contaminants. Efforts to identify a technology that can reliably measure streambank erosion will be simultaneously used to measure the amount of Hg going into the EFPC waters. This technology and relatively novel assessment will replace old techniques such as erosion pins.

1.6 Research Goals, Objectives, and Hypothesis

Goal. This project aimed to quantify changes in volume and soil mass in a streambank to generate estimates of Hg input due to erosion. Our *objectives* for this project were (1) to use TLS technology to generate accurate measurements of streambank retreat in the EFPC, (2) compare those results from the TLS with data taken simultaneously from existing erosion pins, and (3) use the volumes obtained from both techniques along with bulk densities and concentrations of Hg to obtain estimates of Hg being introduced to the EFPC waters due to erosion. With these

objectives in mind, our *hypothesis* established that the TLS technology will generate more reliable streambank retreat measurements than the erosion pins along EFPC.

Chapter II: Materials and Methods

In this chapter, sections 2.1 through section 2.4.2.1 are intended to present the materials and methods used for TLS technology, including the software used and equipment set up in the control and field sites. It also discusses the registration of scans, which is the process of combining multiple images (from one site at different angles) to improve the quality of a point cloud.

2.1 Leica BLK 360 Imaging Laser Scanner

The BLK 360 Imaging Laser Scanner is one of the Leica Geosystems (AG, Heerbrugg, Switzerland 2020) reality capture instruments. It is a compact imaging laser scanner that uses a 360° laser distance meter and high-definition panoramic imaging to create a 3D point cloud. This machinery can capture 360,000 data points within seconds and generate panoramic images in real or thermal imaging within minutes. The accuracy of the instruments ranges between 4 mm at 10 m distance or 7 mm at 20 m distance. This instrument is the designated TLS technology used for this research project, and it was selected for its compactability, low cost, and ease of use in the field.

2.2 Field Work Software

BLK 360 and ReCap Pro are the two operational software packages for working in the field. They are used for controlling the TLS instrument remotely, image processing, and digital storage of the point cloud data.

2.2.1 BLK 360

The BLK 360 software (Leica Geosystems AG, St. Gallen, Switzerland) is the default operating system included with the BLK 360 TLS instrument. It is a simple platform that allows users to control the Lidar and to acquire high-resolution data. After taking each measurement,

users can view the resulting point cloud on a tablet computer or transfer images to a desktop computer for additional processing.

2.2.2 ReCap Pro

Autodesk ReCap Pro (ARP) (Autodesk Inc., San Rafael, CA) stands for "Reality Capture," and it is a more sophisticated program for working with native point clouds from laser scanners. It is a software package to open and process point cloud files. One of the most useful ARP tools was a "noise filter" that allowed removing unnecessary points that are usually associated with heavily dense point clouds. This software was the main program used to control the BLK 360 TLS in the field remotely. This software performed a preliminary registration, that although it was not permanent, provided feedback on whether a sufficient number of scans were obtained for a high-quality point cloud of the streambank. Finally, ARP was used to store the acquired data in the tablet, then using the desktop software version, the images were transferred to a desktop PC for more processing.

2.3 Modeling Software

Cloud Compare (CC) and Trimble RealWorks (TRW) are the designated software used to process and refine the images and to perform volume calculations.

2.3.1 Cloud Compare

CloudCompare (http://www.cloudcompare.org, accessed August 14, 2020) is a 3D point cloud and a triangular mesh processing software. It was designed initially to perform comparisons between two dense 3D point clouds (such as the ones acquired with a laser scanner) or between a point cloud and a triangular mesh. Although the software possesses many useful tools, it was used as a point cloud cleaning software for this project. Meaning that once the dense point clouds were acquired from the field, I used this software to remove unnecessary points to

only work with the area of interest. It was also used to remove most vegetation and debris from the streambank surface since these can generate overestimates of erosion and deposition.

2.3.2 Trimble Real Works

Trimble RealWorks (Trimble Geospatial, Sunnyvale, CA, USA) was used as a point cloud processor and analysis software. This geospatial software was used to perform the final registrations between the different scans taken at different times. Using the first scan as a reference, TRW combines other point clouds after erosion events. A volume calculation tool provided estimates of the difference between both images of the same place at different times. The difference between two values separated by time represented a volume of soil eroded based on the initial scan. Also, the software provided high-quality visual models of the area of interest with a depth color gradient.

2.4 Methodology

The following is a detailed summary of how scans of the creek banks were acquired to obtain point clouds. It includes the materials needed, instrument setup, and how the point clouds were processed after field scans were taken in the field.

2.4.1 Procedure: Basic Setup

Once the bank of interest is located, it is important to know how exposed was the surface of the bank. Some surfaces were covered with dead leaves or branches and vegetation that interfered with the accuracy of the measurement in interrogating the soil. For this reason, the first step was to remove loose debris from the surface of the bank. In case of excess vegetation, these may be trimmed with scissors while avoiding pulling the roots since that will compromise the structure of the bank. This last step is only necessary when taking scans during spring-summer; afterward, the surface in this region will have enough visibility (fall-winter). Then, depending on the size of the bank, three reference targets were be placed randomly across the area of interest, as shown in Figure 9. More targets can be placed for irregular banks if needed since they will facilitate the image registration when taking multiple scans.

The next step is to place a survey marker 8-10 ft from the surface at three different angles. Doing this allows the scanner to generate more accurate point clouds that account for the irregularities in the surface of the bank. Figure 10 shows a simple diagram of how the instrument was set up before taking any scan.

2.4.2 Scanning

After the instrument setup, the scanner was placed on one of the survey markers and using the iPad with the ReCap Pro software, a point cloud was acquired. The same process was repeated on the remaining marked areas. Once the images were taken, the RecapPro software was used to perform a preliminary registration of all the scans, resulting in one big point cloud that is more accurate than the individual images. This preliminary registration provided useful information on the accuracy of the acquired data set.

2.4.3 Image Processing

To process and model the images, I started by uploading the individual point clouds into CC. For this project's purposes, it is important to know that a scan is used in the same context as a point cloud. In this step, the software performed one last registration between the separate scans from one site, allowing to pick reference points across multiple images, increasing the accuracy of the superimposed scans. The final product was a highly dense point cloud with a higher resolution. Next, we cut the 360° image so that we only work with the bank of interest. Then, the bank's point cloud was transferred to TRW. To generate the volume estimates of soil in the creek banks, I used a starting point of reference. In this case, the reference point was the initial scan of the bank taken at the beginning of the experiment. Any erosion or deposition was based on that initial scan; this approach eliminated many uncertainties associated with just comparing one individual scan to another. The diagram above (

Figure 11) summarizes how the point cloud is processed, starting at the field with the equipment setup using the ReCap Pro and BLK 360 to the office work using CC and TRW to register, clean, and obtain volume estimates.

Figure 9: Control Site reference target positioning

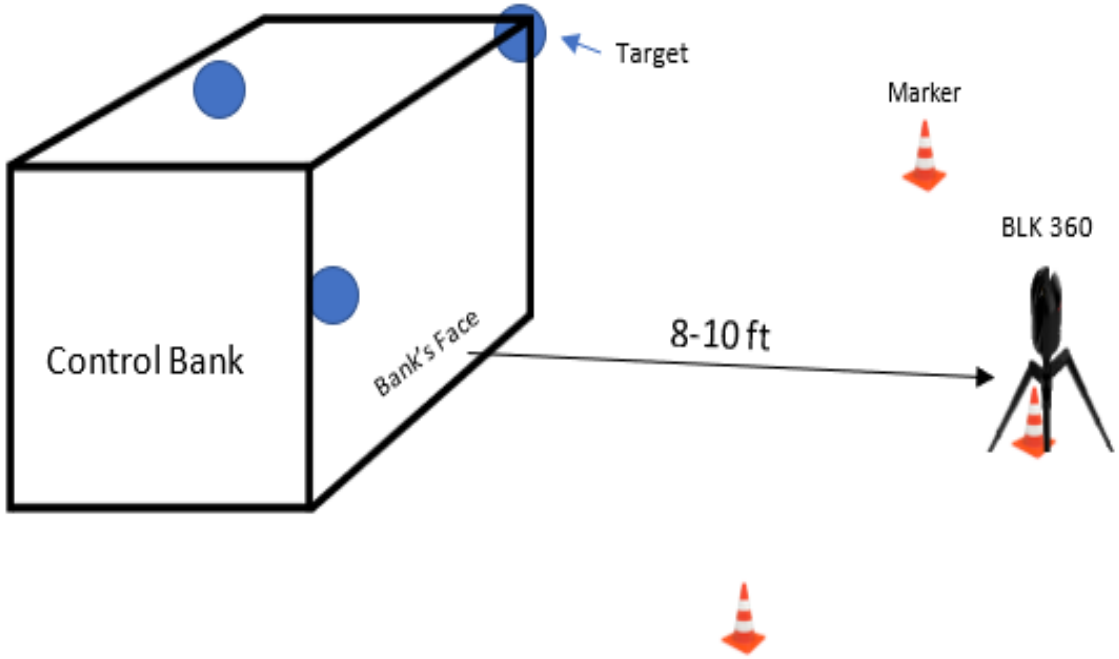

Figure 10:BLK 360 scanner field set up before taking scans

2.5 Initial Tests

2.5.1 Block Test

Before proceeding with fieldwork, a pilot test was conducted to understand and test the accuracy of the scans. This test was used in combination with a control site (next section) to confirm data and methodological procedure. The test consisted of a double-layer brick wall (17 bricks per wall, Figure 12) with known dimensions representing a creek bank. The bricks were placed so that one or more can be easily removed to simulate erosion and deposition. Following the procedure mentioned above, the first set of scans was performed on the full brick wall; this initial scan served as our reference point. To simulate erosion and deposition, scans were taken after removing one and seven blocks (simulating erosion) and after removing and placing right in front of the brick wall two blocks (simulating deposition). Once generated, the point clouds were processed with CC and TRW.

2.5.2 Control Site

Although the block test was expected to provide useful data on the volume accuracy, it is important to understand that it was a very controlled experiment with symmetric surfaces. When working with an actual creek bank, the variations of the surface are very irregular. An additional test was performed in a clean soil bank to determine instrument and software performance with real soil. Simultaneously, the bulk density was measured to relate the mass of soil removed with the soil volume removed.

2.5.2.1 Control Site: Erosion Simulation

This experiment was performed along an old road in the Walker Branch Watershed on the ORR. After following the basic setup procedure (section 2.4.1), I selected an area along the bank's flat surface with a 1ft long by 3ft height. Using a garden trowel, I delineated this rectangle; this was repeated in two more spots on the bank's surface to generate the experimental measurements, in triplicate, of simulated erosion.

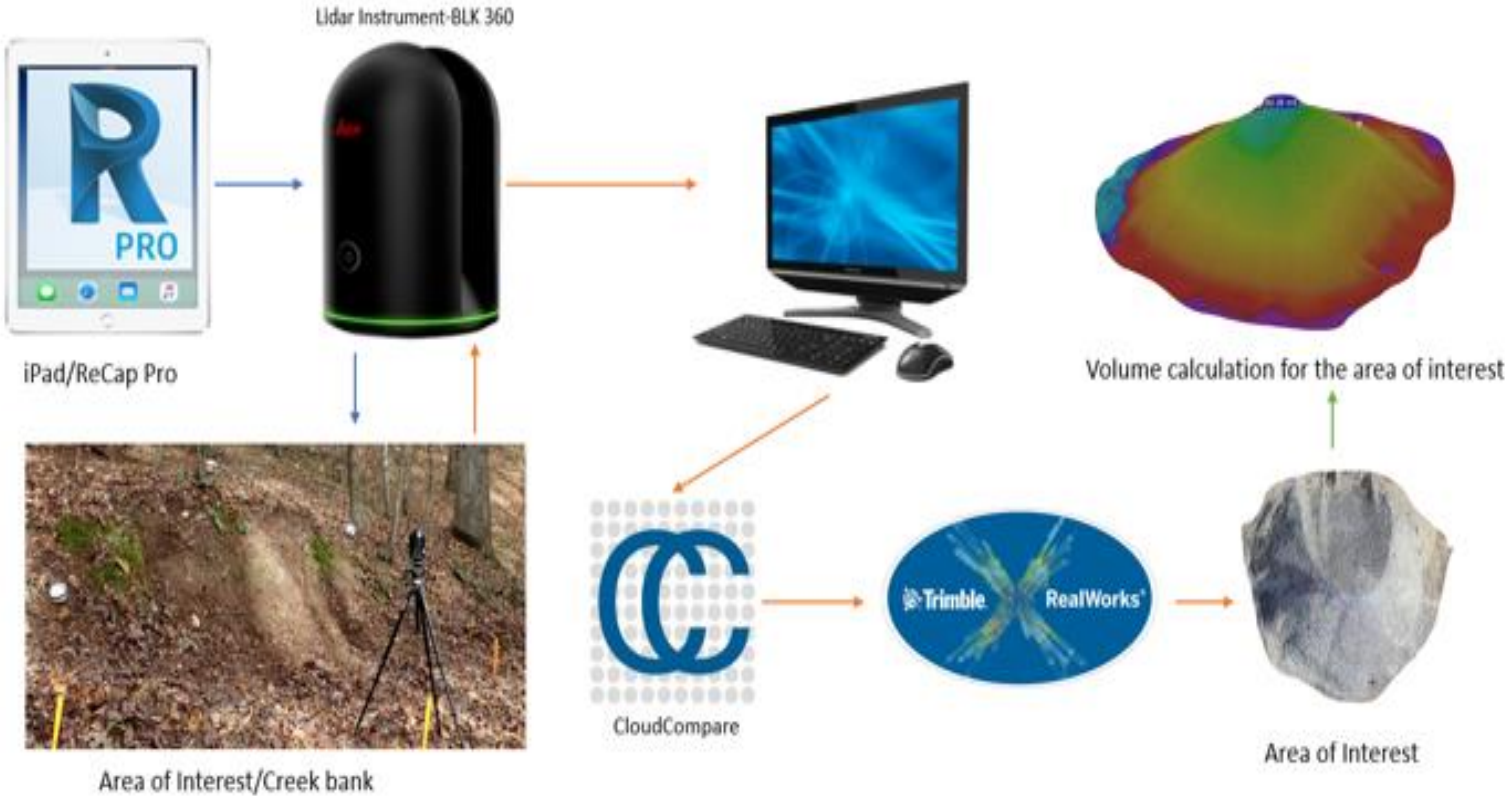

Figure 11: Workflow diagram when working with the BLK 3

Figure 12: Double-layer brick wall simulating a creek bank surface

Afterward, I carefully removed with a hand trowel the most upper part of each rectangle a 1ft by 1ft by 3inch deep cube, as seen in Figure 13. A plastic tarp was positioned under the rectangle before digging; this allowed to recover any loosened soil. The loosened soil from each square was collected in a bucket and weighed using an Ohaus Digital Bench Scale Series 20L (OHAUS Corporation, Parsippany, NJ, USA). The next step was to take the second set of scans following this simulated erosion event. Then I repeated the same process by carefully removing another cube, immediately beneath the first cube, with the same dimensions (Figure 14). This procedure was done one more time until all the delineated rectangles had a depth of 3 inches (Figure 15). This process provided a reference plane (flat surface) and an erosion event simulation to compare against the reference plane.

The images were processed (as described in section 2.3.31), and a volume estimate was obtained from TRW. Each section's volume is about 432 cubic inches (7079.21 cm^3), and this number was compared with that of the software. Once more, this experiment served as a proof of concept before conducting measurements on the EFPC stream banks.

2.5.2.2 Bulk Density Measurements

As mentioned before, bulk density measurements are needed to correlate volume with mass. Due to the different types of bank soils along the creeks, it was important to account for changes in bulk density as a function of creek bank height and changes observed along the length of EFPC. According to the USDA Soil Quality Indicator (June 2008), this soil study will provide validity of comparisons by removing errors associated with differences in soil densities at the time and place of sampling. The following procedure is based on the Soil Quality Test Kit Guide (USDA, 1999), and it consists of a sample collection section and a laboratory analysis.

2.5.2.3 Bulk Density Sample Collection

Bulk density measurements were performed on the control site to develop a representative procedure used in the field sites. For the control site, I took measurements before digging each section. I started by selecting four sampling points per section, as seen in

Figure 16;

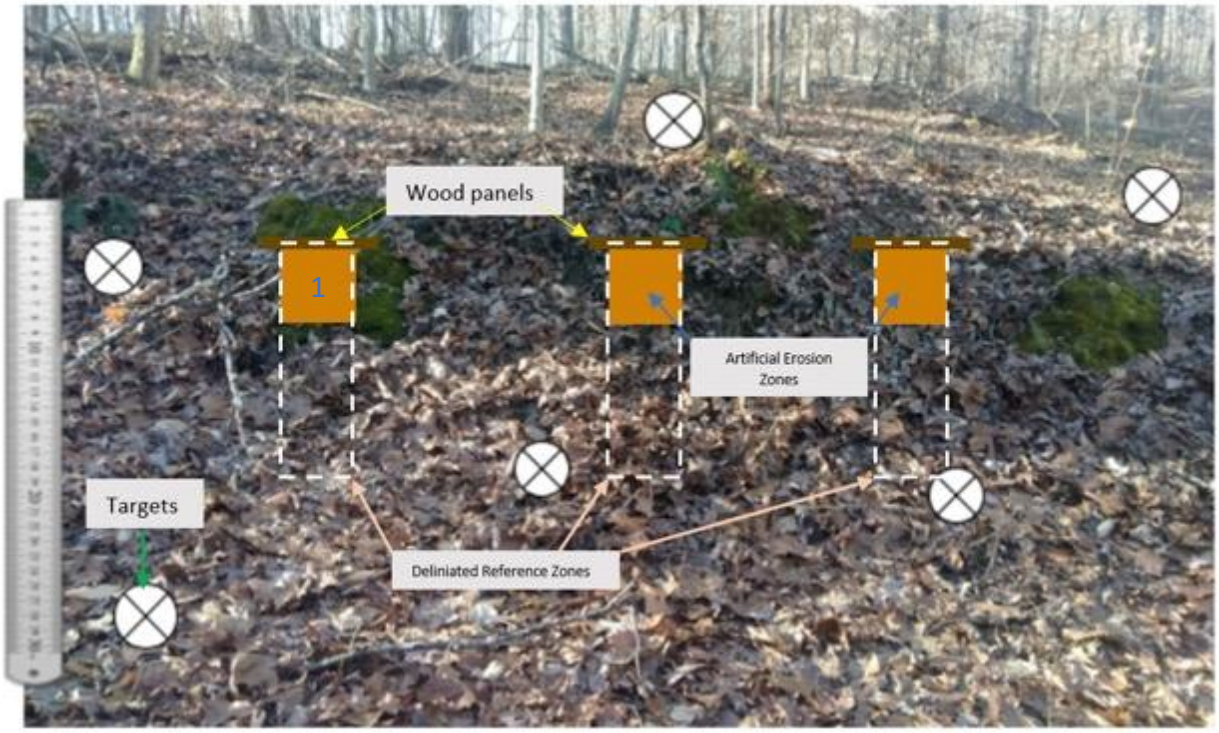

Figure 13: In the first section of erosion simulation, the orange area indicates the 1ft by 1ft by 3inch squared simulating erosion.

Figure 14: Diagram of the artificial zone after the second erosion event.

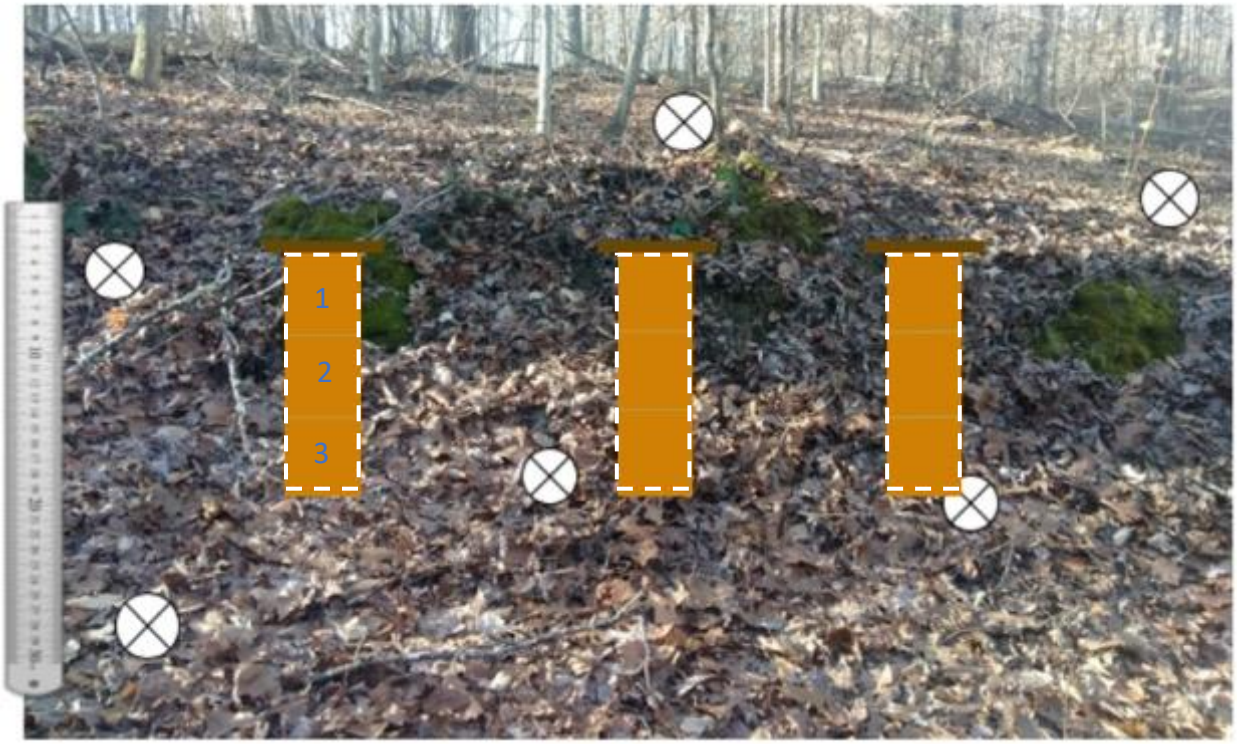

Figure 15: In this diagram, the third erosion zone was added to the delineated area.

since I had nine sections, our total samples were 36. Using a metal cylinder with known dimensions (and with the help of a hand sledge) I inserted the three-inch-diameter core into the surface of the erosion rectangle mentioned above.

To remove the cylinder and avoid losing soil, I dug the soil around the cylinder's outer surface until it was mostly exposed (Figure 17 a). Once the cylinder was loose and easy to remove, I ensure that the soil at the bottom was flat with the bottom part of the cylinder. With the help of a small knife and spatula, I carefully removed the excess soil from the bottom (Figure 17 b). To conclude the sample collecting, each of the core samples were placed inside a labeled plastic bag.

2.5.2.4 Bulk Density Laboratory Analysis

We started by carefully placing the soil from the core into a tray. Samples were then placed in a drying oven at 85° C (Active Standard ASTM D6683 temperatures used for bulk densities are between 70°C and 105°C) for 48 hours. To ensure samples were fully dried, these were removed after the 48 hours, weighed, and placed in the oven again for 24 hours. After no significant change in the weight of the dried soil was detected, each bulk density was determined by dividing the dry weight of the soil sample by the volume of the sample (which is the inner volume of the core).

$$Soil\ bulk\ density\ \left(\frac{g}{cm^3}\right) = \frac{oven\ dry\ weight\ of\ soil}{volume\ of\ soil}$$

2.6 Field Bulk Density Samples

As described in chapter one, EFPC has a characteristic black soil layer known as the HRD. This distinguishing layer makes the soil across the creek banks irregular in texture. Additionally, there are in situ materials weathered from the underlying bedrock, and materials (including HRD) deposited on top of the weathered bedrock material, and then all weathered in place.

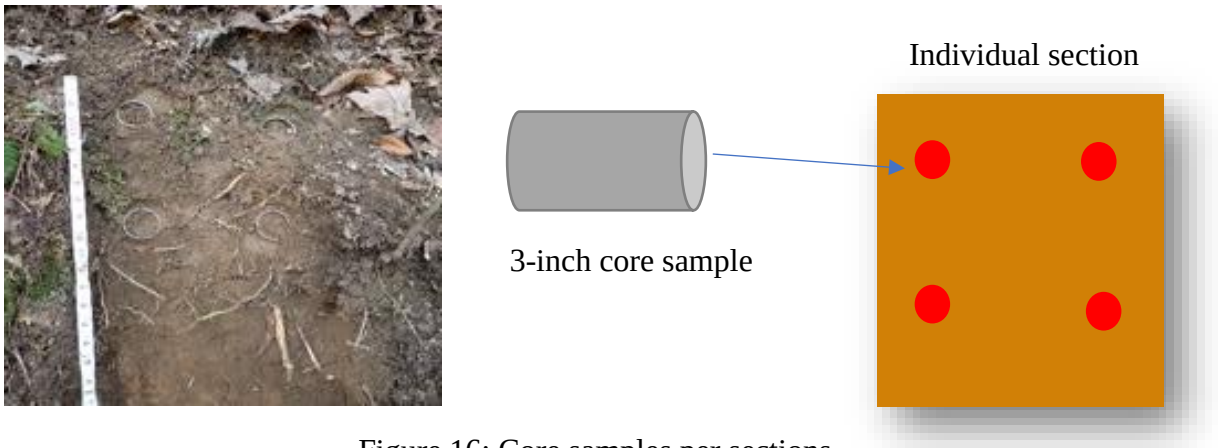

Figure 16: Core samples per sections

Figure 17: (a) the soil around the core was removed, then (b) the excess soil from the bottom was detached from the cylinder's surface.

When collecting the core samples from the field, we followed section 2.4.2.3, but we accounted for the non-homogeneous bank soils in the following manner. Soil samples were collected every 10% depth from the top of the bank to standardize sample collection across all banks, as shown in Figure 18. Following this method ensures the final average bulk density is more representative for the whole bank. In total, two samples were taken per depth, one on each side of the streambank, in order for the scanned surface to remain unaltered for future analysis.

2.7 Experimental Site Locations

This experiment was conducted at nine sites distributed along the 19 kilometers of EFPC (sites identified in Figure 19: EFPC Sampling Sites LocationsTwo previous studies by Dickson et al. (2018) and Dickson et al. (2015) were used as a reference to select sites. The former study focused on the Hg levels, while the latter was intended for soil characterization along the EFPC. The selected sites included areas from high to low erosion levels based on previous erosion pin data (Watson et al., 2016); this way, the project was able to test the technology under a variety of realistic scenarios present in EFPC. Furthermore, the selected sites included erosion pins located within different layers of the bank. This was important since the data collected from the TLS was compared with the data from the erosion pins.

Table 1 summarizes the location of the sites used in this experiment. Added at the beginning are the original names used by previous studies. For this experimental scope, the site names were standardized based on the kilometers from the mouth of the creek (EFK). Data was collected between August 2020 and January 2021; the first set of scans were taken on August 12, 13, and 19 of 2020. The second set followed significant rain events and was collected on October 15-16, 2020. The final scans were taken on January 6, 2021, for 147 total days of the experiment. Simultaneously with the scans, erosion pin measurements were taken at the different sites.

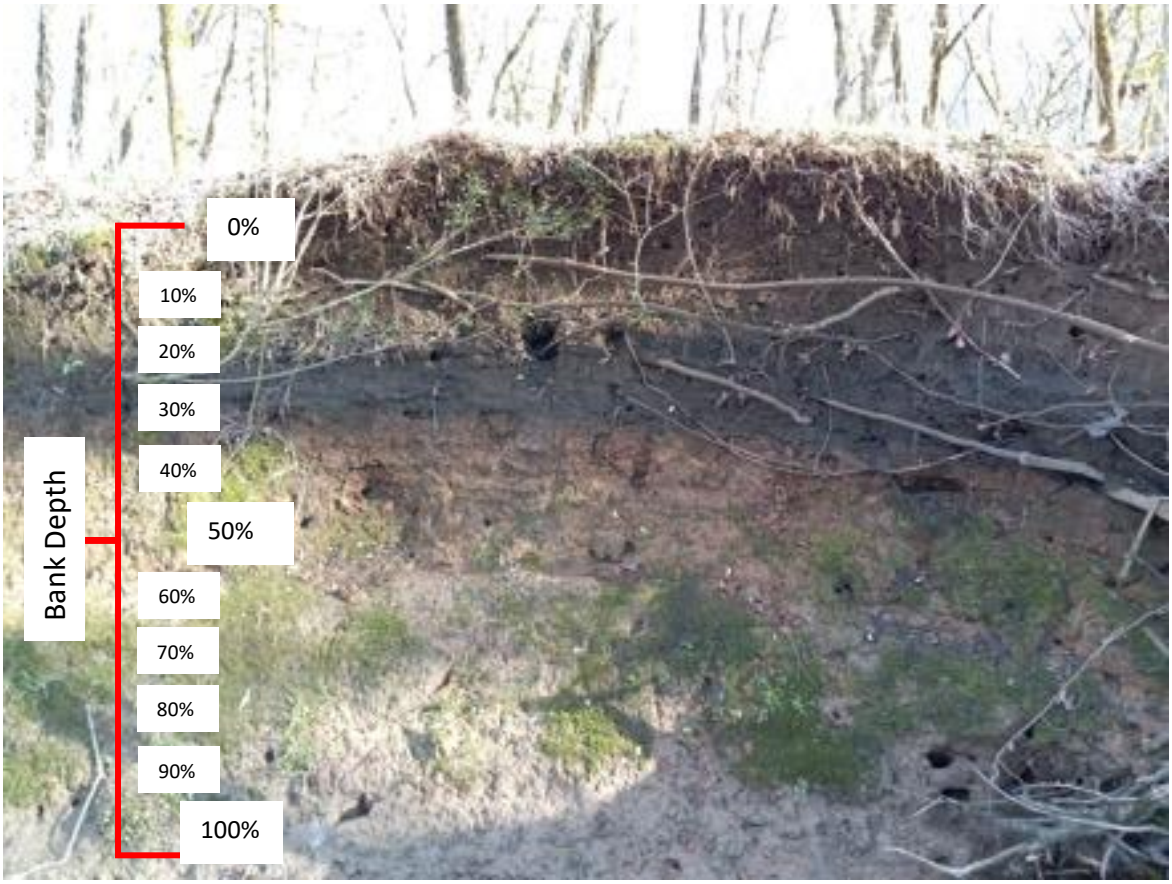

Figure 18: Bulk density sample's collection depths in the field sites

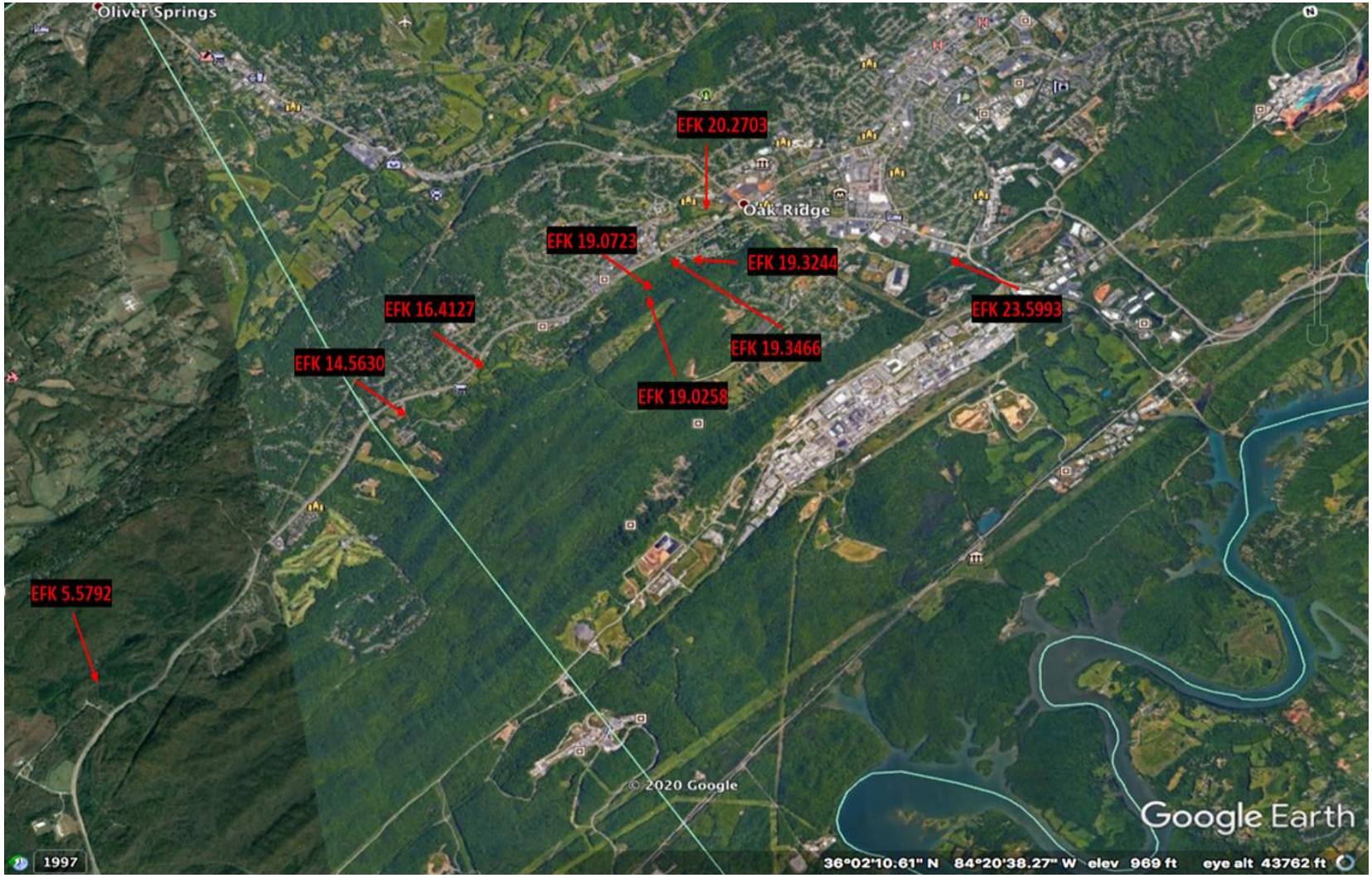

Figure 19: EFPC Sampling Sites Locations

Table 1: EFPC experimental sites and coordinates

Previous Designation	Km from mouth	Latitude	Longitude
BL8	EFK 20.27	36.009790	-84.274850
EP BL-35	EFK 19.32	36.005080	-84.280059
EP BL-43	EFK 19.07	36.004230	-84.282660
EP BL-45	EFK 19.02	36.003880	-84.283000
EP EFK-13.8	EFK 14.56	35.992720	-84.315010
EP EFK 15.7 up SCB	EFK 16.41	35.996614	-84.303500
EP EFK-18.2-SCB	EFK 19.34	36.005400	-84.280583
EP EFK-22.5	EFK 23.59	36.000660	-84.245269
EP EFK-5.4up (SCB)	EFK 5.59	35.966276	-84.358567

2.8 Erosion Pin Experiment

Erosion pins are widely used for measurement of erosion. A previous experiment by Watson et al. (2016) used the erosion pins at different sites on the EFPC, including the selected sites for this experiment. Their method consisted of driving narrow diameter metal rods (0.635cm diameter x 60-90 cm long) into the stream bank, flush with the surface. These were monitored over time, measuring the length of exposure or burial of the pins. Volume estimates from this technique were obtained by combining pin data with reach length and bank height (Peterson et al., 2014). Then to generate values of the mass of soil eroded, bulk density was assumed to be 1.2 g/cm^3 (Hsieh et al., 2009). For this experiment, I continued to use the erosion pins that were still installed; these were monitored after significant rain events (August, October, and January).

Table 2 indicates the position of the erosion pins on the surface of the streambank and the material for the rod. Using the ground surface as a reference, they were placed near the top (T), middle (M), and bottom (B) of the bank height. The numbers following the top, middle, and bottom layer, indicate the depth from the top of the bank at which the pins were placed. As mentioned in the previous section, erosion pin measurements were taken simultaneously with the scans. In the case of the erosion pins, volume estimates were obtained by combining reach length and bank height in combination with the measured exposure (erosion) or depth of burial (deposition). The mass of soil eroded or deposited at each site was obtained after measuring the bulk density for each location. Eventually, the data were compared to the TLS data to see how the technologies differ.

Due to the different pin locations within a bank surface, the final data is normalized so that each pin measurement becomes more representative of the surface erosion. This normalization was made by doing a weighted average of the measurements. It is calculated by creating a ratio between the actual coverage of each pin with the total height of the bank. Then this ratio is multiplied by the corresponding pin measurement. For example, if a 100 cm bank had erosion pins at 25, 50, and 75 cm depth, the coverage area for the first top pin would be 25 plus half the distance between the first and second pin. In this case, the coverage area for the first pin is 37.5 cm, then to obtain the ratio, we divide by the total height of the bank and obtain a ratio of 0.375. The same process is then performed for every pin within each site, and after multiplying each ratio by the pin measurement, the weighted average is obtained. Finally, to make measurements among techniques comparable, the same surface area provided by the

software (the erosion pins were in this area) was used. Then the volume is obtained by multiplying the weighted average of each location by the surface area (TRW area).

Table 2: Erosion pin sites along EFPC and distance from the streambank surface

Site ID	Erosion Pin Depth Location
EFK 23.59	Fiberglass: T 30cm, M 60cm, B 100 cm Metal: T 50cm, B 110cm
EFK 20.27	Metal: T 40cm, M 75cm, B 100cm
EFK 19.34	Fiberglass: T 25cm, M 85cm, B 140cm
EFK 19.32	Fiberglass: T 10cm, M 30cm, B 100cm
EFK 19.07	Fiberglass: T 20cm, M 40cm, B 100cm
EFK 19.02	Fiberglass: T 30cm, M 60cm, B 100cm
EFK 16.41	Metal: T 40cm, B 80cm
EFK 14.56	Fiberglass: T 80cm, B 120 cm
EFK 5.59	Metal: T 40cm, B 80 cm Fiberglass: T 40cm, B 80 cm

Chapter III: Experimental Results

3.1 Block Test

The block experiment test served as a precursor for understanding how the TLS works before the field measurements. As mentioned before, this was a very controlled test on which the dimensions of the material removed were accurately known. I wanted to estimate the volume of material removed from the brick wall in this experiment. I trimmed and processed the reference point cloud (full block wall) and the altered point cloud (different configuration) using TRW, as seen in Figure 20. The software also provided a registration option by identifying matching points between the two images, in this case, the targets. Figure 21 shows the full brick wall (top left) and once brick removed (top right) and the resulting single image at the bottom.

After generating the combined image, I obtained a volume value using the volume tool in TRW. This number represents the volume difference between the two different images, e.g., Figure 21 shows a red rectangle representing the missing space from removing a single brick. The same process was performed for the other configurations (Figure 22, Figure 23, and Figure 24), and the measured volume was compared with the dimensions of the bricks removed to evaluate the accuracy of the TRW volume calculation tool.

Table 3: Erosion and deposition simulation for the block test. summarizes the results from this experiment. The first row labeled 'Simulation of Erosion' represents blocks removed from the structure (they simulate soil removed from the surface of a creek bank). The second row labeled 'Simulation of Erosion and Deposition' represents blocks removed from the surface and placed in front of the structure. This configuration was intended to represent soil from a streambank surface that falls from the top of the bank and settles in the lower section of the bank. The different scenarios tested are described in the column labeled 'Configuration' (it tells us how many blocks were removed and repositioned within the structure). As mentioned in previous sections, all measurements are based on a reference. In this case, the 'Complete Block Wall' was used as the reference to calculate all volumes. Starting from this unaltered reference and using TRW, I obtained the first volume of the whole block wall (TRW volume column). Then volumes from the different configurations were measured by comparing the reference scan and the new configuration. Since the reference scan was altered each time, TRW provided new volumes each

time. The column labeled 'Volume Difference' shows the difference in volume between the reference and the new configuration.

The 'Expected Volume' in Table 3 indicates the actual volume difference expected between the reference and the new configuration based on manual measurements of the blocks. In other words, the volume of the whole structure is known and based on the volume of a single block, 15321 cm^3 (126 cm * 126 cm* 258 cm). Therefore if one block was removed from the initial setup, the volume of this new configuration had to be less. Subtracting the new configuration volume obtained from TRW from the volume of the entire wall gives us an experimental value to compare with the actual dimensions of a block. The last column shows the percentage of error between the experimental values and the real measurements.

3.2 Control Site

The next experiment served as a proof of principle in a more realistic environment. In this field test, we were able to work with a scenario that includes variables such as the irregularity on the soil surface. In this scenario (and the real sites), a bulk density test was performed along with volume comparisons.

3.2.1 Control Site Bulk Density, Volume, and Mass Calculations

Following the procedure previously explained in sections 2.5.2.3-2.6, bulk density measurements on this control site were completed. The TRW volume was calculated following the same method described in the block test. Using the unaltered surface of the bank as a reference, I combined it with the first, second, and third layer removed individually. Figure 25 shows an example of the reference plane (red) and the first layer removed (green). Since I removed soil from the surface, the TRW volume corresponds to the volume difference between both images (in this case, equal to the soil removed).

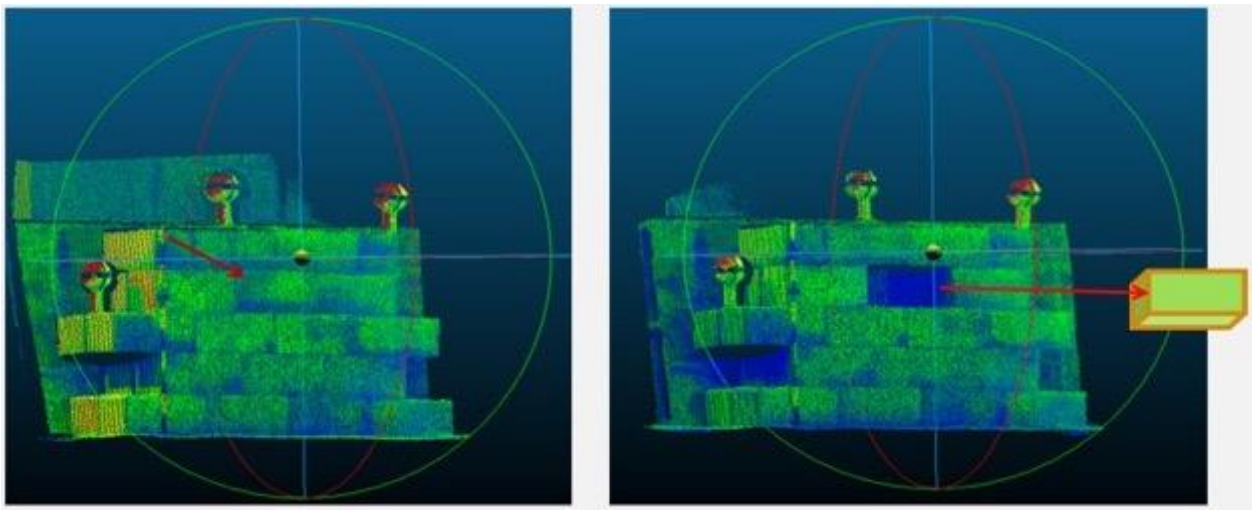

Figure 20: Full block wall (left) and new configuration example: one block removed (right).

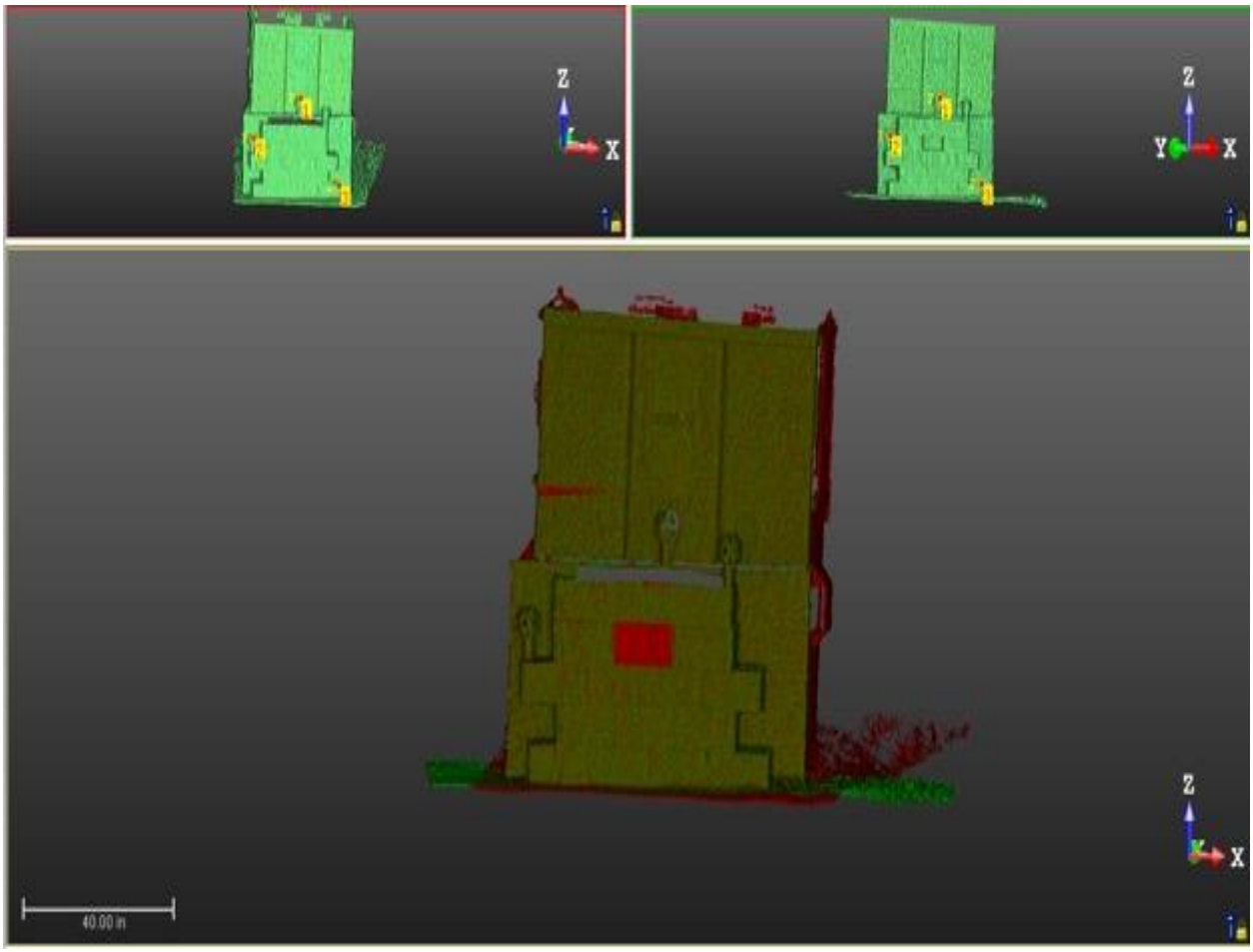

Figure 21: Registration between a point cloud and a reference.

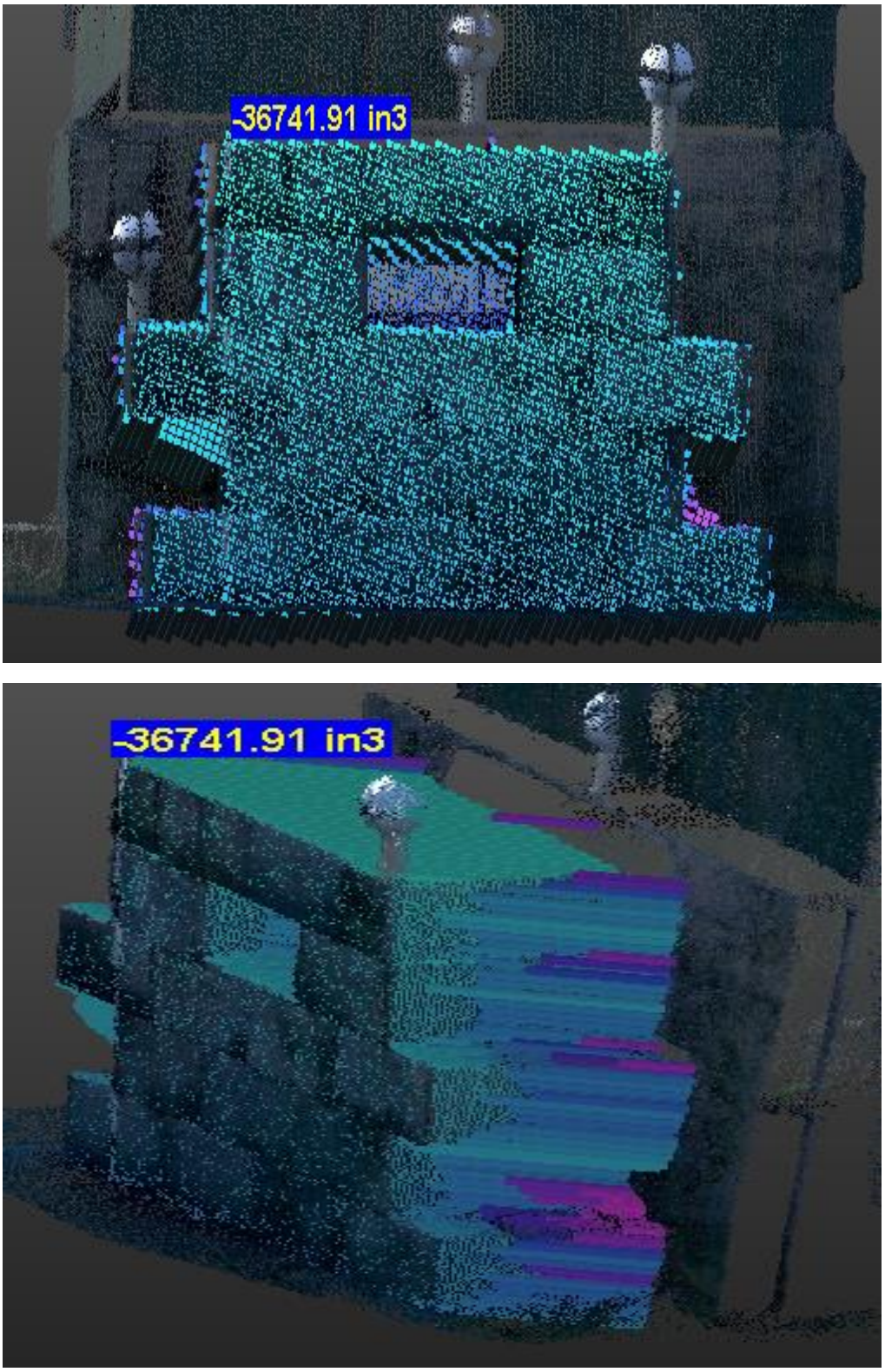

Figure 22: One block removed (image processed with TRW)

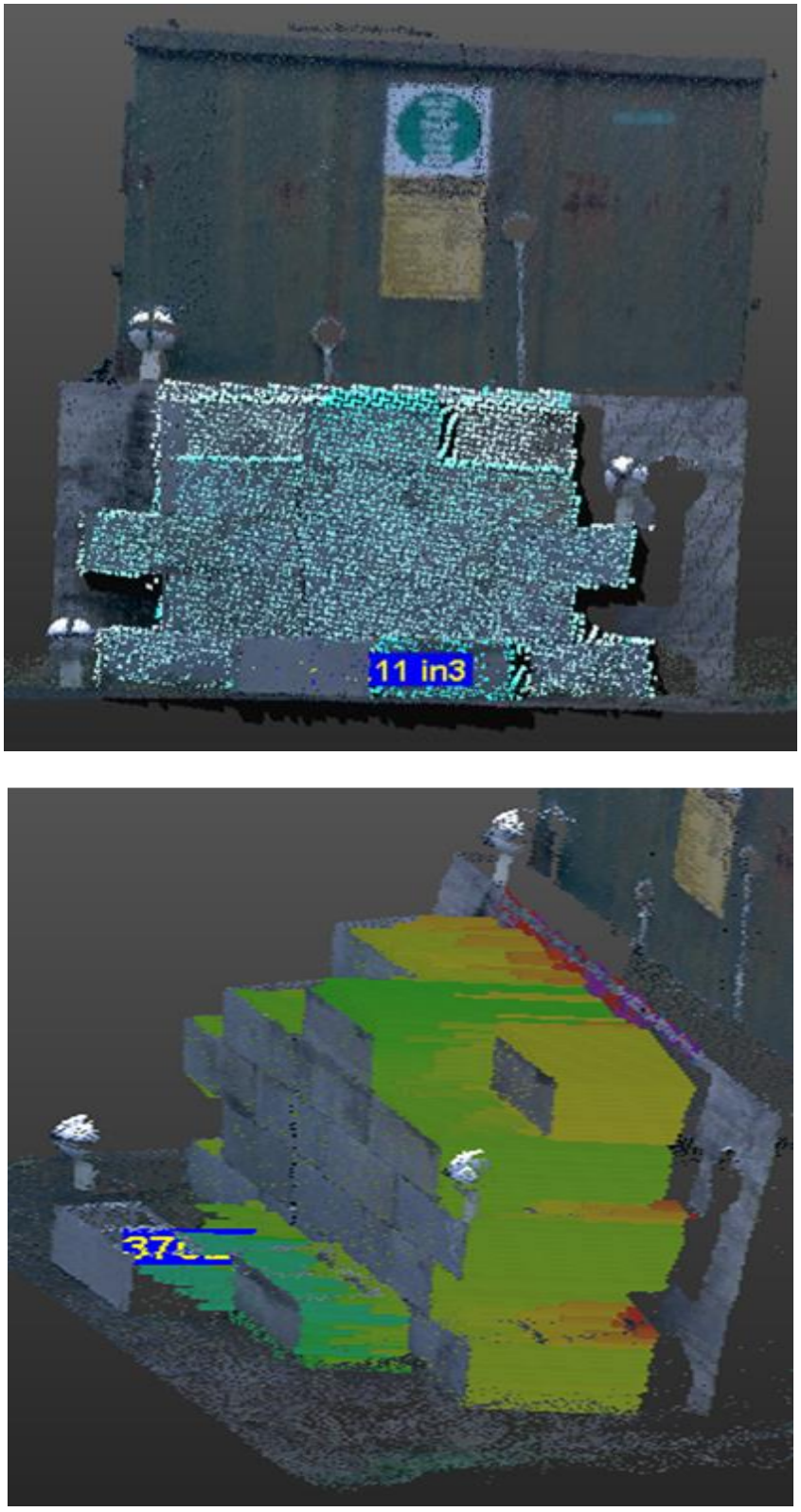

Figure 23: Two blocks removed and placed in front of the brick wall.

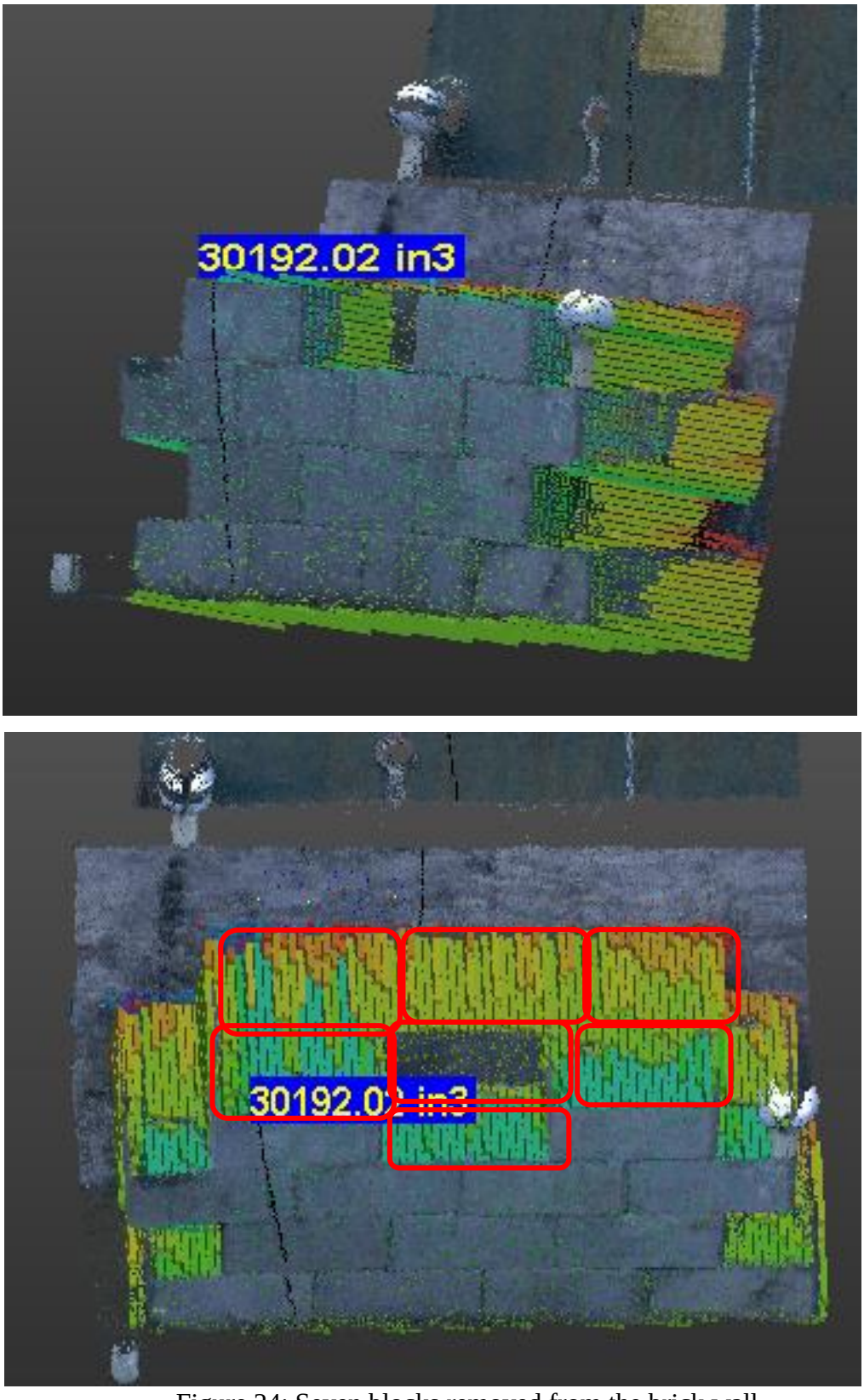

Figure 24: Seven blocks removed from the brick wall.

Table 3: Erosion and deposition simulation for the block test.

	Configuration:	TRW Volume (cm^3)	Volume Difference (cm^3)	Expected Volume (cm^3)	% Error
Simulation of Erosion	Complete Block Wall	614600	0.00	0.00	0.00
	1 Block removed	602100	12500	15350	18.60
	7 Blocks removed	494800	119800	10750	11.50
Simulation of Erosion and Deposition	2 Blocks removed and placed in front of the wall	6145000	-404.4 0.00	0.00	2.36 0.00

The results summarized in

Table 4 present the mass of the soil weighed by hand and provided by the software. Since more portion of the surface area was disturbed as the sections were added, it was expected to have a proportional increment of the error as the surface was disturbed. The average error in mass for all of the columns was around 23%. Two trends were observed, starting with the bulk density; although values were not too different, the bulk density within each column varied slightly. Nonetheless, the bulk density values within the 15 samples of each column were almost identical. The second trend observed was that, apart from one of the soil masses, all the weighted values were higher than those given by the software. This pattern was expected due to the uniformity of the soil, the presence of rock and other debris that might alter the results. Table 5 compares volumes provided by TRW as well as those expected from the dimensions of the sections. The error presented in this last table average 22.9% and as seen before, errors incremented as the surface was being disturbed.

3.3 Experimental Sites in EFPC

The next set of tables and graphs summarize the bulk density measurements, the volumes of released soil into the EFPC waters (using both techniques), and the Hg concentrations at each site using historical data.

3.3.1 Site Bulk Density

The average bulk density in

Table *6* indicates the average among these samples per site. Values ranged from 1.28 to 1.74 g/cm³ with an average standard deviation of 0.18 and a total number of samples of 10 per site. These values were obtained by dividing the dimensions of each core with the dry weights for each sample. In general, values of bulk density average 1.49 g/cm³**,** when compared to a bulk

density of 1.23 g/cm³ obtained during a soil survey across 20 sites along the EFPC by Dickson et al. (2015), the difference is about 19.5%, which is expected not only because they were not performed on the same sites but because of soil heterogeneity.

Table 4: Comparison between actual volume and software volume for the control site experiment. Note: The average bulk density column represents the average between the five samples taken per section, and the mass of soil removed is based on TRW results.

Section	Average bulk density per section (g/cm^3)	TRW Volume (cm^3)	Mass of Soil Removed (TRW), (kg)	Mass of Soil Weighted (kg)	% Error
1A	0.87	7794	6.76	8.16	17.2
1B	0.81	5418	4.39	3.63	21.0
1C	0.87	5854	5.07	7.08	28.4
2A	1.04	13680	14.2	18.6	23.9
2B	0.95	8963	8.47	9.62	11.9
2C	0.92	11030	10.2	13.9	26.6
3A	1.22	16220	19.8	31.8	37.7
3B	1.18	13300	15.8	18.0	12.3
3C	1.14	14420	16.4	25.8	36.3

Table 5: Control site theoretical and TRW volumes per section.

Section	Theoretical Volume (cm^3)	TRW Volume (cm^3)	% Error
1A	7079	7794	10.1
1B	7079	5418	23.5
1C	7079	5854	17.3
2A	14160	13680	3.39
2B	14160	8963	36.7
2C	14160	11030	22.1
3A	21238	16220	23.6
3B	2128	13330	37.4
3C	2128	14420	32.1

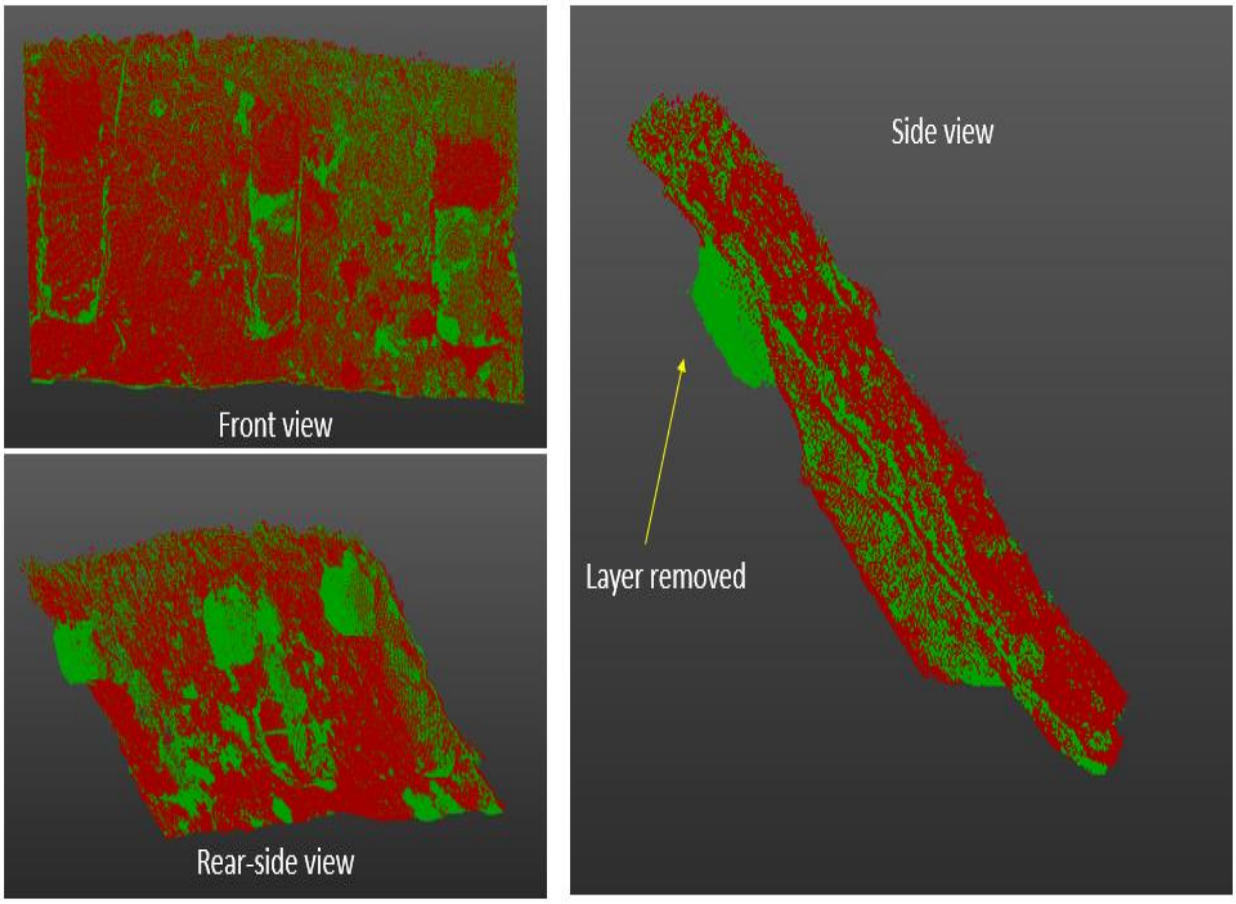

Figure 25: Superimposed point clouds of undisturbed soil surface (red) and the soil surface after removing the first soil layer (green) at the control site.

Table 6: Soil bulk densities at the EFPC field sites

Site	Average Bulk Density(g/cm^3)	Standard Deviation
EFK 23.59	1.60	0.22
EFK 20.27	1.36	0.20
EFK 19.34	1.53	0.13
EFK 19.32	1.44	0.15
EFK 19.07	1.28	0.27
EFK 19.02	1.42	0.19
EFK 16.41	1.57	0.11
EFK 14.56	1.74	0.12
EFK 5.59	1.50	0.20

3.3.2 Soil Volume and Mass Calculations

Starting with the TRW software volume calculations,

Table 7 summarizes the amount of soil introduced into the water per site. It is important to note that these soil values were obtained from a selected surface area that does not include the entire surface of the creek bank. Erosion volumes were obtained by subtracting the erosion from the deposition, which represents the net soil loss into the creek.

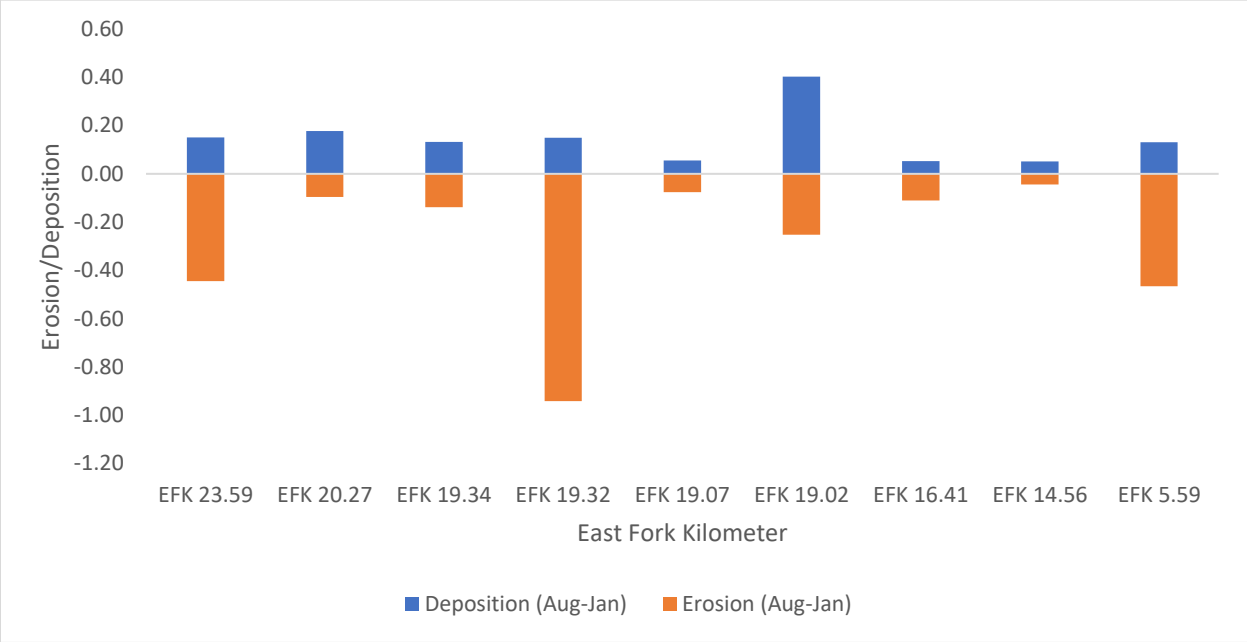

Figure 26 provides a visual aid between the erosion and deposition occurring per site. Despite deposition being overall predominant, there was a pattern observed for erosion. Three particular sites (EFK 23.59, 19.34, and 5.59) had the greatest amount of erosion (2.9, 6.3, and 3.5 times greater than deposition, respectively); what is consistent about them is that those are the three tallest creek banks, and both had either vegetation or visible surface roots during hot months. To facilitate calculations, sites where a net deposition was observed (deposition greater than

erosion) were marked as zero. This adjustment was made since we cannot quantify how much of the deposited soil came from the actual erosion and how much came from other sources such as stream sediment.

The volumes obtained from the erosion pins were based on the weighted average between the different pins located on the bank surfaces. Figure 27 summarizes the erosion and deposition from all nine sites, and Table 8**Error! Reference source not found.** provides the difference between these measurements. Once again, a zero was assigned for those sites where deposition predominates. Although some patterns can be observed in most upstream sites, the erosion pins do not match the erosion measured for the EFK 19.32 (the site with the highest erosion). It also differs drastically when measuring deposition. As shown in the figure mentioned above, only erosion is clearly visible with these techniques. The site where data seem to match the most is at the most upper streambank. This consistency is because erosion in this site was significant, and most of the lower portion of the bank was completely washed out, leaving the pins extremely exposed, as seen in Appendix A1.

One outcome of this experiment is the total Hg introduced into the EFPC waters. Using historical Hg concentration per site (Dickson et al., 2018), I obtained the total mass of Hg released into the creek, as shown in

Table 9.

Sites	Hg total (mg/kg)	Mass of soil into the creek (kg)		Mass of Hg into the creek (kg)		Ratio (Erosion Pin/TLS)
		TLS	Erosion Pins	TLS	Erosion Pins	
EFK 23.59	1070	464	11070	0.49599	11.844	23.9
EFK 20.27	35.9	0.00	394.4	0.00000	0.01417	-
EFK 19.34	763	8.48	2048	0.00648	1.56370	241
EFK 19.32	739	1140	169.9	0.84279	0.12553	0.15
EFK 19.07	429	25.7	0.00	0.01095	0.00000	0.00
EFK 19.02	582	0.00	150.0	0.00000	0.08731	-
EFK 16.41	9.05	88.9	4505	0.00081	0.04079	50.7
EFK 14.56	10.9	0.00	0.00	0.00000	0.00000	-
EFK 5.597	8.10	504	746.7	0.00408	0.00605	1.48

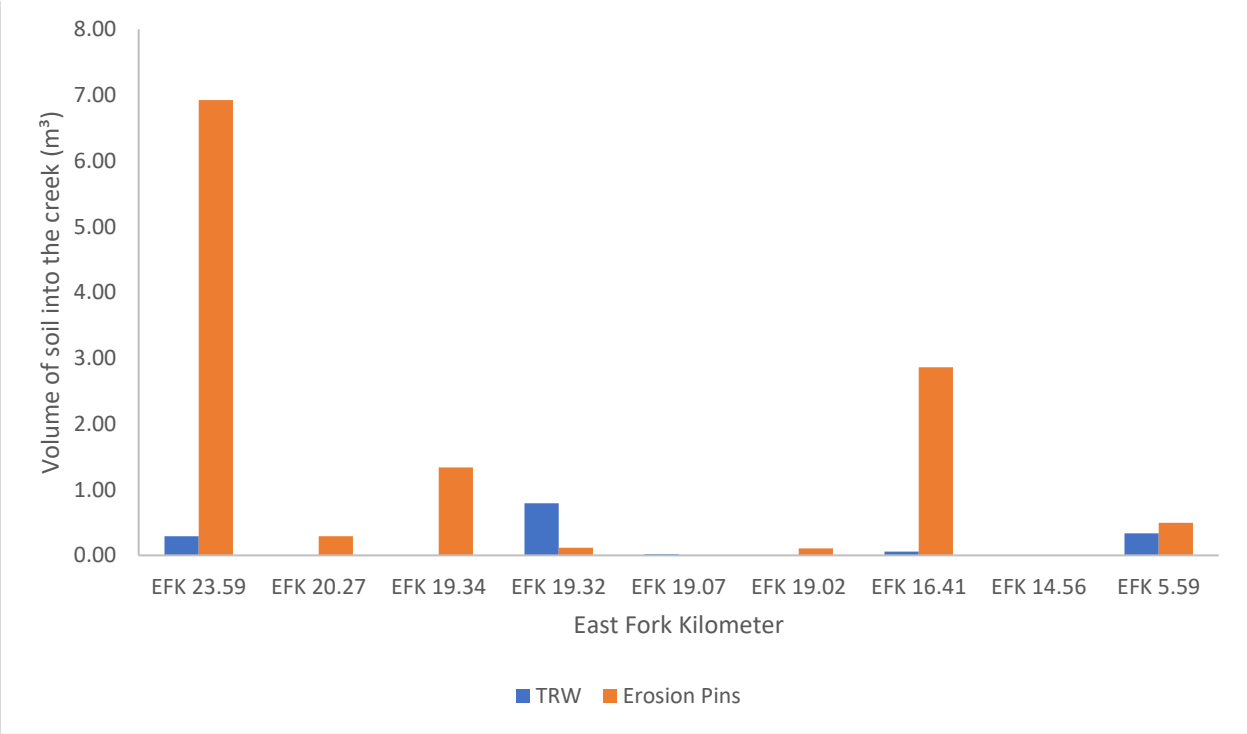

Figure 28 and

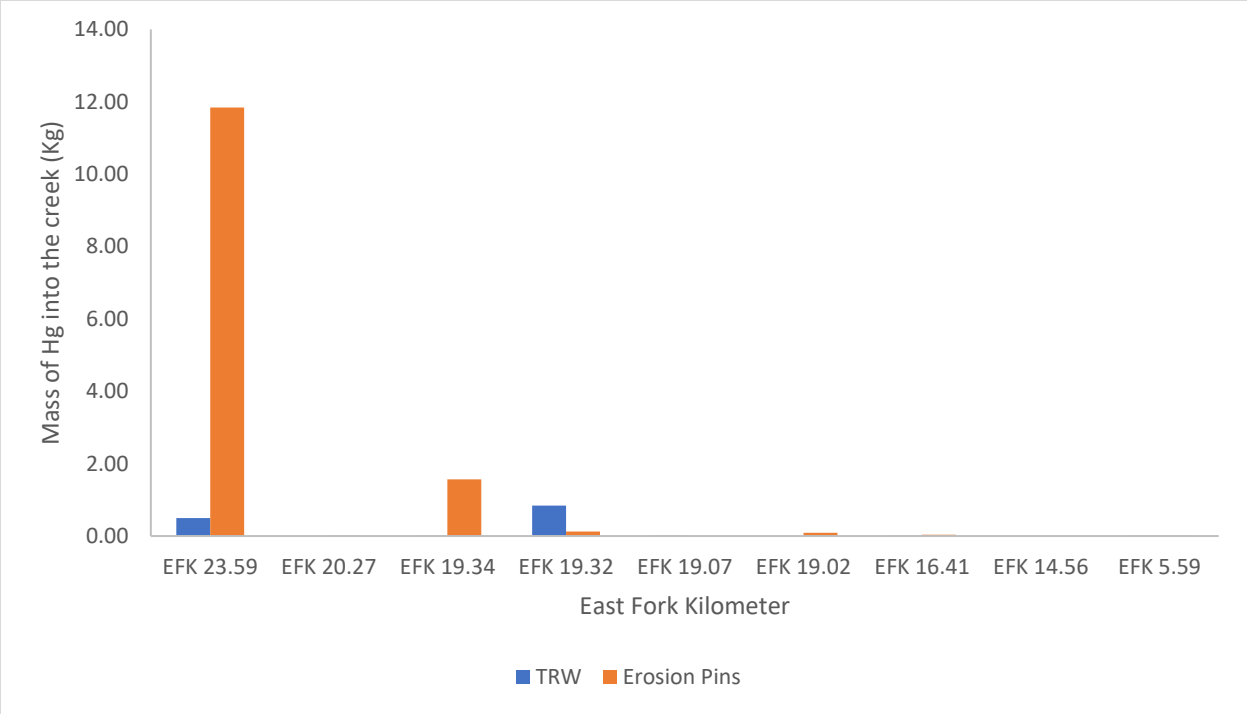

Figure 29 summarize the data for both techniques, and clear variability is observed among techniques. First and as expected, the site with greater erosion was the tallest streambank (EFK 19.32) with soil input into the waters but only for the TLS. Second, a similar pattern was observed on site EFK 23.59, where the TLS showed that it was the third biggest contributor of soil into the creek and the greatest contributor according to the erosion pins. In the case of EFK 5.59, both technologies provided similar data (TRW: 507.97 Kg; Erosion Pins: 743.68 Kg); this was the most consistent site regarding the amount of soil released into the EFPC. Variations in these techniques are very related to the spatial variability associated with the erosion pins. Since the erosion pins only account for what is around the rod's tip, there is too much of the surface area the pin does not consider, therefore high variability in the results.

Table 7: Soil erosion volumes for EFPC field sites obtained from TLS.

Site	TLS Volume, soil loss (m^3)	TLS Bank Surface Area (m^2)
EFK 23.59	0.29	10.3
EFK 20.27	0.00	4.62
EFK 19.34	0.01	6.73
EFK 19.32	0.79	7.10
EFK 19.07	0.02	7.92
EFK 19.02	0.00	7.20
EFK 16.41	0.06	5.65
EFK 14.56	0.00	3.93
EFK 5.59	0.33	14.2

Table 8: Soil erosion volumes for EFPC field sites obtained using the erosion pin method.

Site

	Weighted Average Erosion (m)	TLS Bank Surface Area (m^2)	Erosion Pin Volume of soil loss (m^3)
EFK 23.59	0.67361	10.28	6.92
EFK 20.27	0.06297	4.62	0.29
EFK 19.34	0.19886	6.73	1.34
EFK 19.32	0.01661	7.10	0.12
EFK 19.07	0.00000	7.92	0.00
EFK 19.02	0.01467	7.20	0.11
EFK 16.41	0.50639	5.65	2.86
EFK 14.56	0.00000	3.93	0.00
EFK 5.59	0.03499	14.18	0.50

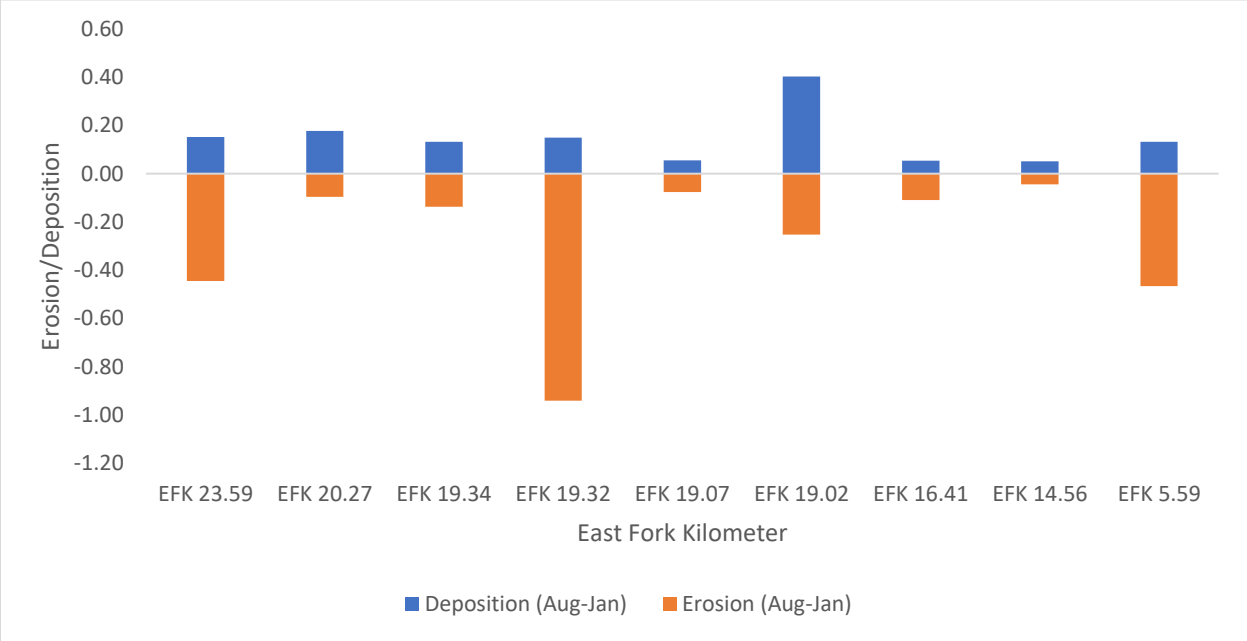

Figure 26: TRW-Volume of soil associated with deposition and erosion from the experimental sites (Aug 2020- Jan 2021).

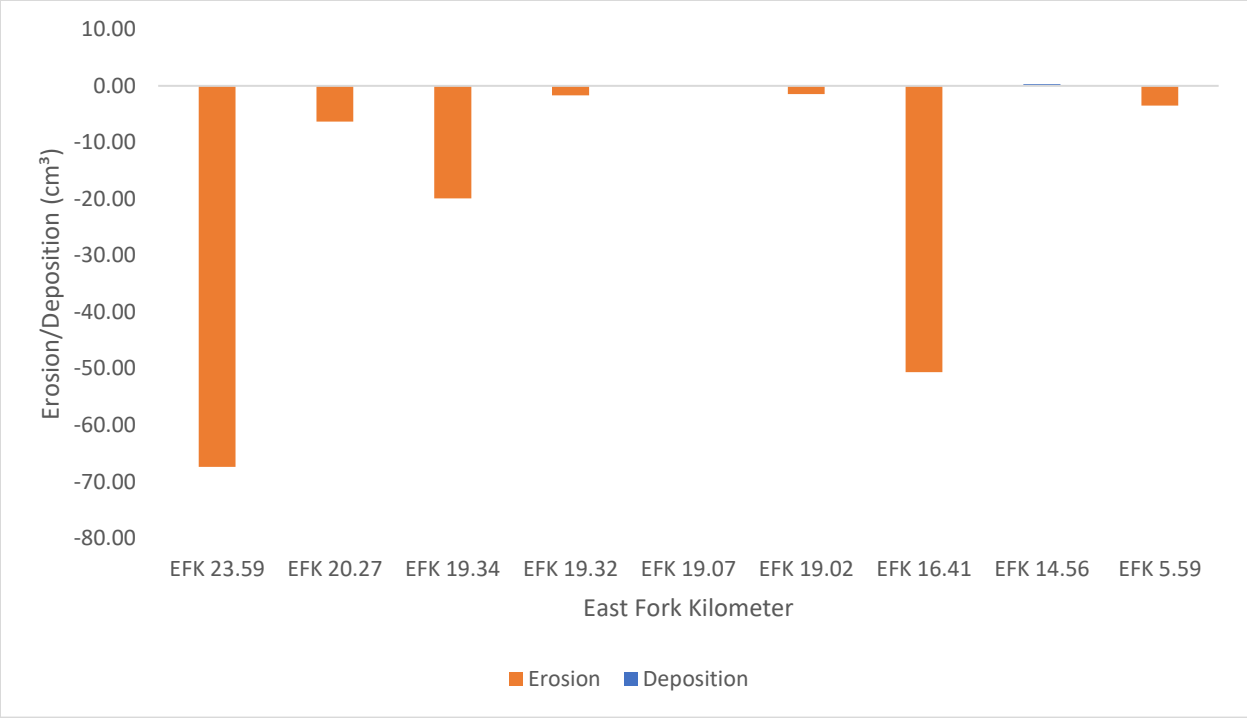

Figure 27: Erosion Pins-Volume of soil associated with deposition and erosion from experimental sites (Aug 2020- Jan 2021).

Table 9: Comparison of soil and Hg loss into EFPC at each site using the TLS and erosion pin techniques.

Sites	Hg total (mg/kg)	Mass of soil into the creek (kg)		Mass of Hg into the creek (kg)		Ratio (Erosion Pin/TLS)
		TLS	Erosion Pins	TLS	Erosion Pins	
EFK 23.59	1070	464	11070	0.49599	11.844	23.9
EFK 20.27	35.9	0.00	394.4	0.00000	0.01417	-
EFK 19.34	763	8.48	2048	0.00648	1.56370	241
EFK 19.32	739	1140	169.9	0.84279	0.12553	0.15
EFK 19.07	429	25.7	0.00	0.01095	0.00000	0.00
EFK 19.02	582	0.00	150.0	0.00000	0.08731	-
EFK 16.41	9.05	88.9	4505	0.00081	0.04079	50.7
EFK 14.56	10.9	0.00	0.00	0.00000	0.00000	-
EFK 5.597	8.10	504	746.7	0.00408	0.00605	1.48

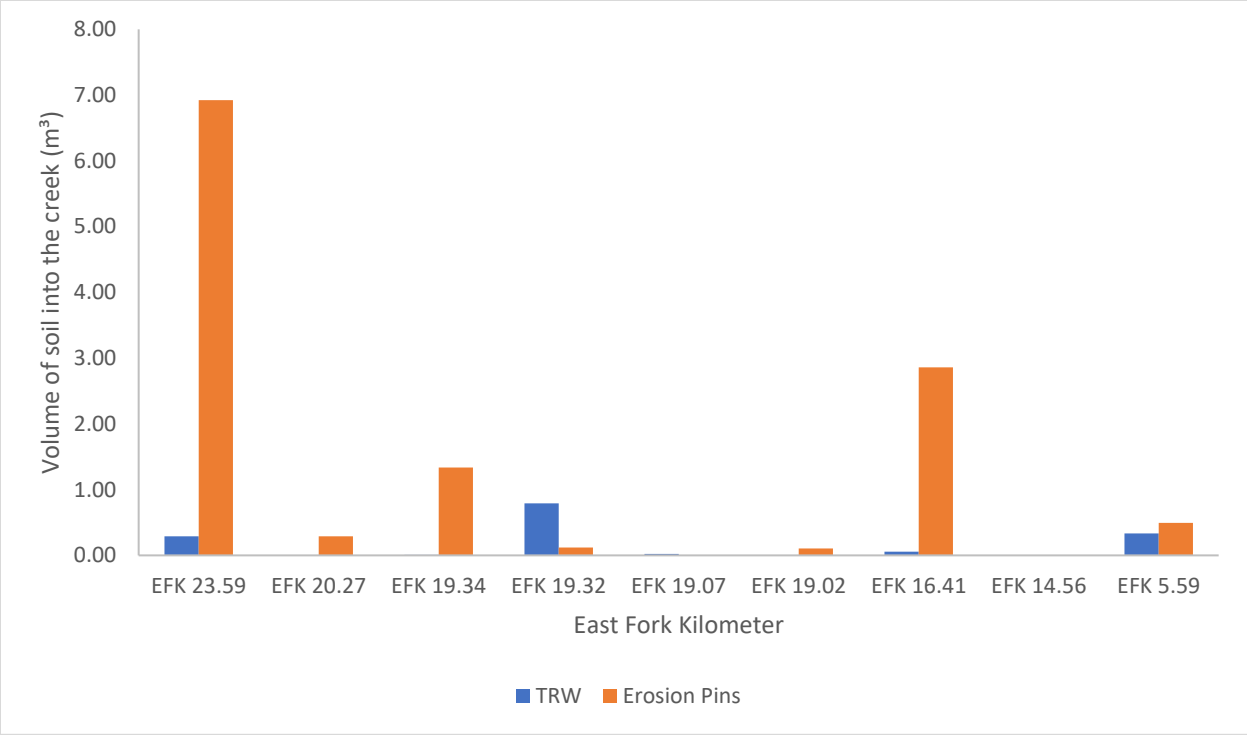

Figure 28: Volume of soil introduced into the EFPC waters per location.

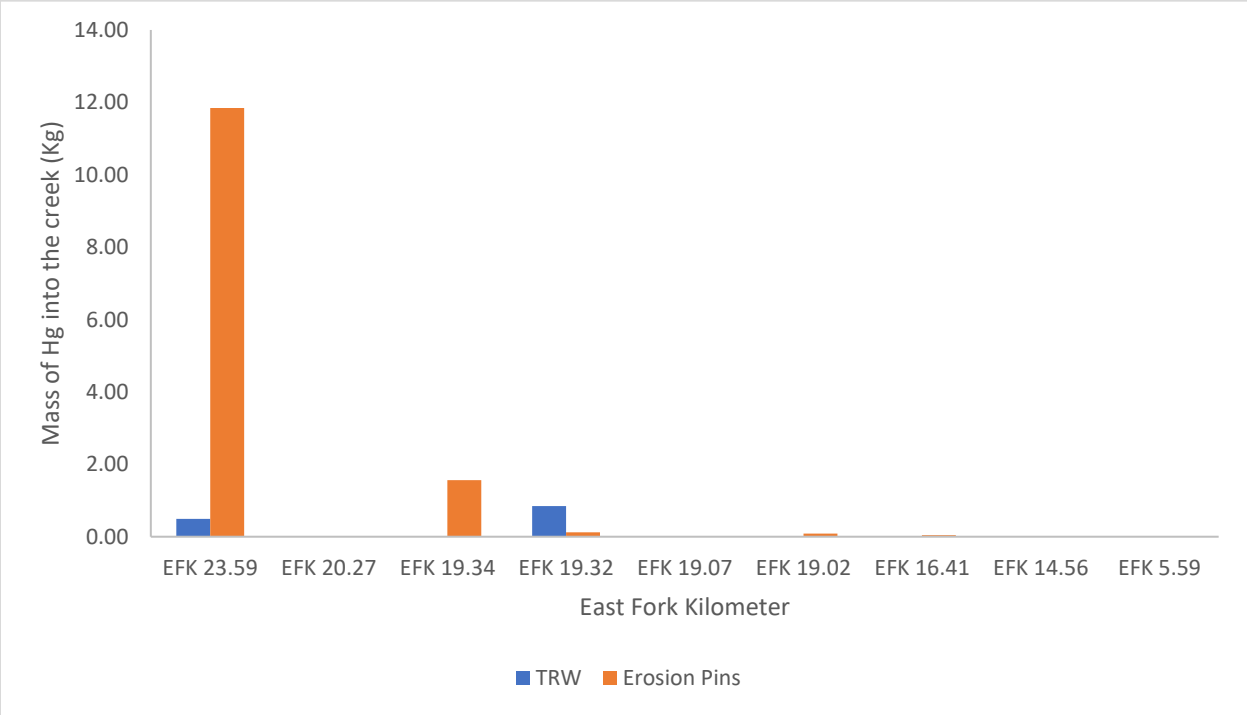

Figure 29: Mass of Hg introduced into the EFPC water per location.

Chapter IV: Discussion

4.1 Site Volume and Mass Measurements

TLS data provided a more reliable representation of a streambank morphology compared to the erosion pin data. To test how much both technologies differ from one another, sites selected for this experiment ranged between low and high erosion, allowing me to compare techniques in different scenarios. According to many studies, there are limitations associated with the erosion pin measurements of streambank erosion, the most important being its lack of accuracy for measuring erosion across the whole surface (Haigh, 1977; Thorne, 1981; Lawler, 1993; Kumar, 2013; Watson et al., 2016). These limitations suggest that the TLS will provide more representative data than the erosion pins. The TLS can obtain millions of points (or measurements) from a streambank, and it can detect small and large changes in the surface and provide more representative and realistic data. The drastic difference in the capacity of the two techniques to measure streambank retreat has been compared in another study, and on average, the reported difference was 787%, with values ranging from 22% to 30003% of soil eroded from a streambank surface (Myers et al., 2009). The same pattern was observed on this research project, where the erosion pins overestimated an average of 64 times higher values of soil and Hg into the stream due to erosion.

Although the experiment was limited to 146 days (August 13, 2020 – January 6, 2021, normal rainfall events), I was still able to see some evident signs of erosions among sites. Here, it is important to remember that the volume of soil into the creek represents the difference between deposition and erosion. As seen in Table 9, there are some cases where a zero was placed for the volume of soil into the creek. They represent those sites where the deposition measured with the TLS was greater than the erosion. Since we cannot account for how much of the deposition comes from other sources, a zero was assigned to indicate there was no net erosion.

One of the scenarios was the erosion at the uppermost bank, EFK 23.59 (erosion pin exposition image in Appendix A1), where a significant portion of the bottom 30 to 40 cm was completely removed between October and January. When analyzing the data from the erosion pin, it was evident that the bottom measurements (below 100 cm depth) will have a huge impact on the overall erosion, regardless of the weighted average performed. This is one of the biggest drawbacks of the erosion pins; since this is a point-specific technique, the erosion obtained may not be representative of the actual scale of erosion. The difference between the results obtained from both methods at this site indicates that the erosion pin measurements overestimated erosion, resulting in a volume of Hg and soil into the creek 24 times higher than the respective volumes obtained from TLS.

Another scenario was the lowermost site, EFK 5.59, which showed the lowest deviation (not accounting for the zero where deposition predominates) between the two techniques (erosion pin/TLS volume ratio of 1.5). Although this number varies significantly from the average soil loss into the creek, it is important to mention that vegetation growth in this site was very high. Although vegetation is not a problem for the erosion pins, it can overestimate surface erosion or deposition with the TLS. In other words, when the laser from the instrument hits an obstruction such as vegetation, the TLS interprets this as the streambank surface. This error was only found on this site, and although it was accounted for by manually removing mistaken points using TRW and by taking scans from different angles to see the true bank surface, there was still a large volume of soil eroded into the creek measured with the TLS. When looking through the data, there is a significant difference between the first scan (August), where vegetation was high, and the last scan (January), where there was almost no vegetation on the streambank surface. This fact led us to conclude that the small ratio of the difference between the pins and the TLS is related to the overestimate given by the TLS due to vegetation.

Site EFK 19.32 appeared to exhibit sheet erosion on its surface. This type of erosion takes place when soil particles are carried evenly over the soil surface. Once again, since erosion pins are a point-specific technique, it was evident that numbers would differ drastically from those obtained using the TLS technique (241 times greater). When sheet erosion happens near the erosion pin, the final value of erosion or deposition for this technique will be very high or very

low and not representative of the real scenario. For instance, when a small number of particles move from the surface and get stuck near the pin, the overall result will be an overestimate of deposition, and in the opposite case, when a small portion of soil moves from near the pin, it will result on an overestimate of erosion. The TLS measurement can account for these types of changes (particles displacing within the surface), and even if the soil is moved within the surface of the bank, it will not be considered as soil deposited into the creek. In other words, streambanks with sheet erosion where the soil moves and stays within the surface will not be accounted for as soil loss into the creek using either technique.

Due to the modification of the data previously explained (zero where the deposition was greater than erosion), there are sites where the difference ratio between techniques can not be calculated. That is the case for sites EFK 20.27 and EFK 19.02, where a zero was assigned for the volume of soil into the creek. Since the ratio is calculated by dividing the volume (of soil or Hg) given by the erosion pins divided by the volume obtained with the TLS, when the TLS was zero, the ratio could not be calculated mathematically (division by zero). On the other hand, the ratio for EFK 14.56 was not determined since both techniques agreed that the deposition was greater than erosion; therefore, no soil appeared to be introduced into the creek regardless of technique. Here is necessary to remember, this does not mean that there was no soil introduced into the creek. These results indicate that we cannot account for how much of the erosion was deposited and how much was released into the EFPC waters. In other words, for any amount of deposition greater than erosion, we can not measure how much of that deposition comes directly from erosion and how much from other sources. Finally, the EFK 19.07 was equal to zero since although the TLS measured soil erosion into the creek, the erosion pin had a zero for the soil into the creek. Therefore, the difference between them was calculated as zero even though there is an actual difference between the estimates from the two techniques.

This study showed that TLS technology proved to be more effective and sensitive to measure soil erosion, especially deposition. Although the erosion pins showed, in some cases, similar patterns, they cannot measure deposition accurately or detect changes across a bigger surface area. When comparing the usability of the techniques, the application of erosion pins is the most cost-effective technique, and it can be monitored easily. Some of the problems with this

technique are that the erosion pins disturbed the surface area; they can be completely washed out in extreme erosion events. The most significant problem with the erosion pins is their poor spatial variability, meaning that their results are extremely generalized and based only on a point within the streambank surface and not the complete surface area. The TLS, in contrast, had the capability of measuring changes in the bank surface with high resolution and sub-centimeter error. This technology also allows us to develop advanced 3D models, it is easy to use in the field, and it does not require much fieldwork time. Some of the drawbacks include the high amount of data that needs to be processed, it is expensive, it requires some software training for modeling data, and in places with high vegetation, the TLS can overestimate changes in soil (despite using tools to remove some of the vegetation). This last problem can be treated if scans are taken for longer periods during cold seasons or by picking sites with low vegetation. For general assessments and rough estimates, the erosion pins still represent a useful and economical tool used in combination with TLS technologies for more accurate data.

Conclusions

Streambank erosion processes represent a significant problem on streams across the United States, especially those where the transport of contaminants represents an important threat to human or animal life. This project objective was to compare a traditional technology used to measure streambank erosion with a relatively new technology. The first one, the erosion pins, is a very cheap technology for easy monitoring that proved to measure erosion better than deposition in this experiment. Since initially, the erosion pin is fully inserted on the streambank surface, in some cases, it provides stability to the soil around it. In addition, deposition in most cases is seen in the lower section of the bank, and since multiple pins are used across the surface, the values of the other pins are greater than that single pin in the bottom section.

In contrast, the TLS technology, although it was very expensive and tedious to process a huge amount of data, was able to measure streambank erosion at a sub-centimeter scale. It also provided high-quality 3D models, showing exactly where soil movement was happening on the surface of the bank through subaerial processes. One of its downsides was that although it can be resolved (by manually removing mistaken points or taking scans from different angles to have a better chance of covering the true streambank surface), interferences on the bank surface can overestimate erosion. Both technologies were able to measure soil introduced into the EFPC, but because of the spatial variability of the erosion pins, they overestimate an average of 64 times greater erosion than the TLS. When comparing the Hg inputs by each technology, the erosion pin again provided overestimations of this contaminant release into EFPC. This is something that needs to be taking into consideration when monitoring erosion. If the data needed are rough estimates or if the monitored site is mostly covered with vegetation, the erosion pins are a cheap and viable alternative. In case a survey for streambank remediation is needed, the best alternative is the TLS. Not only does this technology provides visual models that help us explain erosion processes, but it provides reliable values needed in a cost-dependent project such as streambank restoration.

References

Agriculture, U. S. D. A. (1999). "Soil Quality Test Kit Guide." *Bulk Density Test*, USDA.

ASTM (2019). "Standard Test Method for Measuring Bulk Density Values of Powders and Other Bulk Solids as a Function of Compressive Stress " *ASTM D6683-19*.

Ayers, P., and Wade, D. (2007). "Mapping Site-specific Stream Bank Erosion on the East Fork Poplar Creek." *University of Tennessee, Knoxville*, O. R. N. Laboratory, ed.

Bhan, A., and Sarkar, N. N. (2005). "Mercury in the environment: effect on health and reproduction." *Review of Environmental Health*, 20, 39-56.

Brooks, S., Eller, V., Dickson, J. O., Earles, J. K., Lowe, K. A., Mehlhorn, T. L., Olsen, T., DeRolph, C. R., Watson, D. B., Philips, D., and Peterson, M. J. (2017). "Mercury Content of Sediment in East Fork Poplar Creek: Current Assessment and Past Trends." O. R. N. Laboratory, ed. Oak Ridge, TN.

Brooks, S. C., and Southworth, G. R. (2011). "History of mercury use and environmental contamination at the Oak Ridge Y-12 Plant." *Environ Pollut*, 159(1), 219-228.

Connell, B., Ayers, P., Ludwig, A., and Parham, J. (2019). "Georeference Video Mapping to Classify Streambank Erosion Susceptibility " *Journal of Spatial Hydrology*, 15.

Di Natale, F., Lancia, A., Molino, A., Di Natale, M., Karatza, D., and Musmarra, D. (2006). "Capture of mercury ions by natural and industrial materials." *Journal of Hazardous Materials*, 132(2-3), 220-225.

Dickson, J., Mayes, M., Earles, J., Mehlhorn, T., Lowe, K., Peterson, M., and Pierce, E. (2017). "Soil Investigation of Lower East Fork Poplar Creek.", O. R. N. Laboratory, ed. Oak Ridge, TN.

Dickson, J. O., Mayes, M. A., Brooks, S. C., Mehlhorn, T. L., Lowe, K. A., Earles, J. K., Gonez-Rodriguez, L., Watson, D. B., and Peterson, M. J. (2019). "Source relationships between streambank soils and streambed sediments in a mercury-contaminated stream." *J Soil Sediment*, 19(4), 2007-2019.

E.L., R., O'Neal, M. A., and Pizzuto, J. E. (2009). "Quantifying bank erosion on the South River from 1937 to 2005, and its importance in assessing Hg contamination." Masters of Science in Geography, University of Delaware, Appl Geogr.

Gill, G. A., and Bruland, K. W. (1990). "Mercury Speciation in Surface Fresh-Water Systems in California and Other Areas." *Environ Sci Technol*, 24(9), 1392-1400.

Gilmour, C. C., Podar, M., Bullock, A. L., Graham, A. M., Brown, S. D., Somenahally, A. C., Johs, A., Hurt, R. A., Bailey, K. L., and Elias, D. A. (2013). "Mercury Methylation by Novel Microorganisms from New Environments." *Environ Sci Technol*, 47(20), 11810-11820.

Guzzi, G., and La Porta, C. A. M. (2008). "Molecular mechanisms triggered by mercury." *Toxicology*, 244(1), 1-12.

Guzzi, G., and La Porta, C. A. M. (2008). "Molecular mechanisms triggered by mercury." *Toxicology*, 244(1), 1-12.

Harada, M. (1995). "Minamata Disease - Methylmercury Poisoning in Japan Caused by Environmental-Pollution." *Crit Rev Toxicol*, 25(1), 1-24.

Hsieh, Y. P., Grant, K. T., and Bugna, G. C. (2009). "A field method for soil erosion measurements in agricultural and natural lands." *J Soil Water Conserv*, 64(6), 374-382.

Hunter, D., Bomford, R. R., and Russell, D. S. (1940). "Poisoning by Methyl Mercury Compounds." *Quarterly Journal of Medicine*, 33, 193-213.

Kiesel, J., Schmalz, B., and Fohrer, N. (2009). "SEPAL- a simple GIS-based tool to estimate sediment pathways in lowland catchments " *Advances in Geosciences*, 21, 23-32.

Kraepiel, A. M. L., Keller, K., Chin, H. B., Malcolm, E. G., and Morel, F. M. M. (2003). "Sources and variations of mercury in tuna." *Environ Sci Technol*, 37(24), 5551-5558.

Lawler, D. M. (1993). "The Measurement of River Bank Erosion and Lateral Channel Change - a Review." *Earth Surf Proc Land*, 18(9), 777-821.

McKenzie, N., Coughlan, K., and Cresswell, H. (2002). *Soil Physical Measurement and Interpretation for Land Evaluation*, Australia.

Mergler, D., Anderson, H. A., Chan, L. H. M., Mahaffey, K. R., Murray, M., Sakamoto, M., and Stern, A. H. (2007). "Methylmercury exposure and health effects in humans: A worldwide concern." *Ambio*, 36(1), 3-11.

Oken, E., and Bellinger, D. C. (2008). "Fish consumption, methylmercury and child neurodevelopment." *Curr Opin Pediatr*, 20(2), 178-183.

Parks, J. M., Johs, A., Podar, M., Bridou, R., Hurt, R. A., Smith, S. D., Tomanicek, S. J., Qian, Y., Brown, S. D., Brandt, C. C., Palumbo, A. V., Smith, J. C., Wall, J. D., Elias, D. A., and Liang, L. Y. (2013). "The Genetic Basis for Bacterial Mercury Methylation." *Science*, 339(6125), 1332-1335.

Podar, M., Gilmour, C. C., Brandt, C. C., Soren, A., Brown, S. D., Crable, B. R., Palumbo, A. V., Somenahally, A. C., and Elias, D. A. (2015). "Global prevalence and distribution of genes and microorganisms involved in mercury methylation." *Sci Adv*, 1(9).

Poulain, A. J., and Barkay, T. (2013). "Cracking the Mercury Methylation Code." *Science*, 339(6125), 1280-1281.

Resop, J. P., and Hession, W. C. (2010). "Terrestrial Laser Scanning for Monitoring Streambank Retreat: Comparison with Traditional Surveying Techniques." *J Hydraul Eng*, 136(10), 794-798.

Roe, A. (2003). "Fishing for Identity: Mercury Contamination and Fish Consumption Among Indigenous Groups in the United States Amy." *Sage Journals*, 23, 368-375.

Rosgen, D. L. (2001). "A Practical Method of Computing Streambank Erosion Rate." *The Seventh Federal Interagency Sedimentation Conference*, Wildland Hydrology, Inc., Reno, Nevada.

Rulot, F., Dewals, B. J., Erpicum, S., Archambeau, P., and Pirotton, M. (2012). "Modelling sediment transport over partially non-erodible bottoms." *Int J Numer Meth Fl*, 70(2), 186-199.

Sanfeliu, C., Sebastia, J., Cristofol, R., and Rodriguez-Farre, E. (2003). "Neurotoxicity of organomercurial compounds." *Neurotox Res*, 5(4), 283-+.

Seminove, A. (2018). "Minamata Disease—Review." *World Journal of Neuroscience*, 8.

Starr, R. (2018). "Maryland Trust Fund Geomorphic Monitoring " *Stream Habitat Assessment and Restoration Program U.S. Fish & Wildlife Service, Chesapeake Bay Field Office Coastal Program 46.*

Thorne, C. R. (1981). "Field Measurements of rates of bank erosion and bank material strength." *Erosion and Sediment Transport Measurement*, 10, 133.

Timothy, G. S. (2001). "Minamata: Pollution and the Struggle for Democracy in Postwar Japan.", H. U. A. Center, ed. Cambridge, 385.

Ullrich, S. M., Tanton, T. W., and Abdrashitova, S. A. (2001). "Mercury in the aquatic environment: A review of factors affecting methylation." *Crit Rev Env Sci Tec*, 31(3), 241-293.

Wallschlager, D., Desai, M. V. M., Spengler, M., and Wilken, R. D. (1998). "Mercury speciation in floodplain soils and sediments along a contaminated river transect." *J Environ Qual*, 27(5), 1034-1044.

Wallschlager, D., Desai, M. V. M., Spengler, M., Windmoller, C. C., and Wilken, R. D. (1998). "How humic substances dominate mercury geochemistry in contaminated floodplain soils and sediments." *J Environ Qual*, 27(5), 1044-1054.

Watson, D., Bevelhimer, M., Brandt, C., C., D., Brooks, S. C., Mayes, M., Olsen, T., Dickson, J., Peterson, M., and Ketelle, D. (2017). "Evaluation of lower East Fork Poplar Creek mercury sources - model update.", ORNL, ed.Oak Ridge, TN.

Watson, D., Brooks, S. C., Mathews, T., Bevelhimer, M., DeRolph, C., Brandt, C., Peterson, M., and Ketelle, D. (2016). "Evaluation of Lower East Fork Poplar Creek Mercury Sources. ", O. R. N. Laboratory, ed.Oak Ridge, TN.

Whiteacre, D. M. (2009). "Reviews of Environmental Contamination and Toxicology." *Springer, New York*.

Wolman, M. G. (1959). "Factors Influencing Erosion of a Cohesive River Bank." *Am J Sci*, 257(3), 2042-2216.

Zagar, D., Knap, A., Warwick, J. J., Rajar, R., Horvat, M., and Cetina, M. (2006). "Modelling of mercury transport and transformation processes in the Idrijca and Soca river system." *Sci Total Environ*, 368(1), 149-163.

Partnership, U. N. G. M. (2020). "Overarching frame-work: UNEP Global Mercury Partnership." *United Nations Environment Programme*, <www.unep.org/globalmercurypartnership>.

Programme, U. N. E. (2019). "Global Mercury Assessment 2018." *UN Environment*.

Riscassi, A., Miller, C., and Brooks, S. (2016). "Seasonal and Flow-Driven Dynamics of Particulate and Dissolved Mercury and Methylmercury in a Stream Impacted by an Industrial Mercury Source." *Environ Toxicol Chem*, 35(6), 1386-1400.

Appendix

A1. EFK 23.5993 (EP EFK 22.5, August 12, 2020/ January 6, 2021; behind dentist's office)

A2 EFK 20.2703 (BL 8, August 18, 2020; AMVET Area)

A3 EFK 19.3466
(BL 35, August 13, 2020/January 6, 2021; Brunners area, next to a water vein)

A4 EFK 19.3244
(EP EFK 18.2 SCB, August 13, 2020/ January 6, 202; closest to the bridge in Brunners)

A5 EFK 19.0723
(BL 43, August 4, 2020; coupon experiment bank)

A6 EFK 19.0258
(BL 45, August 13, 2020; downstream of mesh experiment)

A7 EFK 16.4127
(EP EFK 15.7 UP SCB, August 18, 2020/ January 6, 2021; behind the electric power plant)

A8 EFK 14.5630
(EP EFK 13.8, August 4, 2020; behind wastewater plant)

A9 EFK 5.5972
(EP EFK 5.4 Up SCB, August 4, 2020/ January 6, 2021; New Horizon)

B1 EFK 23.5993 Aug-Jan (note erosion/deposition images are inverse)

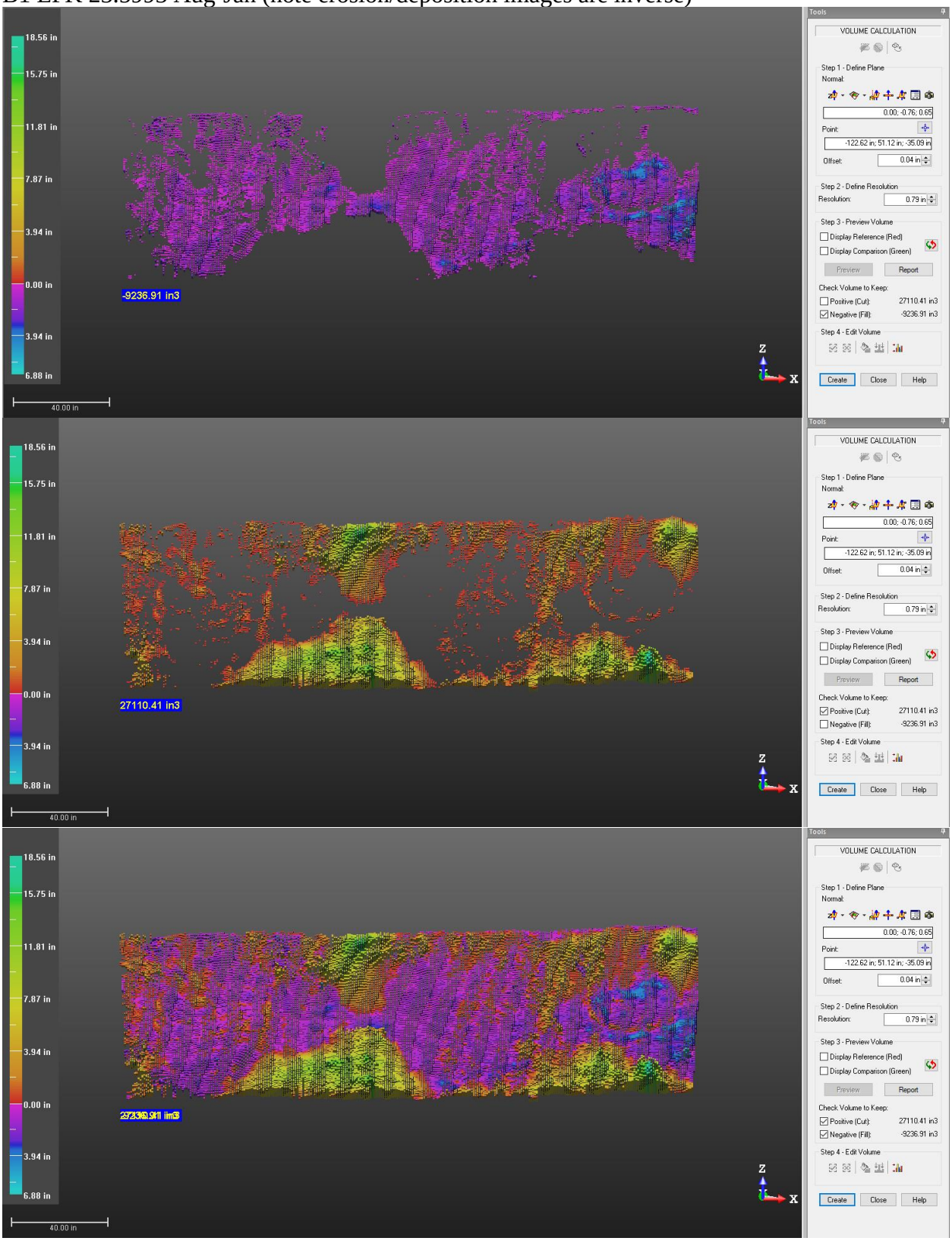

B2 EFK 23.5993 Aug-Oct

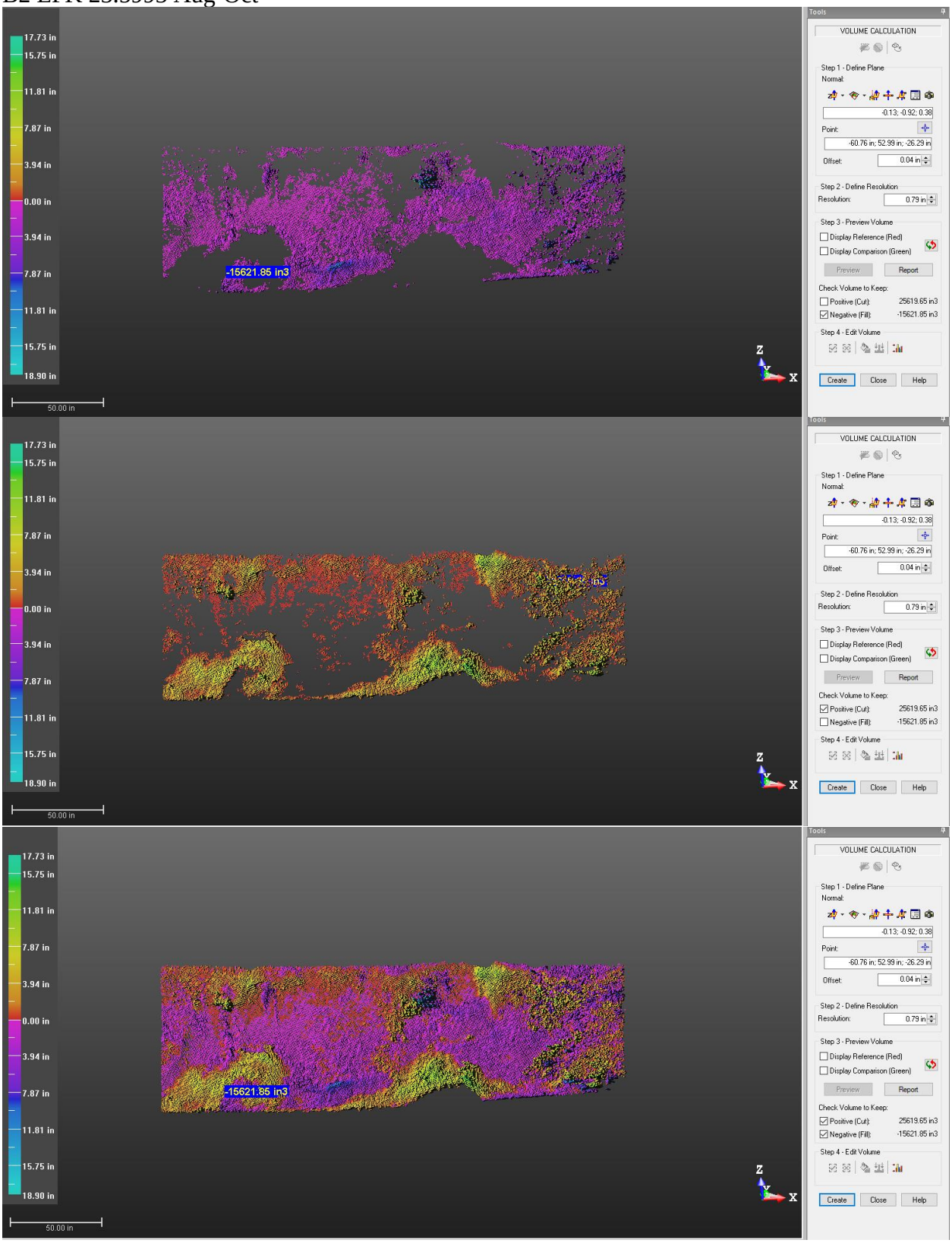

B3 EFK 20.2703 Aug-Jan

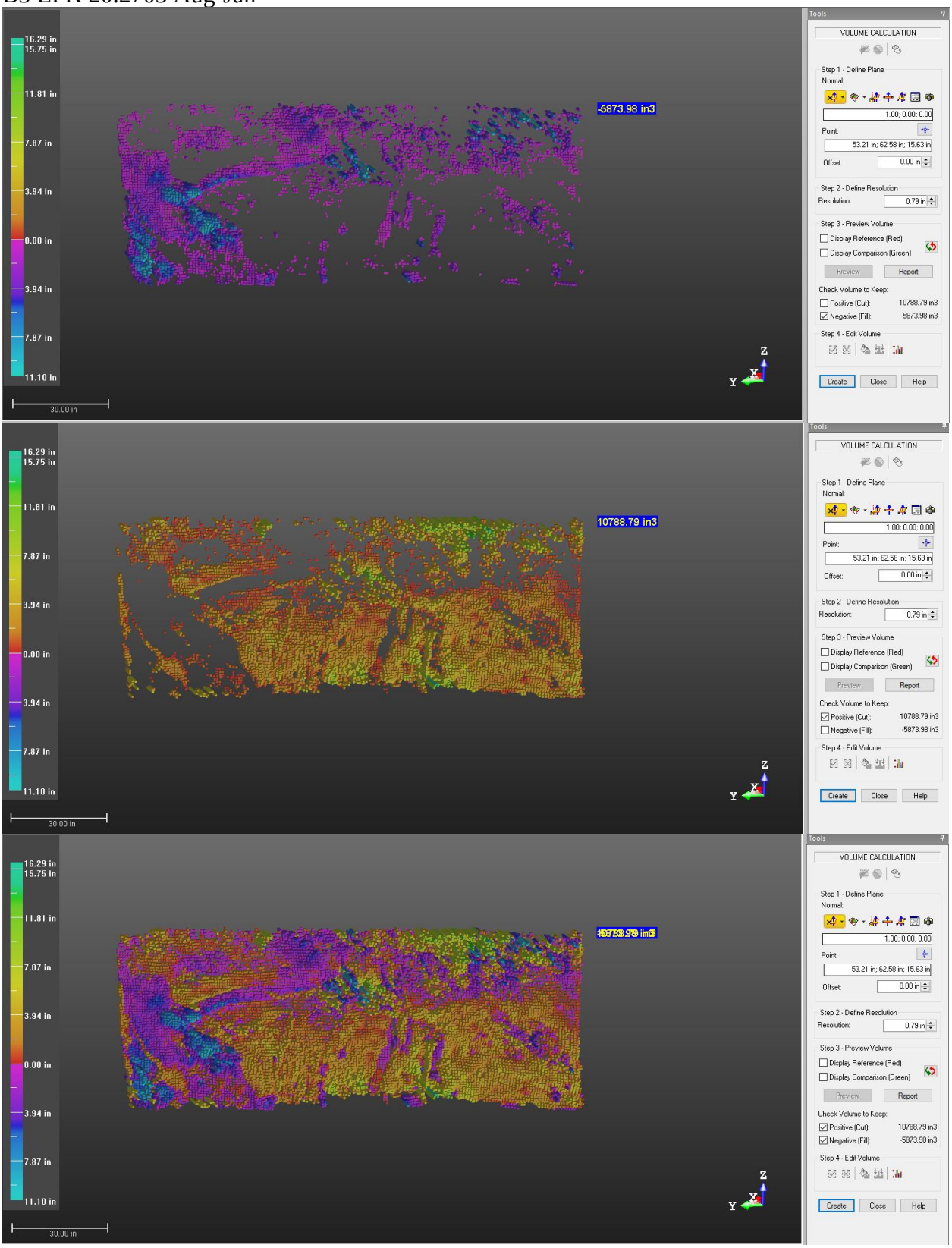

B4 EFK 20.2703 Aug-Oct

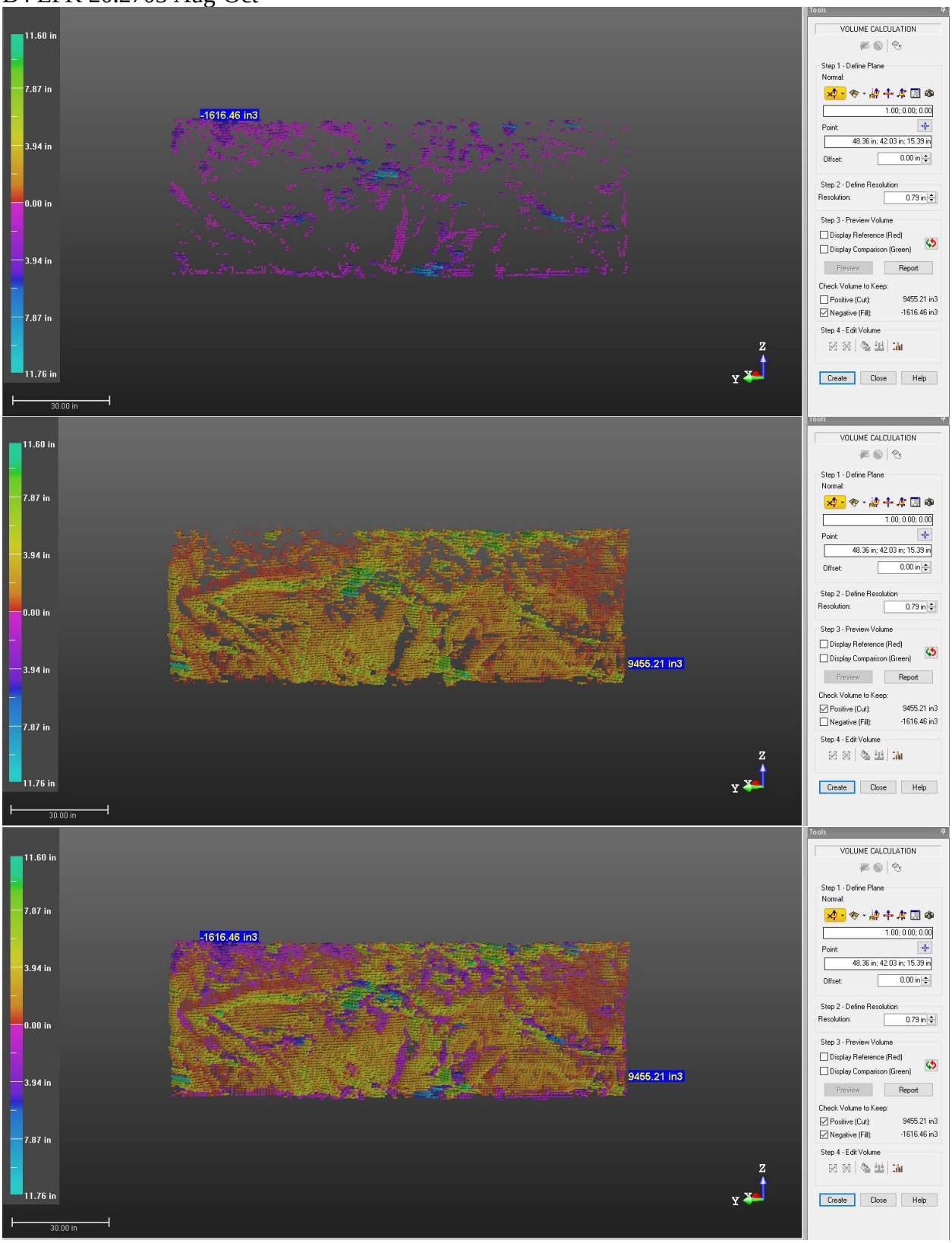

B5 EFK 19.3466 Aug-Jan

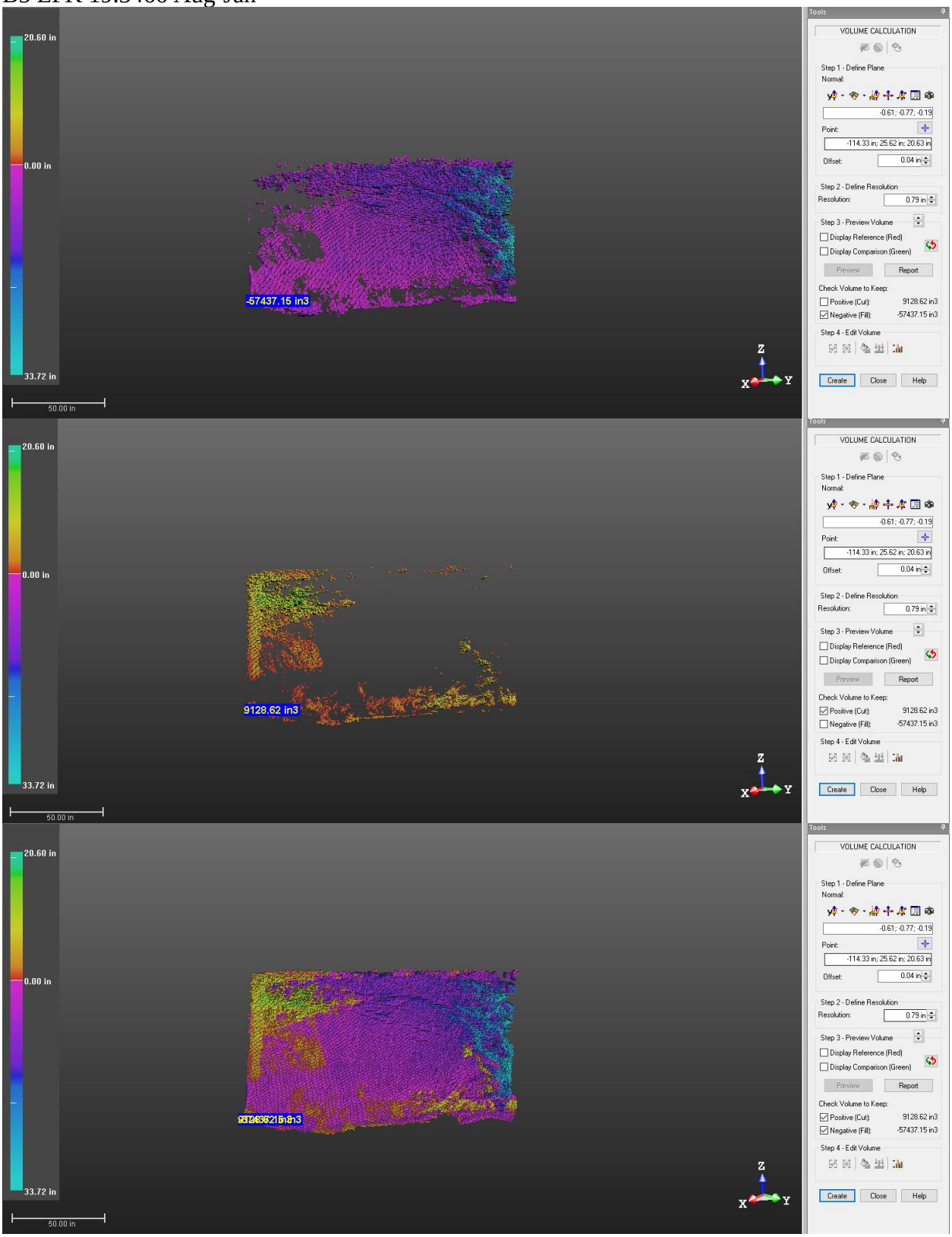

B6 EFK 19.3466 Aug-Oct

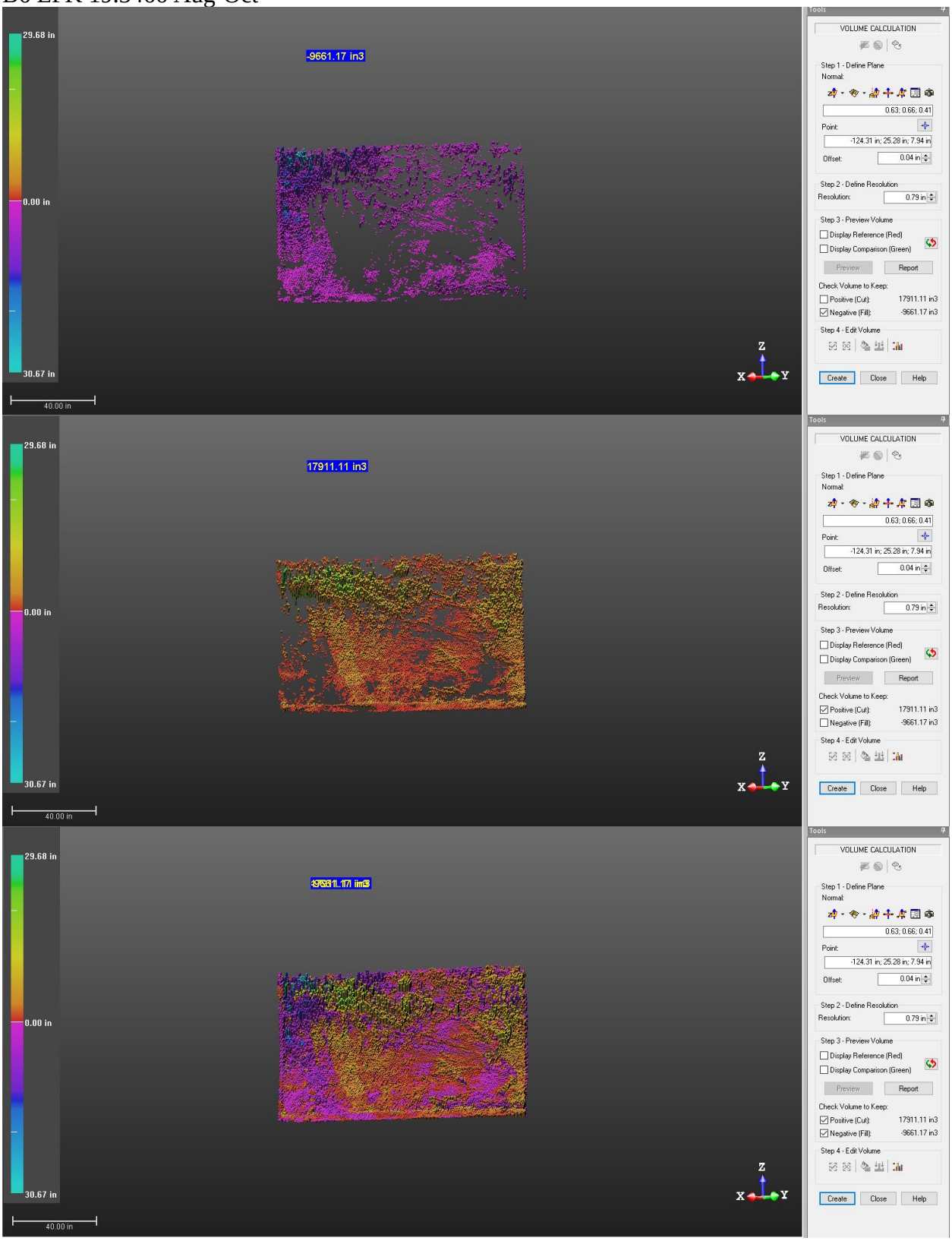

B7 EFK 19.3244 Aug-Jan

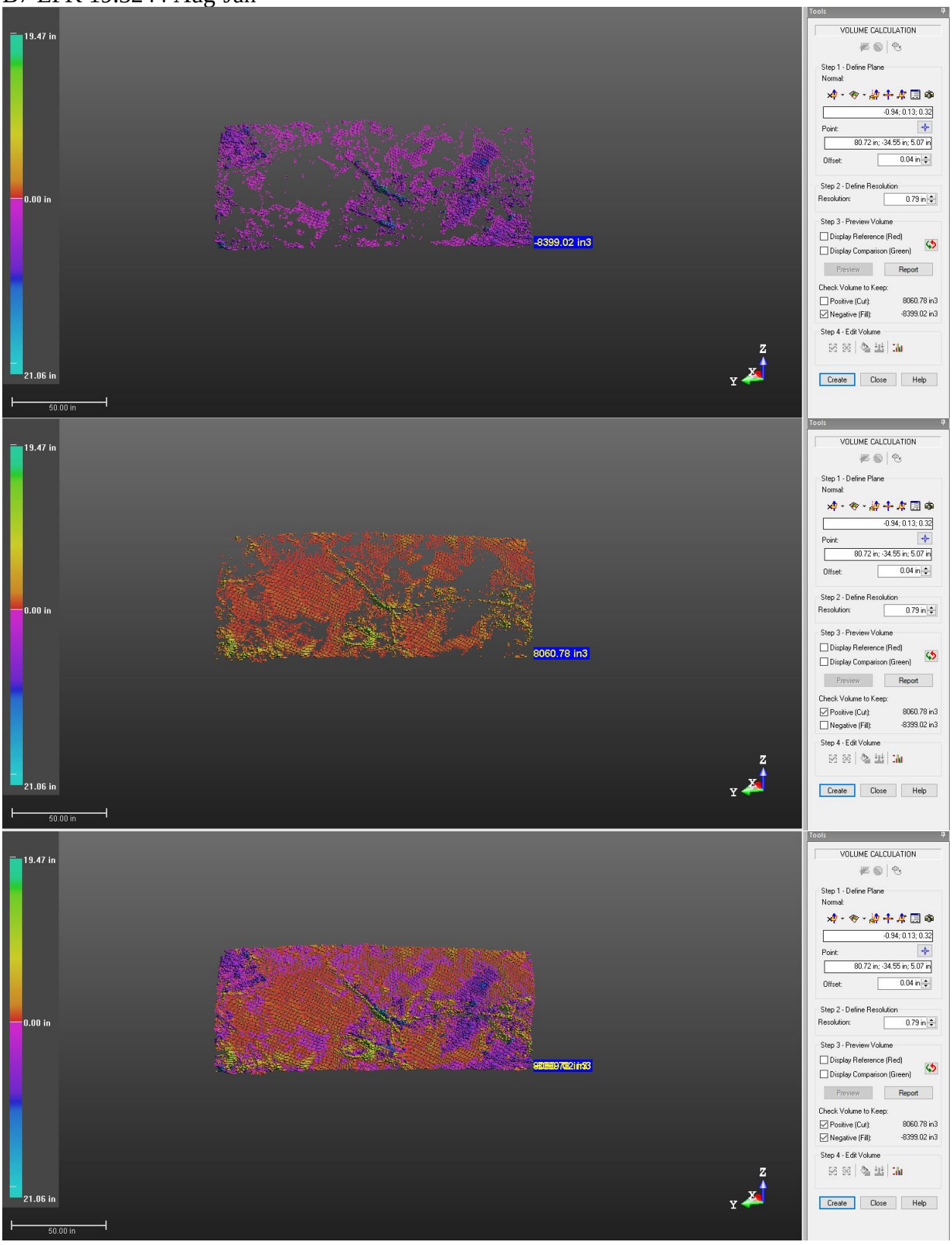

B8 EFK 19.3244 Aug-Oct

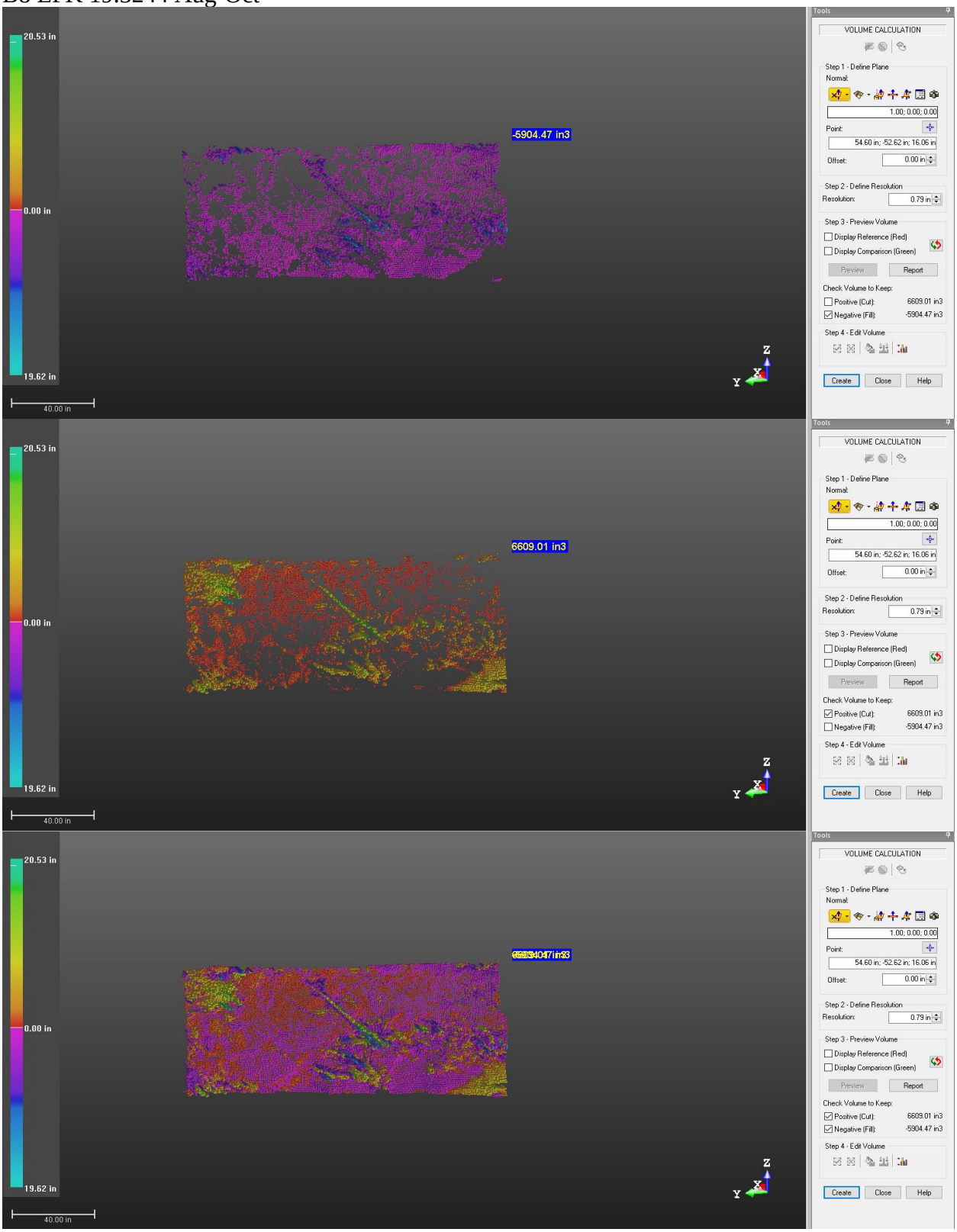

B9 EFK 19.0723 Aug-Jan

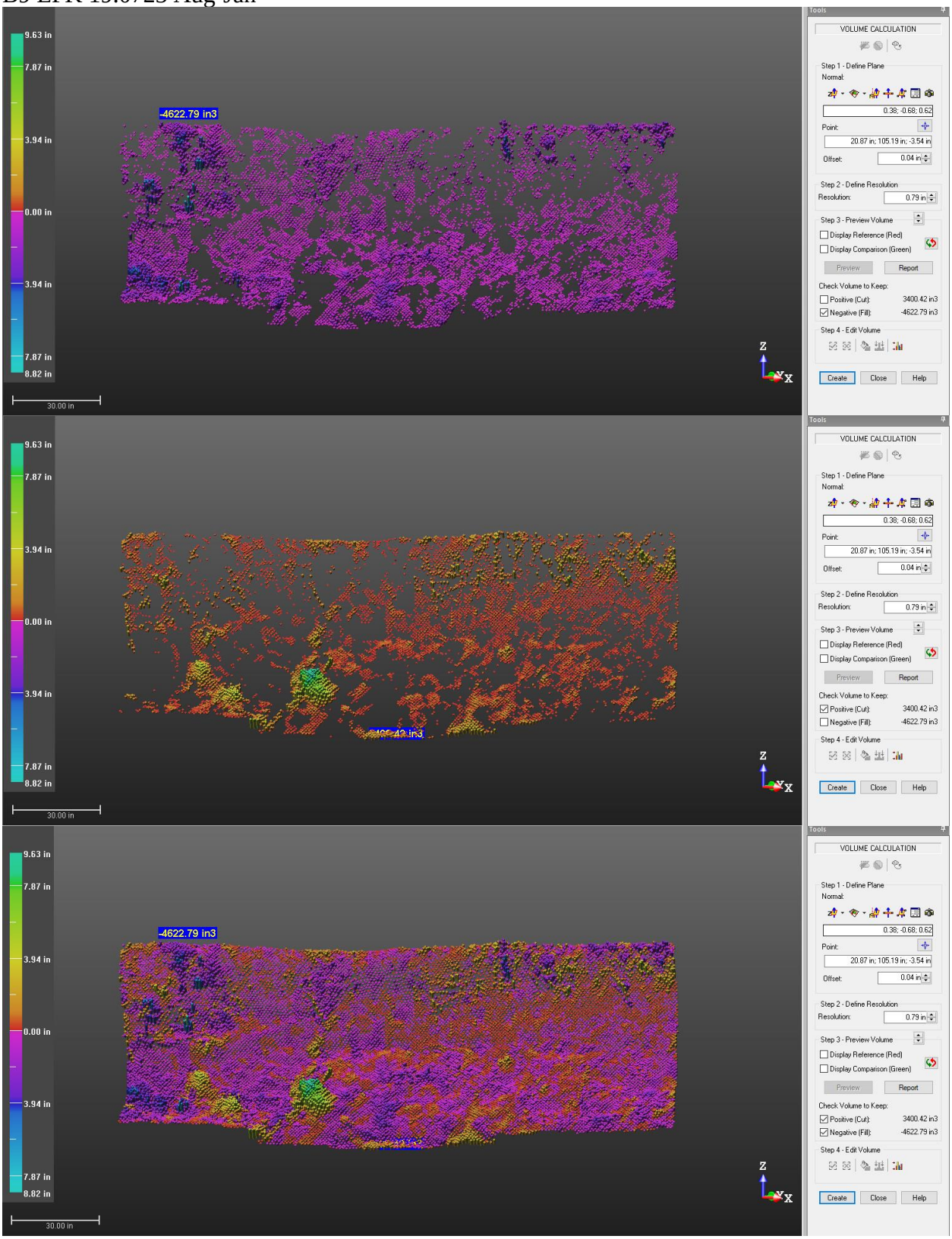

B10 EFK 19.0723 Aug-Oct

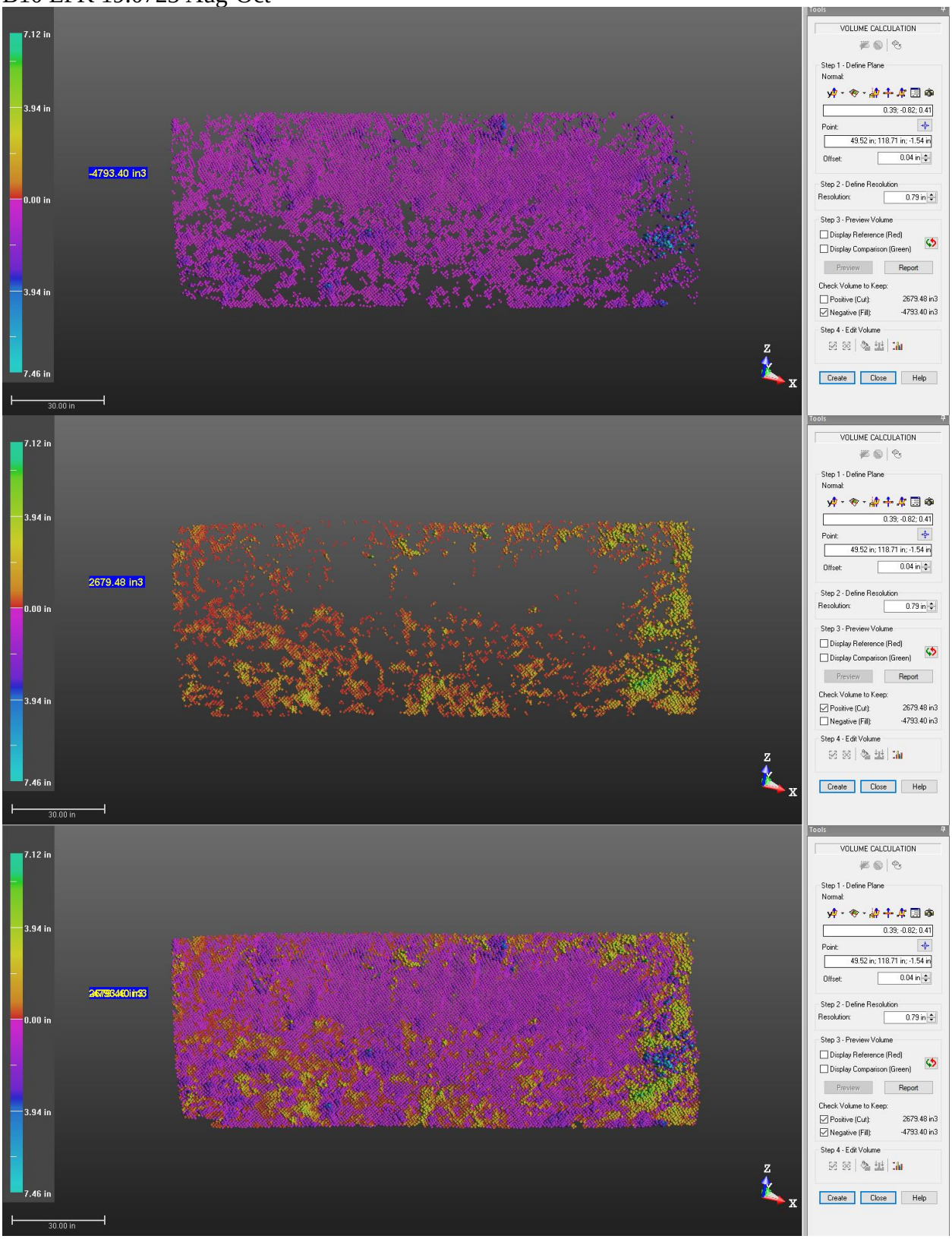

B11 EFK 19.0258 Aug-Jan

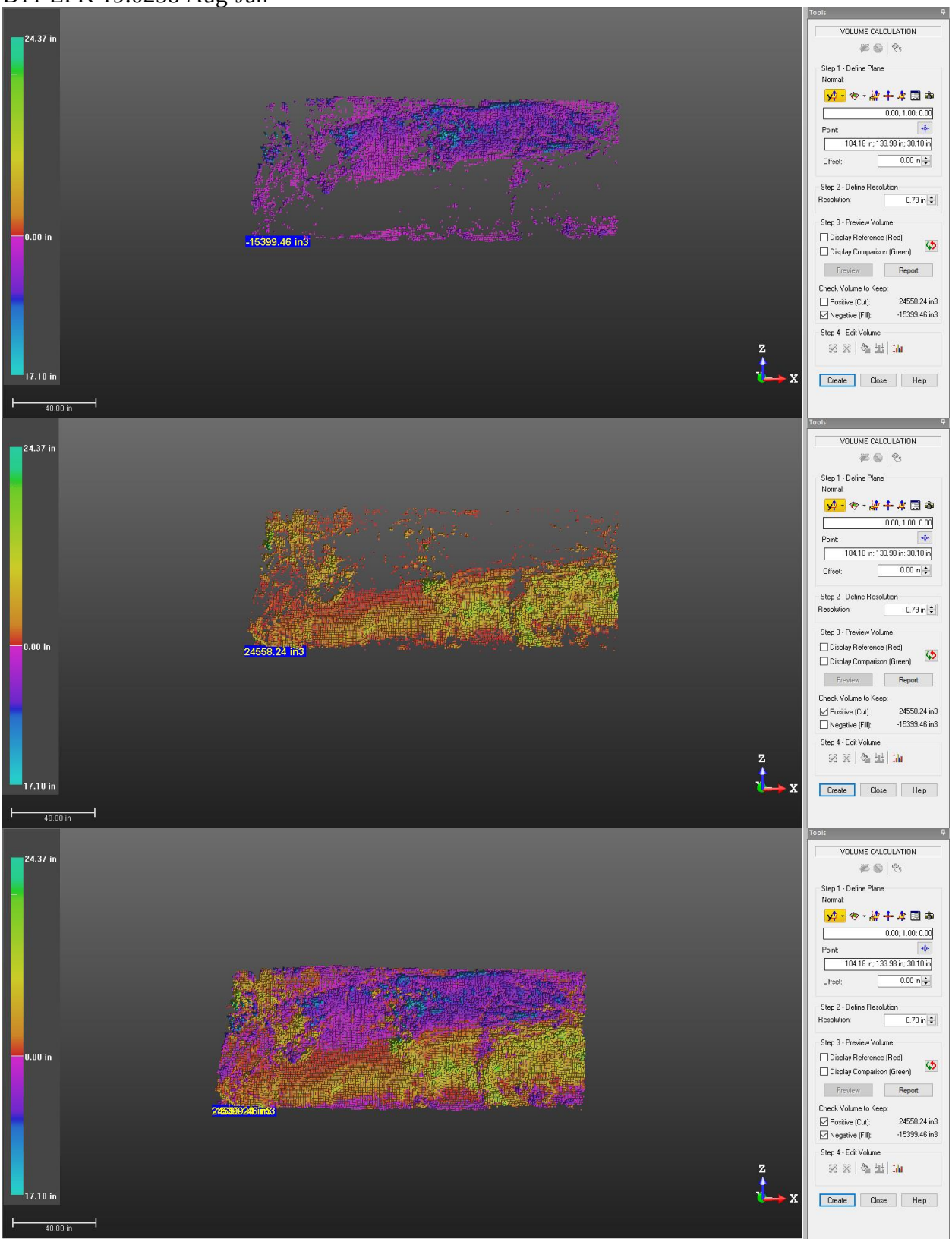

B12 EFK 19.0258 Aug-Oct

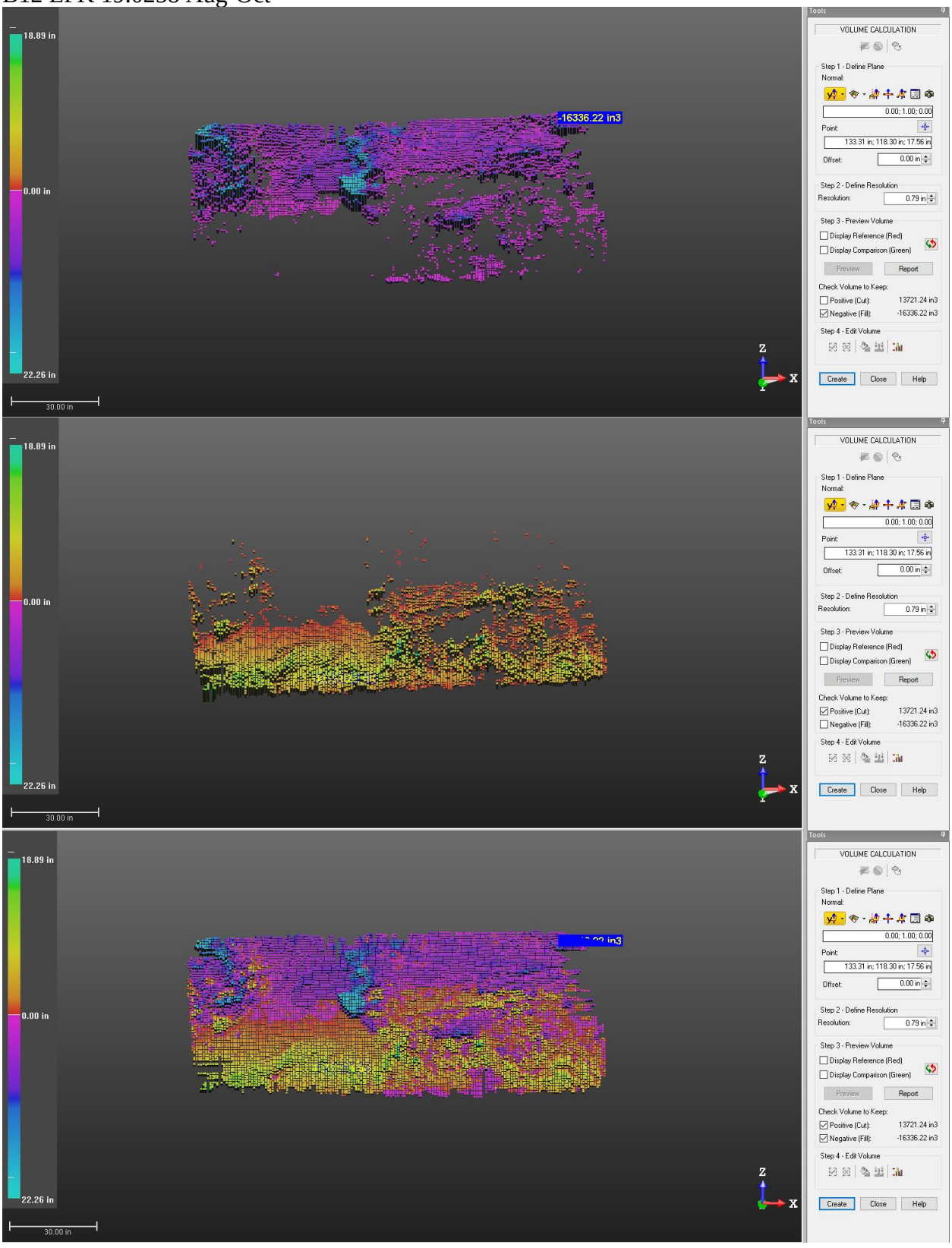

B 13EFK 16.4127 Aug-Jan

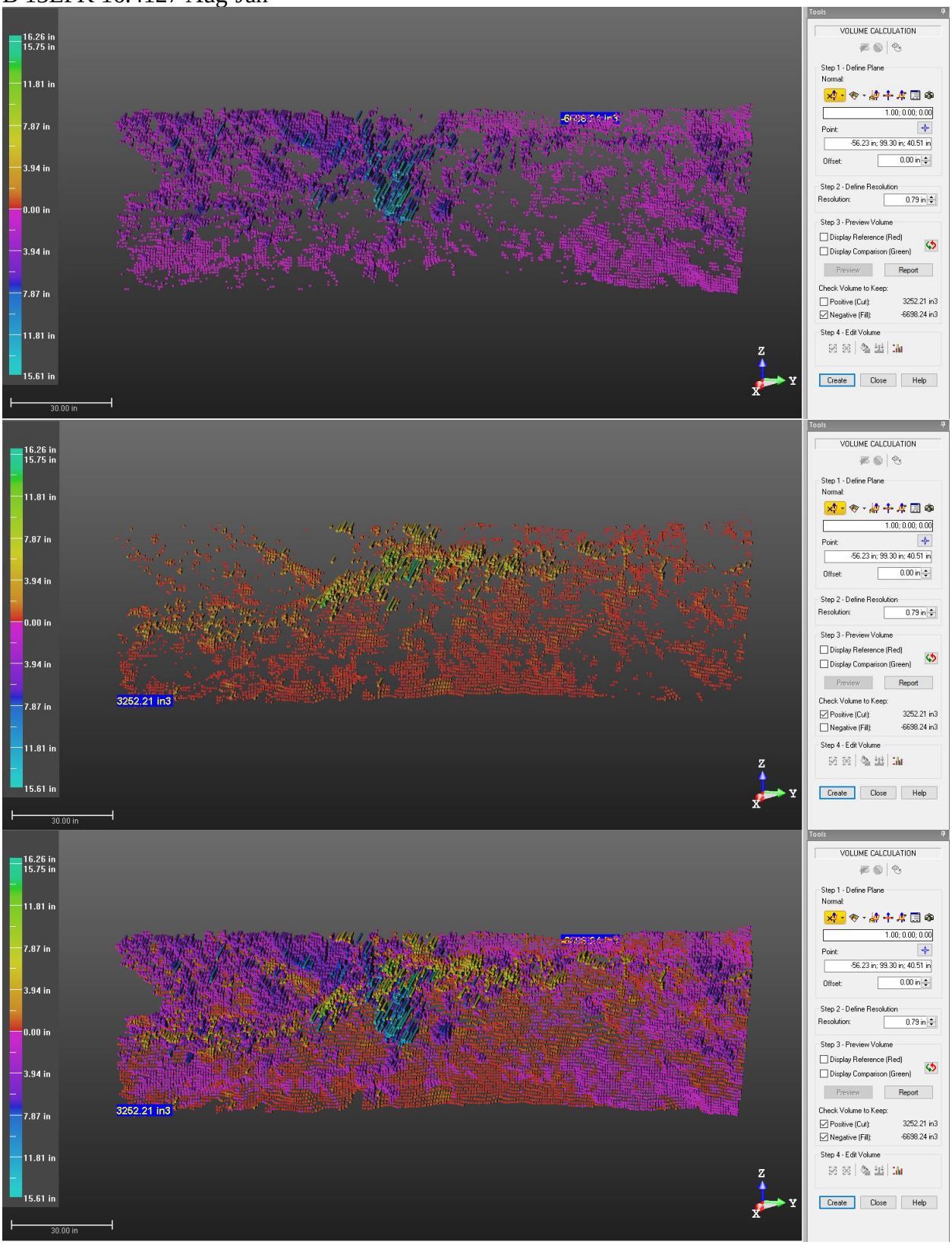

B14 EFK 16.4127 Aug-Oct

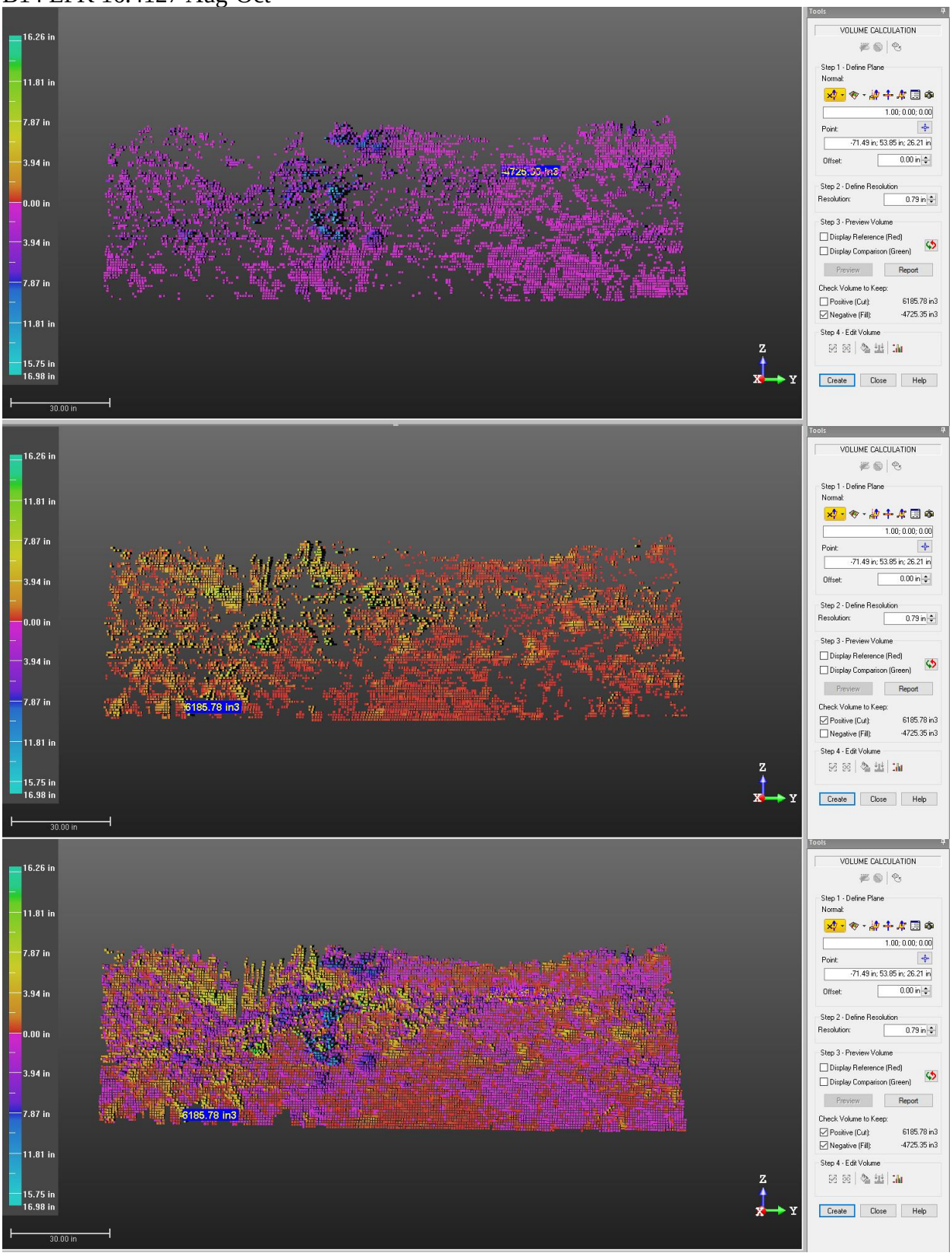

B15 EFK 14.5630 Aug-Jan

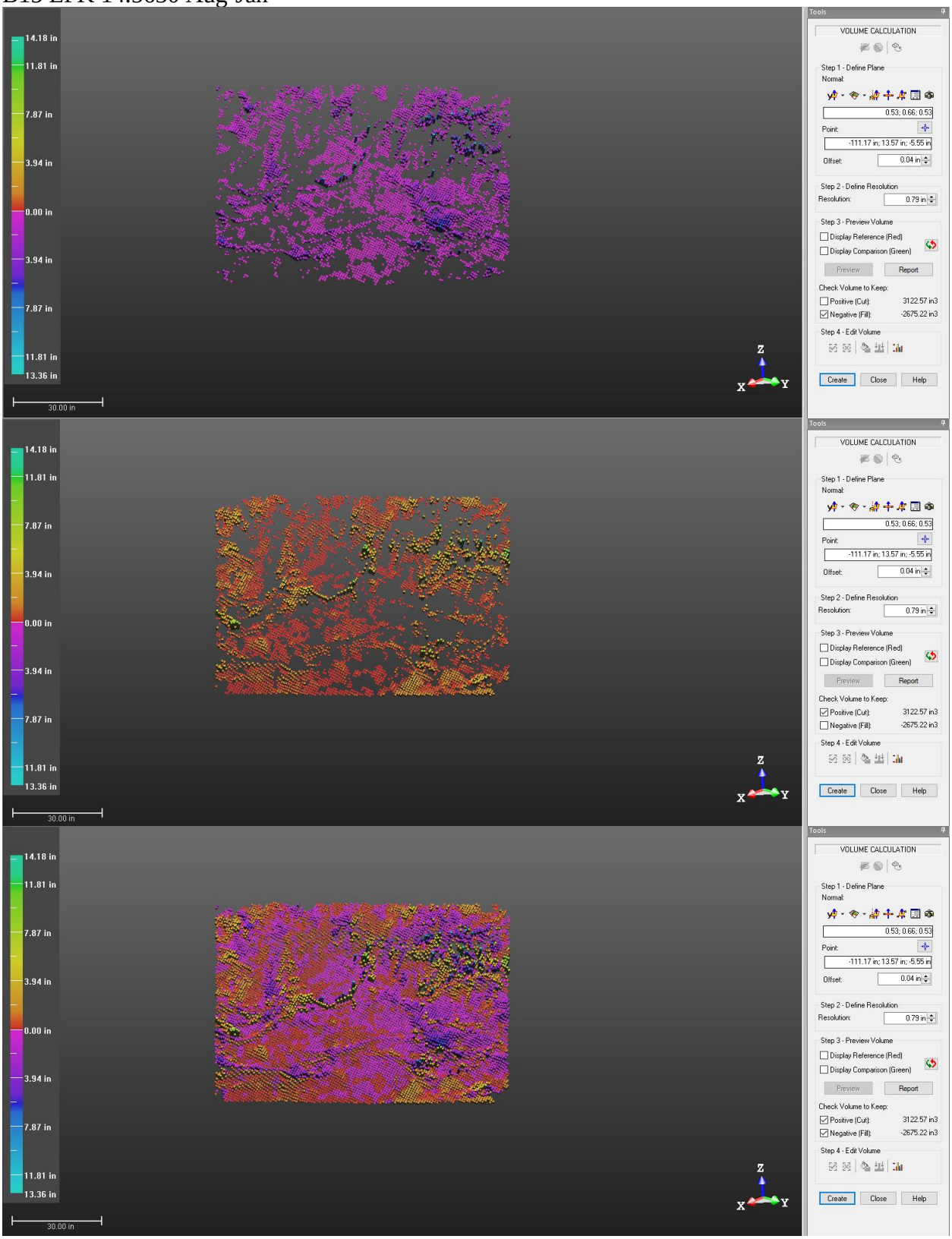

B 16 EFK 14.5630 Aug-Oct

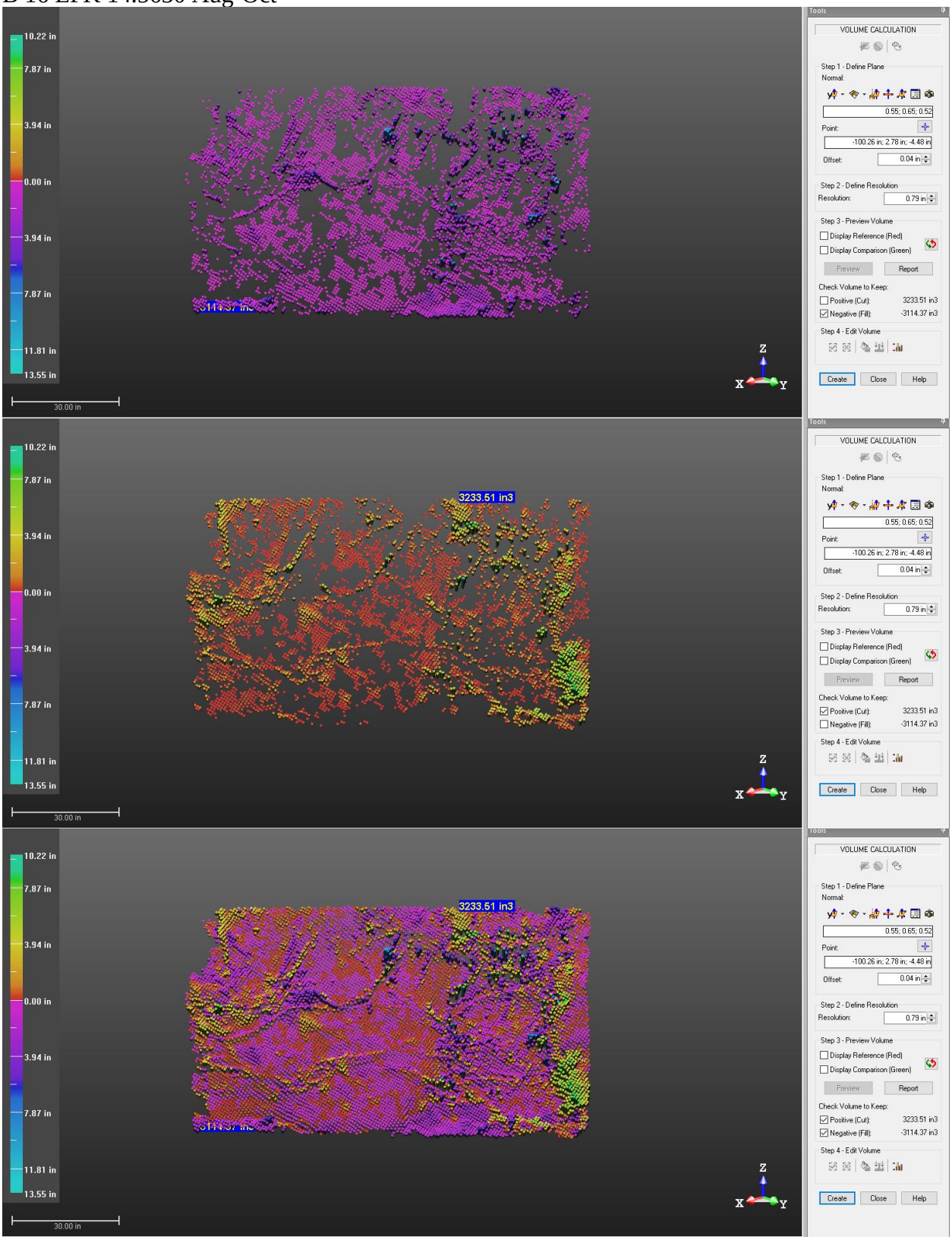

B17 EFK 5.5972 Aug-Jan

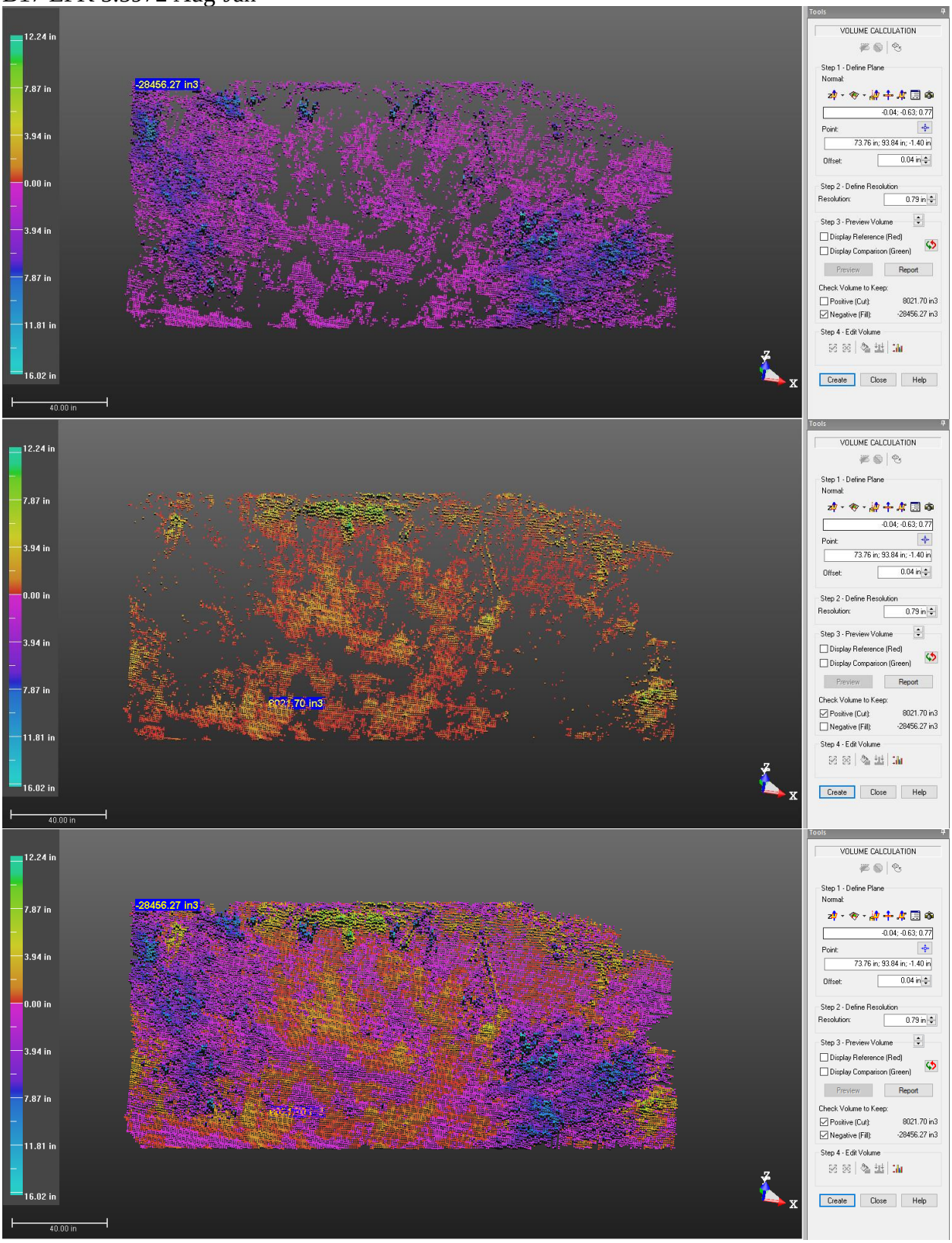

B18 EFK 5.5972 Aug-Oct

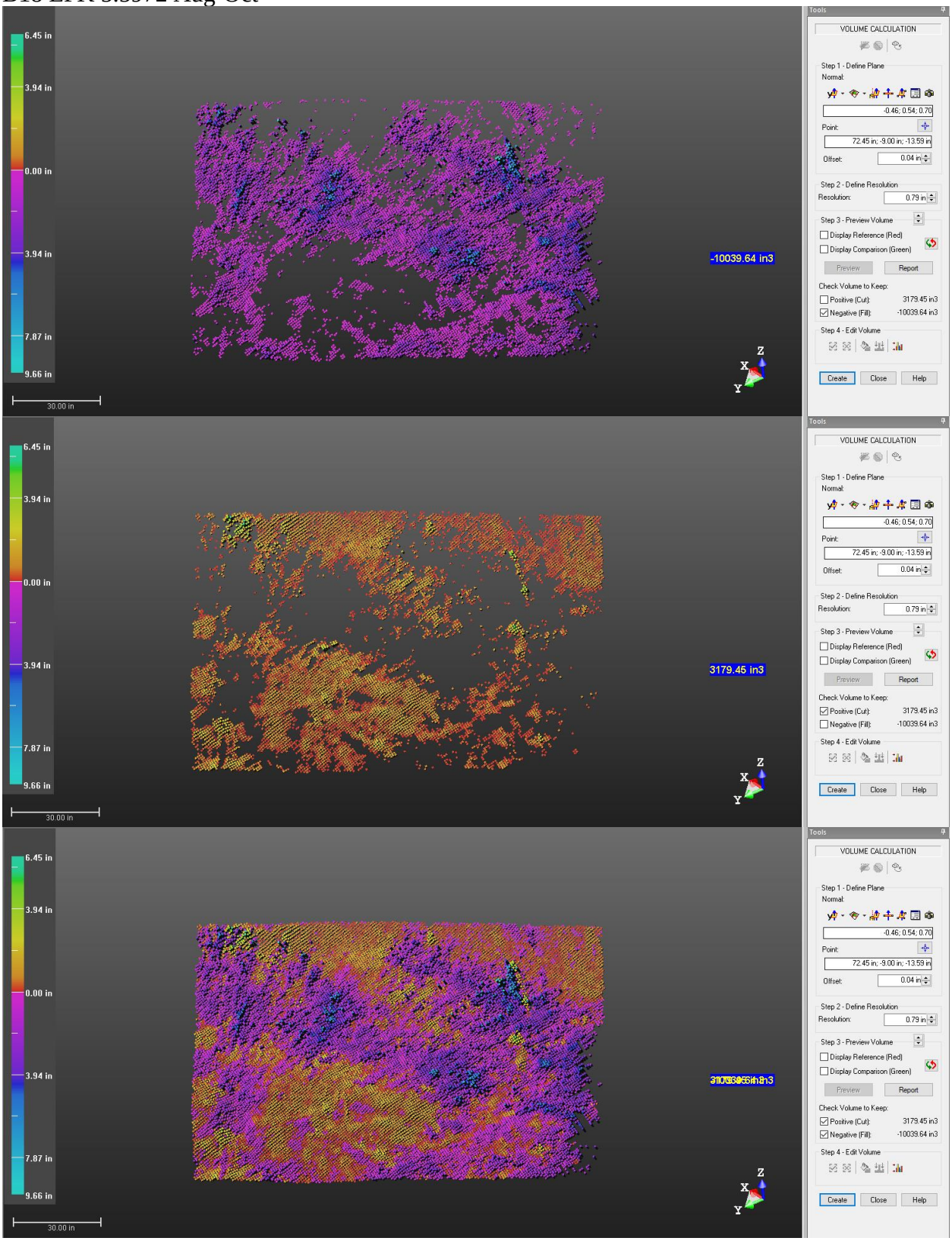

C1

Depth Percentage	10%	20%	30%	40%	50%	60%	70%	80%	90%	100%
Site	**Length of the core sample (cm)**									
EFK 23.59	7.50	5.00	6.70	6.00	7.50	7.00	8.50	5.50	6.50	6.50
EFK 20.27	5.50	5.00	5.70	6.00	7.00	5.50	6.50	7.30	6.00	8.50
EFK 19.34	5.00	6.30	6.10	5.40	5.00	5.40	6.00	6.00	5.00	6.00
EFK 19.32	4.80	5.00	7.50	6.00	7.00	7.50	5.30	5.40	5.40	6.90
EFK 19.07	6.80	5.00	5.80	7.00	9.50	5.30	6.00	7.00	8.00	5.50
EFK 19.02	5.50	4.80	5.00	5.40	6.20	3.60	5.00	5.00	5.00	4.60
EFK 16.41	4.80	7.00	4.60	4.50	6.50	5.20	5.50	4.10	4.50	6.00
EFK 14.56	7.00	5.80	6.80	7.00	6.00	6.00	7.00	5.50	5.60	5.80
EFK 5.59	6.80	6.80	6.50	9.00	7.00	7.00	6.20	6.20	6.30	7.50

Site ID	Volume of core sample (cm^3)									
EFK 23.59	33.93	22.62	30.31	27.14	33.93	31.67	38.45	24.88	29.40	29.40
EFK 20.27	24.88	22.62	25.79	27.14	31.67	24.88	29.40	33.02	27.14	38.45
EFK 19.34	22.62	28.50	27.59	24.43	22.62	24.43	27.14	27.14	22.62	27.14
EFK 19.32	21.71	22.62	33.93	27.14	31.67	33.93	23.98	24.43	24.43	31.21
EFK 19.07	30.76	22.62	26.24	31.67	42.98	23.98	27.14	31.67	36.19	24.88
EFK 19.02	24.88	21.71	22.62	24.43	28.05	16.29	22.62	22.62	22.62	20.81
EFK 16.41	21.71	31.67	20.81	20.36	29.40	23.52	24.88	18.55	20.36	27.14
EFK 14.56	31.67	26.24	30.76	31.67	27.14	27.14	31.67	24.88	25.33	26.24
EFK 5.59	30.76	30.76	29.40	40.71	31.67	31.67	28.05	28.05	28.50	33.93

Site	Soil Dry Weight (g)									
EFK 23.59	49.9000	47.1459	48.1249	40.4165	46.2548	53.3570	63.7100	37.8096	52.6177	39.5572
EFK 20.27	31.9780	33.4862	41.5193	36.4111	43.4158	34.9175	31.3523	32.7297	38.6493	60.8860
EFK 19.34	40.8302	45.0630	38.0559	34.7853	33.9649	36.2060	43.0902	44.7323	34.7030	36.9333
EFK 19.32	31.4076	29.6271	39.0120	35.4625	44.5576	52.3788	36.4980	39.6009	39.9485	45.6980
EFK 19.07	39.4669	33.9203	33.7994	25.4684	36.6179	36.7379	39.2586	44.1940	41.4615	38.8874
EFK 19.02	39.2934	31.1171	31.1139	28.3846	28.4832	23.3060	36.0940	34.6154	36.1201	30.9115
EFK 16.41	32.6194	49.8319	35.8603	33.1761	49.3849	35.6070	38.5462	30.2073	33.1903	35.7327
EFK 14.56	48.9088	45.8880	52.5169	58.3095	49.9944	48.9269	55.7809	45.5258	45.8075	39.8965
EFK 5.59	54.0806	56.4240	50.5712	61.2620	45.6995	44.9087	38.9002	36.3778	37.0540	47.0817

Site	Bulk Density (g/cm^3)									
EFK 23.59	1.4708	2.0844	1.5878	1.4890	1.3633	1.6850	1.6569	1.5196	1.7894	1.3453
EFK 20.27	1.2853	1.4805	1.6102	1.3415	1.3710	1.4034	1.0662	0.9911	1.4239	1.5834
EFK 19.34	1.8051	1.5812	1.3791	1.4240	1.5016	1.4821	1.5876	1.6481	1.5343	1.3607
EFK 19.32	1.4464	1.3098	1.1498	1.3065	1.4071	1.5438	1.5223	1.6211	1.6353	1.4640
EFK 19.07	1.2830	1.4997	1.2882	0.8043	0.8521	1.5323	1.4464	1.3956	1.1457	1.5630
EFK 19.02	1.5793	1.4330	1.3756	1.1620	1.0155	1.4311	1.5958	1.5304	1.5969	1.4855
EFK 16.41	1.5022	1.5737	1.7233	1.6297	1.6795	1.5137	1.5492	1.6287	1.6304	1.3165
EFK 14.56	1.5445	1.7489	1.7072	1.8414	1.8419	1.8026	1.7615	1.8298	1.8082	1.5206
EFK 5.59	1.7581	1.8342	1.7198	1.5047	1.4432	1.4182	1.3869	1.2970	1.3002	1.3877

Vita

José L. Martínez Collado was born in Mayagüez, Puerto Rico. He aspired to become a first-generation college student and serve as an inspiration for his three siblings. From a young age, he demonstrated a great passion for science and education; his hard work in school allowed him to be one of his class's top students and be part of the honors program. After graduating from high school, José decided to pursue his bachelor's degree from the University of Puerto Rico at Mayagüez. During this time, he was able to do many types of research in material science, chemistry, and environmental engineering. Before graduating, he was able to do two internships at Oak Ridge National Laboratory. After graduating in 2018, he was allowed to return to ORNL for a post-bachelor. During this time, José was accepted and eventually completed his Master's degree in Environmental Engineering from the University of Tennessee, Knoxville.